Bauhaus Summer School

# „Model Validation and Simulation"

Graduate Courses for Structural
Engineering Application

4th – 16th August 2013

# Content

# Foreword

WITT, Karl J.
Dean of the Faculty

Like some other Universities, the Faculty of Civil Engineering of the Bauhaus-Universität Weimar makes its experience and expertise in teaching and research available to foreign students during the summer break. Unlike most Universities, however, the aim this Summer School is to provide a course and a workshop to graduated students at the highest level of recent development of numerical methods and sophisticated modelling in different disciplines of modern civil engineering far beyond traditional graduate courses. In addition, it challenges the students to bring their own issues and develop their present topics of research with the experts. And finally a selected social program gives an opportunity for intercultural exchange and complements the experience Weimar.

In August 2013 about 50 students, 22 lecturers from 20 countries have participated our annual Summer-School. This volume summarizes some of the results, abstracts of selected student research works as well as the organized social events.

On behalf of our Faculty I would like to thank everyone for their contribution to the scientific input, the organization and the realization of this event and the realization of this booklet.
Particular thanks to all the lecturers who spent part of their annual leave to come to Weimar. In addition, I express my thanks to the German Academic Exchange Service (DAAD) for the sponsorship of this event.
The successful Bauhaus Summer School 2013 and this booklet would not have been possible without this generous financial support.

Weimar, August 2014

ABRAHAMCZYK, Lars &
SCHWARZ, Jochen
Earthquake Damage
Analysis Center,
Bauhaus-Universität Weimar

# Bauhaus Summer School – Model Validation and Simulation 2013: Course Description

## Participants

The course targets post-graduate students, i.e., second (M.Sc.) and third cycle (Ph.D.) from different institutions and countries to enable knowledge transfer between the participants. By providing students with advanced, scientifically-based interdisciplinary knowledge, skills and methods, they are trained to react to demanding engineering tasks in the areas of planning, construction and realization of structures under specific site, action and loading conditions. In addition the soft skills of each participant will be trained like team working and task sharing in an internationally composed project group.

Since 2011, the Summer School has been supported by the Life-long Learning Programme. Students from nearly over the world attended the summer courses during the last three years, which leads to a very intercultural exchange of ideas, thinking and life styles (cf. Figure 1).
Its innovative character results from the ambitious engineering tasks and advanced modeling demands. Major course topics are derived from current research fields of the participating institutions.

They are introduced by key lectures in civil engineering and con-densed during the project related training of simulation and mo-deling techniques. The acquired knowledge is applied to scien-tific and practically relevant projects within a compact course. Such a "hands-on approach" is commonly not included in regular teaching programmes. Several targets harmonically overlap.

The students will be trained in the use of modern software tools, design concepts and their practical applications. In general the project work is intensively assisted by the lecturer from different institutions ensuring a broader view to the existing problems and solution strategies.
The interdisciplinary teamwork in the projects combined with an intensive assistance by the academic staff shall enable the students to prepare and present a final presentation of the project results.

Especially thanks to the ERASMUS grand as part of the Lifelong Learning Programme students from the project partner could be supported and the mobility and exchange between the European Union are increased (cf. Figure 2).
Additionally the exchange between the participating project partners allowed not only an intensive guidance of the students by the entire attending lecturer also an opportunity for the scien-tific exchange of ideas and preparation of common collaboration projects could be achieved.

## Targets and Objectives

Model validation plays a central role in the work of civil and structural engineering. In practice engineers are dealing day-to-day with models to solve the specific problems in design. Materials with different properties are often combined; interaction phenomena (e.g. between soil and structure, structural and equipment) have to be considered. Often simplifications are requested which could impact the quality of numerical simulations.

Expert knowledge from different fields has to be transformed following the demands and needs of interdisciplinary cooperation. Due to the complexity of the problems (handled within the projects), models have to be validated through real measurements and simulations. The course covered the hybrid methods of model calibration using instrumental testing methods.
Experimental facilities were used for providing the data base for the reinterpretation and the comparison with numerical results.

The Course offers the platform to discuss the transfer of real existing buildings into different basic type structural models, to compare their robustness with respect to increasing abstractness and reduced dimensionality and to estimate the characteristic response parameters under dynamic loading and particular interaction effects (cf. project reports).

In order to structure and reflect the complexity of the chain reactions inherent to the impact extreme loadings (caused by natural phenomena or disasters), the programme explores in detail closely linked research disciplines and engineering-related areas of the natural sciences. It examines the central role that structural engineering plays in lessening the impact of extreme loadings e.g. natural disasters and focuses on the engineering methods that can be used to assess and (possibly) reduce the vulnerability of built environment and special structures.
Targeting to international objects relevant projects the programme highlights the demands on engineering modeling and simulation techniques at both regional and global levels. The objectives of this summer course are to demonstrate and to apply them.

The summer course offers the possibility for an exchange of modern scientific knowledge in a realistic training setting among the young scientists as well as the improvement of the partnerships for further common activities. Towards the end of the course, students are requested to present and discuss their work in front of a broad scientific audience.

The participants are invited to create their own networks for their future career, to train their management as well as language abilities and to train the ability to work in an international team.
In sum, the summer course of the Bauhaus-Universität Weimar provides a platform for networking by the participants and the involved European partner universities or institutions. The participants are invited to find new partnerships and to contribute to the development of an efficient networking between the participating institutions (Figure 2).

## Course Topics

The summer course is divided into two main parts: lectures and
project work. This time sharing ensures theoretical and practical
oriented work under holistic aspects and the use of modern
analyses methods and tools for numerical simulation in structural
and mechanical engineering. The young scientists get experience
and modern scientific knowledge under realistic training settings.
The offered formats and forms of training can be summarized as
follows (see Figure 3):

• **Lectures**: The necessary theoretical basics, the current state
of research (in project targeting fields) as well as special topics
are presented by lecturers and leading scientists from the
partner institution and invited guest speakers.

• **Special Theme Sessions**: Special lectures by partners and
lecturers from Bauhaus-Universität Weimar related to the
project work are offered; thus specific project related topics
could be discussed and trained.

• **Presentation of the Participants** (workshop character):
Participating students were requested to present their work in
a special session and to defend their results in front of a broad
scientific audience. Therefore each participant had to submit a
short abstract together with his/her application. On the basis
of these abstracts 15 titles were elected as presentation by the
participants, which also shall honor the effort and work of the
participant. (cf. Reports)

• **Excursion**: An excursion to a railway construction sites emphasizes the practical relevance of the course topics and illustrates existing requests for real existing structures and in more detail. Discussions with professionals provide the opportunity to link theoretical knowledge to practical experience.

• **Project Work**: (including presentation and submission of final results): This (for the participants mostly demanding) part of the course offers the possibility to work in interdisciplinary teams on different projects. The offered six projects are related to structural modeling, numerical and experimental geodynamics, earthquake engineering and seismic hazard and risk assessment, simulation and testing of steel and glass structures, wind engineering as well as numerical models in civil engineering. The project work was conducted in small groups and intensively supervised. The outcome - presented by the herein compiled reports - reaches an impressive level of results and graphical elaboration. (cf. **Project Reports**)

At the national level, no similar workshop to the International Summer School "Model Validation and Simulation" is known. The relevance of the course topics is undisputable. Not at least the number of applicants indicates the existing demand for such an international and interdisciplinary oriented format of training and exchange between young scientists in structural and mechanical engineering.

Referring to recent European and international code developments, participants are invited to present national design practice and experience from applications, focusing on the efforts that contribute to new concepts, evaluation strategies and the quality assurance of structural models.

The Summer School combines theory and practice on the basis of advanced research and tool development. The modular structure of the programme allows the participants to address current and trendsetting problems and research topics.

Key aspects of the Summer School are linked to the Research Training Group 1462 ("Model Validation in Structural Engineering") which is involved with the project "Calibration of Numerical Models in Civil Engineering Applications".

## Bauhaus Summer School 2013
## Model Validation and Simulation
## August 5th - August 16th

**schedule 1st week - Lecture hall C**

| | Monday, 5th | Tuesday, 6th | Wednesday, 7th | Thursday, 8th | Friday, 9th | Saturday, 10th |
|---|---|---|---|---|---|---|
| 09:00 - 10:30 | Opening 2013 (Dean, IO, GRK, ...) *Lecture hall C, M13* | Stochastic methods for modeling uncertainties and quantifying reliability \| *Prof. Helmuth Pradlwarter (Uni Innsbruck)* *Lecture hall C, M13* | Unsaturated Soils - Fundamentals and Overview of Applications \| *Dr. Snehasis Tripathy (Cardiff)* *Lecture hall C, M13* | Damage Detection of Civil Engineering Structures by Evaluating the Changes of Linear and Nonlinear Dynamic Characteristics \| *Prof. Stefan Maas (Luxembourg)* *Lecture hall C, M13* | Project work | Excursion: DB railway line for high-speed passenger and freight traffic incl. "Osterberg" tunnel, "Unstrut" viaduct and Erfurt main station |
| 11:00 - 12:30 | Presentation of the Staff and Projects (6 different projects will be offered, registration to the projects) *Lecture hall C, M13* | Self-Centering Rocking Frames \| *Prof. Attila Joó (BME)* *Lecture hall C, M13* | Optical 3D reconstruction for geometric validation \| *Prof. Volker Rodehorst (BUW)* *Lecture hall C, M13* | System identification and parameter estimation in structural dynamics and building acoustics \| *Dr. Edwin Reynders (KU Leuven)* *Lecture hall C, M13* | will be announced | |
| 12:30 - 13:30 | | | Lunch | | | |
| 13:30 - 15:00 | Project work (Introduction) | Project work | Interdisciplinary experience exchange with specialised courses of Bauhaus Summer School 14:00 - 17:00 | Presentation by Participants (Lecture hall) | Project work | 8 a.m to around 5 p.m |
| 15:30 - 17:00 | will be announced | will be announced | | Project work / *will be announced* | Closure / *will be announced* | |
| 17:30 - 19:00 | Icebreaker Party *student club " Schütze"* | Sightseeing Weimar Group I (17:30 - 19:00) *meeting point ( the Egg)* | Project work *will be announced* | Project work *will be announced* | Sightseeing Weimar Group II (17:30 - 19:00) *meeting point ( the Egg)* | |
| | Cultural events as part of the Bauhaus Summer School 2013 | | | Cooking evening *student club " Schütze"* | | |

**schedule 2nd week - Lecture Hall C**

| | Monday, 12th | Tuesday, 13th | Wednesday, 14th | Thursday, 15th | Friday, 16th | Saturday, 17th |
|---|---|---|---|---|---|---|
| 09:00 - 10:30 | Assessment of Historic Structures: The Fatih, Istanbul, Case Study \| *Prof. Polat Gülkan (METU)* *Lecture hall C, M13* | Seismic strengthening of R/C structures using devices for passive energy dissipation \| *Prof. Diiyan Blagov (UACEG)* *Lecture hall C, M13* | Spatially varying earthquake ground motion and dynamic response of long bridges: assessment from a structural engineering perspective \| *Assoc. Prof. Anastasios Sextos (AUTH)* *Lecture hall C, M13* | Project work | Presentation of project works | Departure |
| 11:00 - 12:30 | Simulations and Methods for Earthquake Performance Assessment of Buildings \| *Prof. Ahmet Yakut (METU)* *Lecture hall C, M13* | Presentation by Participants (Lecture hall) *Lecture hall C, M13* | Modelling of composite steel-concrete bridges \| *Prof. I. Vayas (NTUA)* *Lecture hall C, M13* | will be announced | Closure *Lecture hall C, M13* | |
| 12:30 - 13:30 | | | Lunch | | | |
| 13:30 - 15:00 | Presentation by Participants (Lecture hall) | Project work | Interdisciplinary experience exchange with specialised courses of Bauhaus Summer School 14:00 - 17:00 | Preparing of presentation | Preparation of final report \| Presentation Bauhaus Summer School | |
| 15:30 - 17:00 | Seismic Instruments \| Werner Bolleter (SYSCOM Inc.) *Lecture hall C, M13* | will be announced | | will be announced | | |
| 17:30 - 19:00 | Project work *will be announced* | Soccer challenge *sports ground "Falkenburg"* | Project work *will be announced* | Cooking evening (optional) *student club " Schütze"* | Fare well party (18:00) *student club " Schütze"* | |
| | Cultural events as part of the Bauhaus Summer School 2013 | | Cultural events as part of the Bauhaus Summer School 2013 | | | |

Figure 3 – Time Schedule of the Bauhaus Summer School "Model Validation and Simulation" (MVS 2013)

# Project Reports

DRAGOS, Kosmas
Aristotle University of
Thessaloniki

MEIXEDO, Andreia
Faculty of Engineering of
University of Porto (FEUP)

BONIFÁCIO, Cristiana
Faculty of Engineering of
University of Porto (FEUP)

SASSANI, Alireza
Middle East Technical
University (METU), Ankara

KAMEZI AMIRI, Abbas
TU Vienna

SCHOMMER, Sebastian
University of Luxembourg

MAKISHA, Nikolay
Moscow State University of
Civil Engineering

DEEB, Maher
Bauhaus-Universität Weimar

ZABEL, Volkmar
Bauhaus-Universität Weimar

# Project 1 – System Identification, Model Updating and Simulation

## Abstract

During the Weimar Summer School course "Model Validation and Simulation" the project "System Identification, Model Updating and Simulation" has been performed. The project was about modal analysis of civil structures. As an example a down scaled "tower" was given. This tower was made of PVC water pipes, with a basement of concrete. Four acceleration sensors had been placed on the pipe by pipe clamps. So it was possible to measure the response of the structure for different excitations. Impulse forces were applied using a hammer from different directions. The force excitation in Newton and the resulting accelerations given by the sensors in m/s² have been recorded. For the measurements the sensors had been arranged in different setups with one sensor as reference, so it was possible to combine the setups later. The measured response was analyzed in order to identify the modal parameters including the natural frequencies, the mode shapes and the damping ratios of the structure using MACEC toolbox.

Parallel to the real measurements a simulation has been prepared. The first step was to create two FEA models of the structure using the software packages ANSYS and SLang. The aim was to compare

the results calculated by the different software. In the models were developed using beam elements considering the material properties of a PVC pipe. The models were used to calculate the modal parameters of the tower.

## The Structure

As an example a "tower" like structure was studied Figure 1. It was made of PVC water pipe standing in a basement of concrete and had a height of 3 m. Moreover, in the same figure, the four acceleration sensors can be seen which were attached to the tower by pipe clamps. It was possible to move them up and down easily to arrange them in different setups. On the outside of the pipe the height in centimeters was measured and marked from the surface of the basement. The markers have the same position as the nodes in FEA models. So it was logical to put the sensors onto the marks. In perfect case one sensor should be positioned on every mark. Because of the lack of sensors different setups with respectively 4 sensors were used. One of the sensors stayed at the top on the 3 m mark as a reference. The other 3 sensors had been placed on 3 following marks. Due to the reference sensor it was possible to combine the setups later.



Figure 1 – PVC pipe with concrete basement

## The FEA

In addition to the real measurements a simulation based on FEA models has been created. Two FEA models of the structure have been developed using software ANSYS (ANalysis SYStem) and SLang (Structural Language). The reason to do so was to compare the results calculated by the different software.

Except of the different software the models were exactly the same. They were made of beam elements with the material properties of a PVC pipe and 6 DOF (Degrees of freedom). The nodes of the elements aligned along the vertical z-axis with equal distances of 0.2 m. The lowest node has been fixed by restraining all of its DOFs.

The models were used to calculate 10 modes of the tower. After that the mode shapes of the structure were simulated in the MATLAB toolbox MACEC.

## Preparation of FEA in SLang

For the purpose of modal analysis "SLang" software were used. This is a program prepared for FE static and dynamic analysis. In order to build up the FE model, there is an auxiliary program so-called "PreSLang" which gives the possibility of creating objective model in a GUI (Graphical User Interface). Once the model is created, an output file via export option could be made in order to be used by SLang for the main analysis.

## FE model of the pipe specimen

The pipe specimen was modelled by the use of pipe element as well as shell type element, so that the results of natural frequencies and eigenvectors could be compared. However to avoid any unnecessary complications associated with the definition and working with shell element, we ended up with using only the pipe element modelled specimen throughout the further steps.

Following the arrangement of measurement points on the laboratory specimen, in the FE model, 16 nodes have been defined. The pipe elements are assigned in between each adjacent pair of nodes.

The length of the model is 3.00 m long, which was divided into 15*0.20 m parts located between adjacent nodes and each part is a pipe element. Before performing the analysis, all the elements were merged together. The pipe model PreSLang is shown in figure 1 and the model properties are given in table 1.
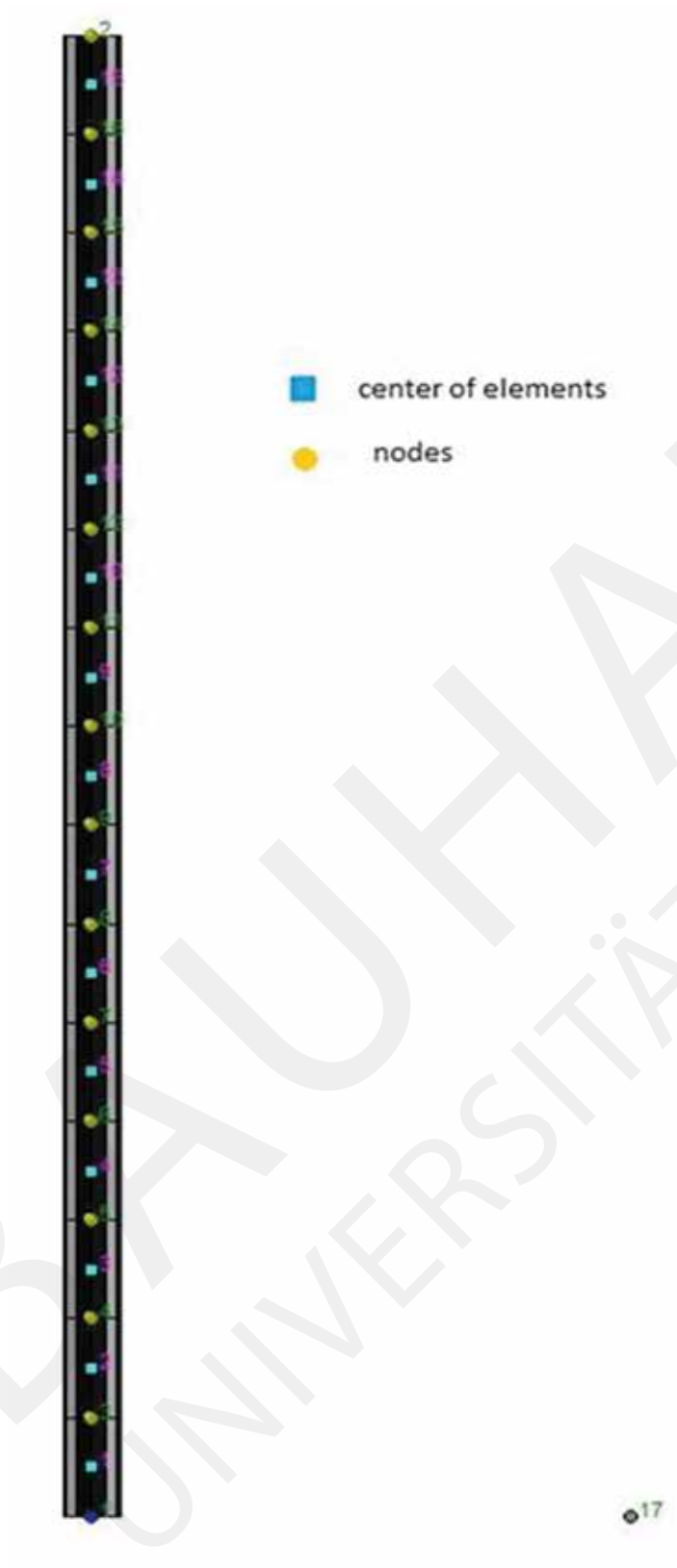
Figure 2 – The graphical expression of model in PreSLang. Node 17 is reference node

Table 1 – The properties of the nodes and elements of the model
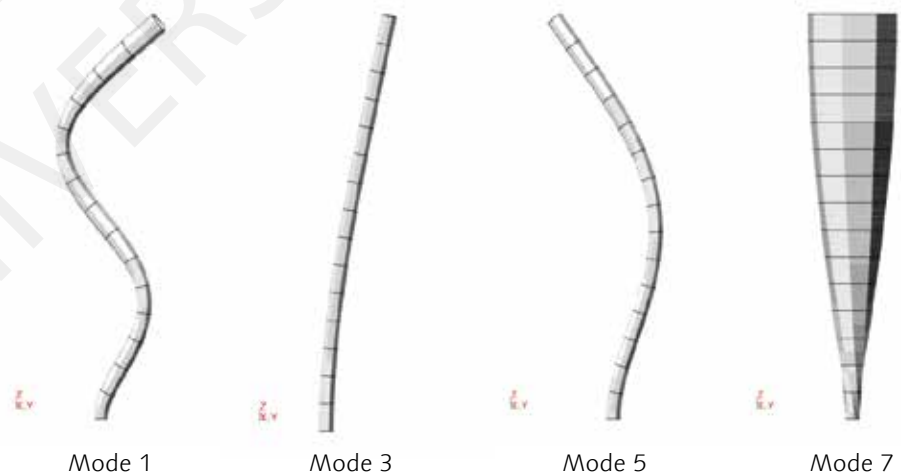
| ELEMENTS | | | | NODES | | |
|---|---|---|---|---|---|---|
| Material Data | | Physical Data | | Number | | DOF |
| Mass density (kg/m3) | Elastic Modulus (N/m2) | Poison's ratio | Central radius (m) | Wall thickness (m) | 1 | Rigidly clamped |
| 1400 | 3e+09 | 0.4 | 0.0534 | 0.0032 | 2-16 | 3D-6 |

The exported file of FE model is used for solving the corresponding eigenvalue problem of the undamped free equation of motion of the structure. Consequently the natural frequencies and modal shapes are provided for the first 12 modes by SLang as given in Table 2 and Figure 3 respectively. Note that we have the orthogonal modes due to the symmetry of the circular cross section of the structure.

Table 2 – The natural frequencies of the initial FE model

| Mode Number | Natural Frequency (Hz) |
|---|---|
| 1 | 3.4368 |
| 2 | 3.4368 |
| 3 | 21.538 |
| 4 | 21.538 |
| 5 | 60.31 |
| 6 | 60.31 |
| 7 | 72.935 |
| 8 | 118.2 |
| 9 | 118.21 |
| 10 | 122.05 |
| 11 | 195.46 |
| 12 | 195.46 |

Figure 3 – Graphical presentation of the mode



Mode 1          Mode 3          Mode 5          Mode 7

*for similar mode shapes only one is shown.

Mode 8                          Mode 11                          Mode 10

Note that the 7th and 10th modes are torsional and longitudinal respectively which are out of our interest for system identification but those are provided merely as a report of solution to the eigenvalue problem.
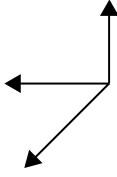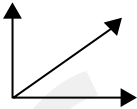
## System Identification by means of MACEC

For the purpose of system identification MACEC, which is a MATLAB toolbox, was utilized. In order to start identification, the record of accelerations corresponding to the measurement channels for each setup were demanded which had been already obtained from the experiment.

Some preliminary files including a grid and beam file must be constructed in MACEC in advance. These two files contain the location of nodes and the connection between. The step by step proceeding with MACEC as well as the chosen method of identification is in the following concisely provided.

1. Inserting the file which contains the measured acceleration data of channels.
2. Converting the data into "mcsignal".
3. Processing the modification and data, which includes the removing of the offset for all channels and decimation. First we can have a look to the FFT of the data of the channels to investigate the frequency range of excitation due to the hammer impact. Decimation is applied to capture the range of interest for the frequency that lies into the excited frequency range. Since the method of stochastic subspace system identification was applied there was no need to generate the frequency response function (FRF), hence the channel corresponding to the measured data of impulse was eliminated.
4. Adjustment of degrees of freedom of the channels. Two perpendicular channels in the XY plane were defined for each node. Subsequently, due to the difference between the coordination systems of the FE model and that used for data acquisition, the

*for similar mode shapes only one is shown.

Table 3 – Transformation of the coordinates between transducers and the FE model

| transducer | FE model |
|---|---|
|  |  |
| z | -y |
| y | -x |

following transformation of the coordinates must be necessarily implemented in MACEC (see Table 3).

5. Selection of the identification method: The stochastic subspace method was selected. In this section the covariance driven method was selected to be applied. Two mutually perpendicular channels 7 and 8 both located in the top node (node 2) were set as reference channels to reduce the amount of calculations. Then the order of the system corresponding to the size of the problem was estimated. Subsequently the QR factorization and SV (singular values) decomposition of the system matrix were calculated. The singular values should approach to zero in the estimated order.

6. At the final step, the Modal Analysis is executed to derive the natural frequencies of the stable global modes. There is an option in the program for plotting the power spectral density (PSD) of the data which is giving the opportunity to pick the stable modes for determination of mode shapes. The criteria for choosing the stable modes are a) a reasonable damping ratio (approximately less than 5%), b) real mode shapes (against the imaginary part), c) MPC factor close to 1.

7. Plotting the graphic presentation of the mode shapes.

8. We execute the forgoing steps for each setup separately and then combine the identification results of all setups in order to obtain a complete representation of the mode shapes and their corresponding frequencies.

Although it was attempted to excite the structure in one single direction, however it was practically impossible and the structure was also excited in other perpendicular directions as an undesirable side effect of the excitation. Therefore, after the combination of the results of each setup the mode shapes had a spatial distribution (instead of single-plane distribution). This was an undesirable incidence for our purpose, because we aimed to compare these mode shapes with the in-plane mode shapes obtained from the initial FE model in order to generate the updated FE model. To cope with this problem, in the next stage the system identification was implemented in one single

direction, I. e. identification for all setups were done separately in X and Y directions. These mode shapes and their corresponding frequencies are shown in Figure 4 and Table 4 respectively.

| Equivalent Mode Number | Natural Frequency (Hz) |
|---|---|
| 1 | 2.988675 |
| 2 | 19.05725 |
| 3 | 53.31688 |
| 4* | 68.1351 |
| 5 | 103.5391 |
| 6 | 165.9107 |

Table 4 – The combined identified natural frequencies in Y direction
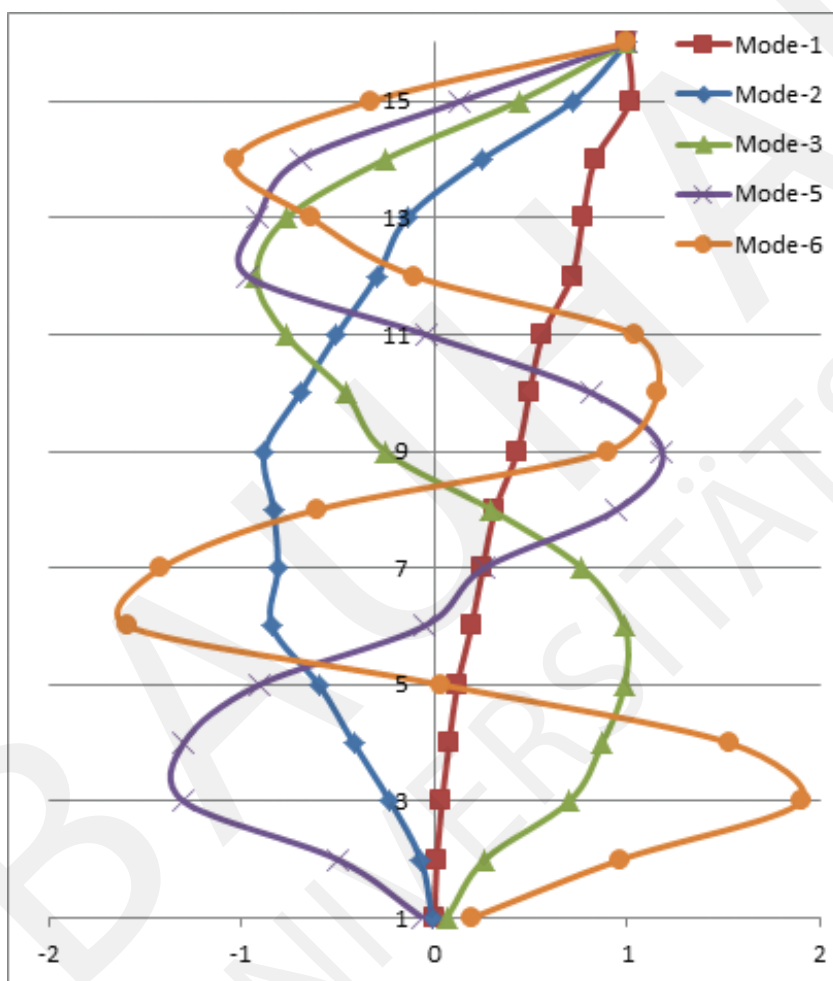


Figure 4 – The combined identified mode shapes in Y direction

*The 4th identified mode is torsional and equivalent to 7th mode of the initial model (c.f. Table 2). This is a useless unidentified torsional mode since it just has the y component of the torsional displacement.

## The measurements in the laboratory

Measurements of the response of the structure for different excitations should be accomplished. For this purpose an impulse was applied with a hammer. The force excitation in Newton and the resulting accelerations given by the sensors in m/s² have been recorded. The measurements started from above with the sensors attached to the upper 4 marks. For the next setups the non-reference sensors were respectively putted down 3 marks lower. This can be seen in the middle of Figure 5. With this approach 5 setups were measured. For every setup there were 2 tests. At the first one the excitation was applied every time on the same point coming from the same direction. At the second test the impact point and the direction was altered for every setup.



Figure 5 – 3 different setups
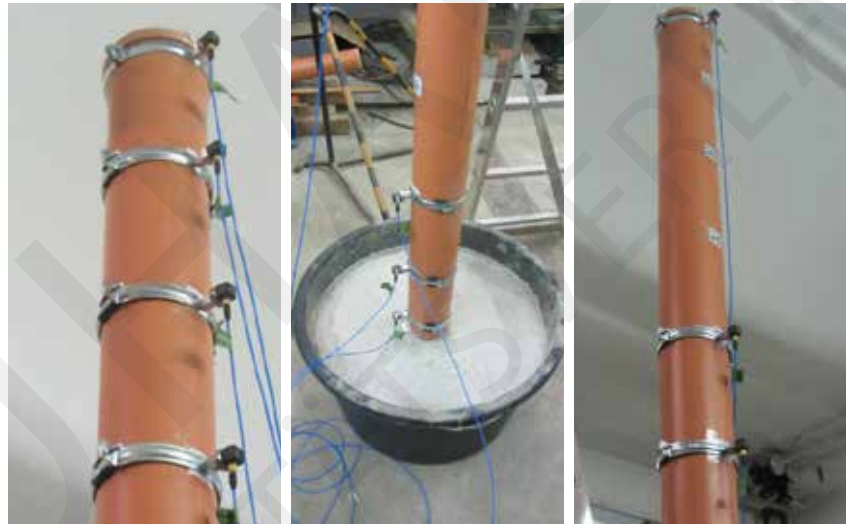


Figure 6 – Applying the excitation force

## Modal Analysis of the measured data
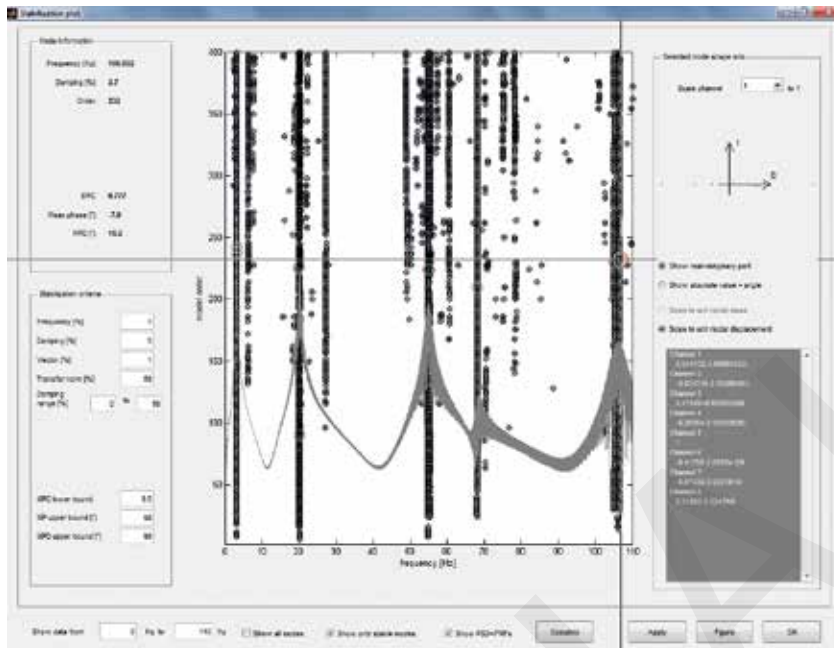


Figure 7 – Example for a modal analysis in MACEC

The measured data has been analysed in the MATLAB toolbox MACEC.

Table 5 – Measured modes of the structure

| | Mode | Frequency | Dampling | MPC | Order |
|---|---|---|---|---|---|
| Setup 1 Test 1 | 1 | 2,754 | 1,1 | 0,995 | |
| Setup 1 Test 1 | 2 | 2,822 | 1,0 | 0,990 | |
| Setup 1 Test 1 | 3 | 19,477 | 1,6 | 0,989 | |
| Setup 1 Test 1 | 4 | 19,735 | 1,8 | 0,963 | |
| Setup 1 Test 1 | 5 | 53,829 | 1,7 | 0,997 | |
| Setup 1 Test 1 | 6 | 54,240 | 1,8 | 0,979 | |
| Setup 1 Test 1 | 7 | 59240 | 0,2 | 0,990 | |
| Setup 1 Test 1 | 8 | 102,755 | 0,8 | 0,919 | |
| Setup 1 Test 1 | 9 | 104,518 | 1,9 | 0,929 | |
| Setup 1 Test 2 | 1 | 2,739 | 2,2 | 0,990 | |
| Setup 1 Test 2 | 2 | 2,829 | 1,3 | 0,710 | |
| Setup 1 Test 2 | 3 | 19,451 | 1,8 | 0,996 | |
| Setup 1 Test 2 | 4 | 19,799 | 1,7 | 0,867 | |
| Setup 1 Test 2 | 5 | 53,930 | 1,8 | 0,972 | |
| Setup 1 Test 2 | 6 | 54,274 | 1,7 | 0,955 | |
| Setup 1 Test 2 | 7 | 59,283 | 0,4 | 0,922 | |
| Setup 1 Test 2 | 8 | 104,127 | 1,3 | 0,931 | |
| Setup 1 Test 2 | 9 | 104,684 | 1,9 | 0,941 | |
| Setup 2 Test 1 | 1 | 2,912 | 0,7 | 0,995 | |
| Setup 2 Test 1 | 2 | 2,955 | 0,8 | 0,999 | |
| Setup 2 Test 1 | 3 | 18,695 | 1,5 | 0,935 | |
| Setup 2 Test 1 | 4 | 19,414 | 1,5 | 0,986 | |
| Setup 2 Test 1 | 5 | 52,314 | 2,2 | 0,969 | |
| Setup 2 Test 1 | 6 | 52,889 | 1,7 | 0,979 | |
| Setup 2 Test 1 | 7 | 60,776 | 1,7 | 1,000 | |
| Setup 2 Test 1 | 8 | 105,630 | 0,6 | 0,940 | |
| Setup 2 Test 1 | 9 | 106,350 | 2,3 | 0,990 | |
| Setup 2 Test 2 | 1 | 2,906 | 1,7 | 1,000 | 174 |
| Setup 2 Test 2 | 2 | 2,914 | 1,2 | 0,925 | 18 |
| Setup 2 Test 2 | 3 | 18,797 | 1,2 | 0,999 | 348 |
| Setup 2 Test 2 | 4 | 18,968 | 0,9 | 1,000 | 210 |
| Setup 2 Test 2 | 5 | 52,142 | 1,8 | 0,999 | 89 |
| Setup 2 Test 2 | 6 | 52,561 | 2,2 | 0,997 | 316 |
| Setup 2 Test 2 | 7 | 60,872 | 1,8 | 0,999 | 30 |
| Setup 2 Test 2 | 8 | 104,880 | 2,0 | 0,927 | 72 |
| Setup 2 Test 2 | 9 | 106,175 | 2,0 | 0,987 | 256 |
| Setup 3 Test 1 | 1 | 3,036 | 1,6 | 0,954 | 340 |
| Setup 3 Test 1 | 2 | 3,070 | 0,7 | 0,994 | 304 |
| Setup 3 Test 1 | 3 | 18,085 | 2,4 | 0,625 | 168 |
| Setup 3 Test 1 | 4 | 18,100 | 1,9 | 0,687 | 210 |
| Setup 3 Test 1 | 5 | 53,709 | 1,8 | 0,961 | 242 |
| Setup 3 Test 1 | 6 | 54,377 | 1,8 | 0,952 | 244 |
| Setup 3 Test 1 | 7 | 63,328 | 1,9 | 0,995 | 184 |
| Setup 3 Test 1 | 8 | 103,162 | 1,7 | 0,960 | 178 |
| Setup 3 Test 1 | 9 | 103,787 | 1,7 | 0,966 | 184 |
| Setup 4 Test 1 | 1 | 3,096 | 1,6 | 0,878 | 184 |
| Setup 4 Test 1 | 2 | 3,117 | 0,8 | 0,658 | 104 |
| Setup 4 Test 1 | 3 | 18,976 | 1,2 | 1,000 | 208 |
| Setup 4 Test 1 | 4 | 19,204 | 1,2 | 0,998 | 200 |
| Setup 4 Test 1 | 5 | 50,249 | 1,7 | 0,988 | 184 |
| Setup 4 Test 1 | 6 | 51,316 | 1,4 | 0,966 | 185 |
| Setup 4 Test 1 | 7 | 66,292 | 1,7 | 1,000 | 124 |
| Setup 4 Test 1 | 8 | 100,960 | 0,6 | 0,976 | 264 |
| Setup 4 Test 1 | 9 | 102,088 | 2,0 | 0,994 | 255 |
| Setup 5 Test 1 | 1 | 3,099 | 0,9 | 0,977 | 242 |
| Setup 5 Test 1 | 2 | 3,154 | 0,9 | 1,000 | 238 |
| Setup 5 Test 1 | 3 | 19,929 | 1,3 | 0,998 | 226 |
| Setup 5 Test 1 | 4 | 20,184 | 1,4 | 0,998 | 88 |
| Setup 5 Test 1 | 5 | 54,845 | 1,7 | 0,995 | 224 |
| Setup 5 Test 1 | 6 | 55,239 | 1,7 | 0,997 | 224 |
| Setup 5 Test 1 | 7 | 68,043 | 1,7 | 0,999 | 210 |
| Setup 5 Test 1 | 8 | 105,003 | 1,7 | 0,982 | 230 |
| Setup 5 Test 1 | 9 | 106,477 | 1,7 | 0,999 | 232 |

## Comparing the results

| Setup / Model | 1 Setup | | 2 Setup | | 3 Setup | |
|---|---|---|---|---|---|---|
| | | Numerical Model | | Numerical Model | | Numerical Model |
| 1 Mode | 2,74452 | 3,12870 | 2,93815 | 3,22917 | 3,06206 | 3,29065 |
| 2 Mode | 19,62089 | 20,44115 | 18,89437 | 20,32208 | 17,86350 | 19,80208 |
| 3 Mode | 54,34921 | 57,14755 | 52,49444 | 56,08412 | 54,17411 | 57,13907 |
| 4 Mode | 103,36550 | 110,51106 | 104,95570 | 111,16566 | 102,54130 | 109,52147 |
| 5 Mode | 166,54150 | 181,70540 | 165,59090 | 181,07740 | 166,10790 | 181,40378 |

| Setup / Model | 4 Setup | | 5 Setup | | Without Mass Numerical Model |
|---|---|---|---|---|---|
| | | Numerical Model | | Numerical Model | |
| 1 Mode | 3,09724 | 3,31545 | 3,10141 | 3,31984 | 3,42861 |
| 2 Mode | 18,96386 | 20,29998 | 19,94362 | 20,70743 | 21,36171 |
| 3 Mode | 50,56787 | 55,24837 | 54,99875 | 57,51187 | 59,47823 |
| 4 Mode | 101,81980 | 109,18017 | 105,01310 | 111,28019 | 115,87507 |
| 5 Mode | 165,85560 | 181,33799 | 165,45760 | 181,46731 | 190,48165 |

Table 6 – Measured and calculated eigenfrequencies

The experimental results and the numerical calculated ones have been compared. In Table 6 can be seen the results for the eigenfrequencies of the first 5 modes.

In the following diagrams (Figure 8 to Figure 12) comparisons of the measured and the numerical calculated mode-shapes for one setup are visualized.
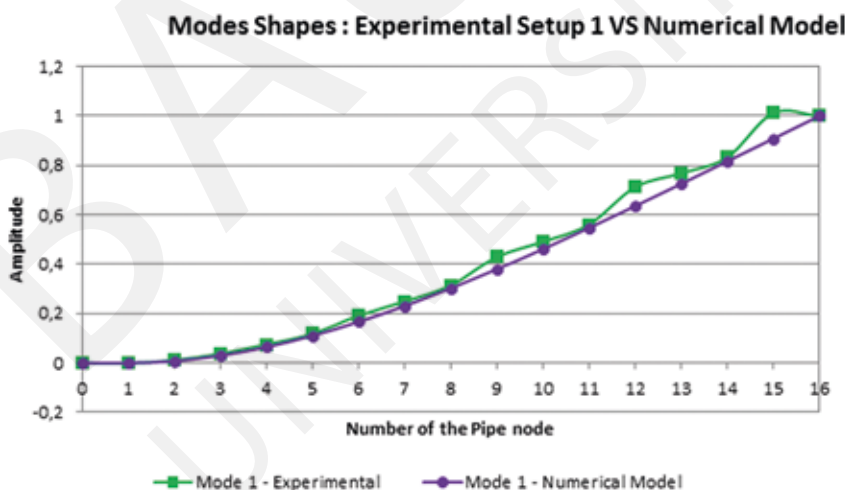


Figure 8 – Comparison of Mode 1

**Modes Shapes : Experimental Setup 1 VS Numerical Model**

**Modes Shapes : Experimental Setup 1 VS Numerical Model**

**Modes Shapes : Experimental Setup 1 VS Numerical Model**
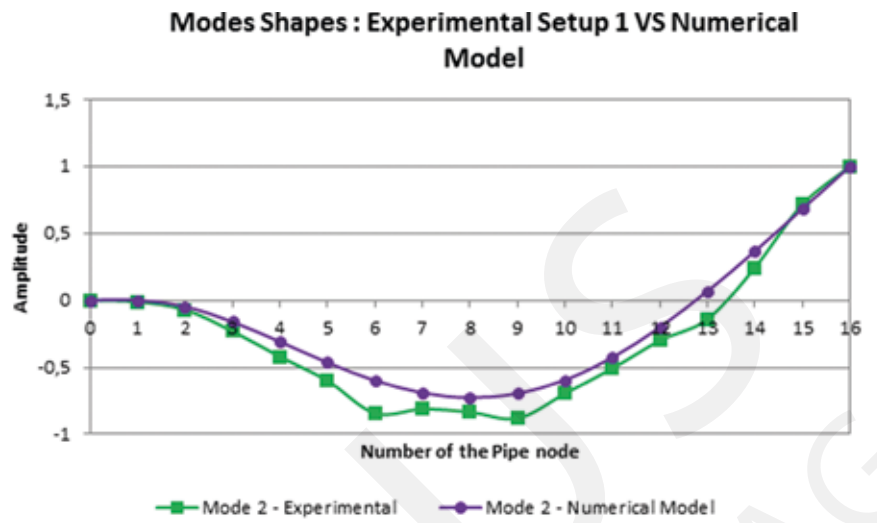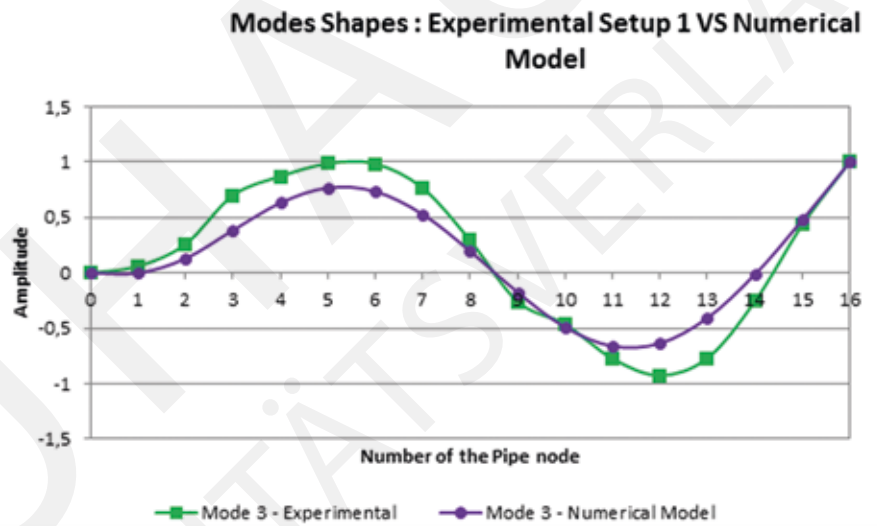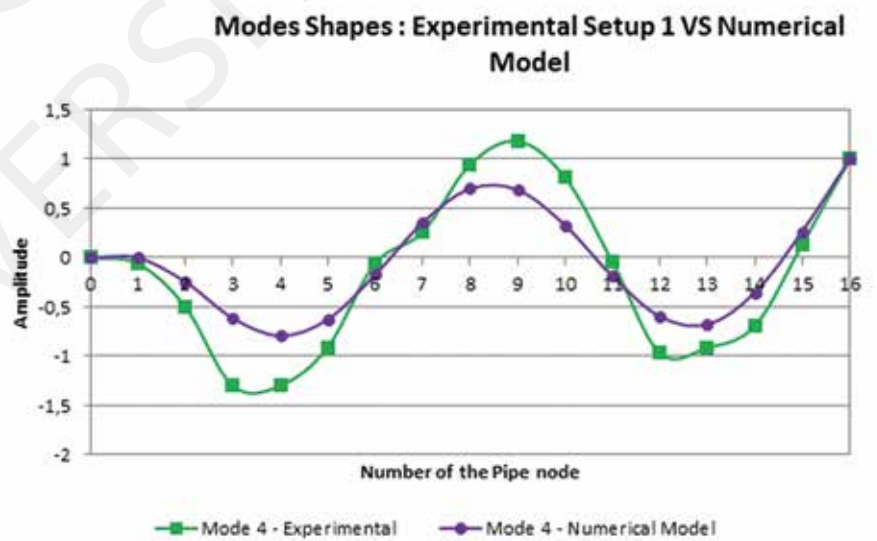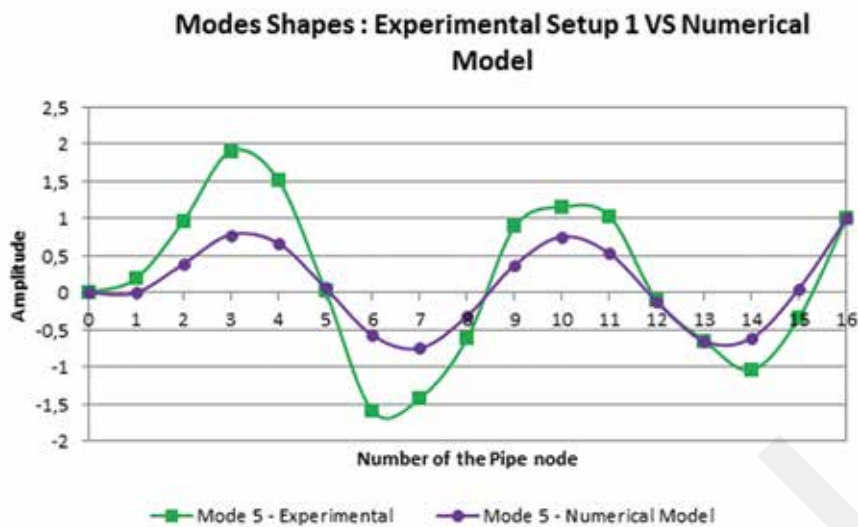
Figure 12 – Comparison of Mode 5

It was expected that the differences between simulation and reality would be reduced by the optimisation of the numerical model.

## The effect of the accelerometer mass

By attaching the accelerometers onto the tower their additional inertia took effect. As a result the measurements have been corrupted. This hasn't been considered in the first FEA models, so the results of the numerical calculations differed from the measured ones. In Figure 13 results of the numerical simulation is seen as line "Mode 1 – Without Mass". The other lines show measured results from the different setups 1 to 5. For every setup it can be seen that the calculated amplitudes of the mode shapes are higher than the measured ones, what can be explained by the additional inertia. It can also be seen that the effect appears mostly at the top of the pipe which is node 16. There also the amplitude of the mode shape is the highest.

In setup one the sensors were placed in the nodes 13-16, so at the top of the pipe. The corresponding mode shape has the highest difference between measured and simulated trend. Above all the amplitude at node 16 is the lowest.

In the higher modes (2-5) which are pictured in Figure 14 to Figure 17 it can also be asserted, that the additional sensor mass has the highest effect on the mode shapes at the places were the sensors are attached.

Figure 13 – Modeshapes of Mode 1
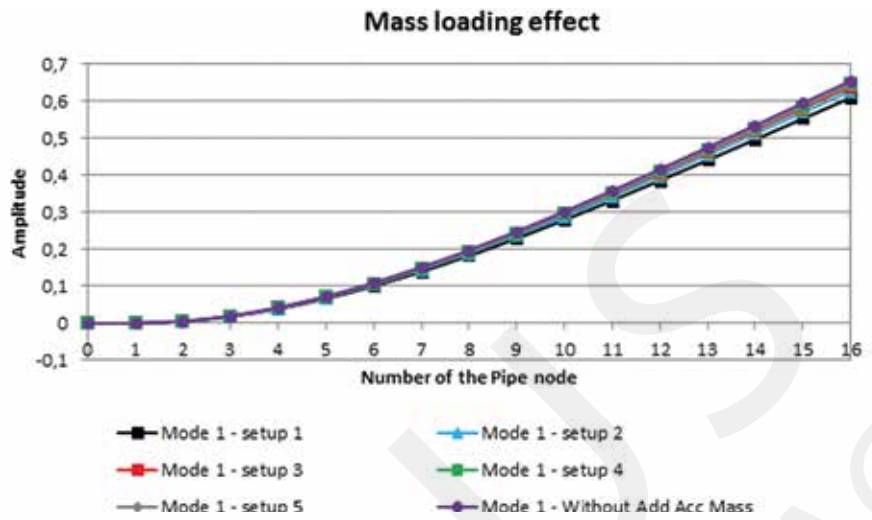


Figure 14 – Modeshapes of Mode 2
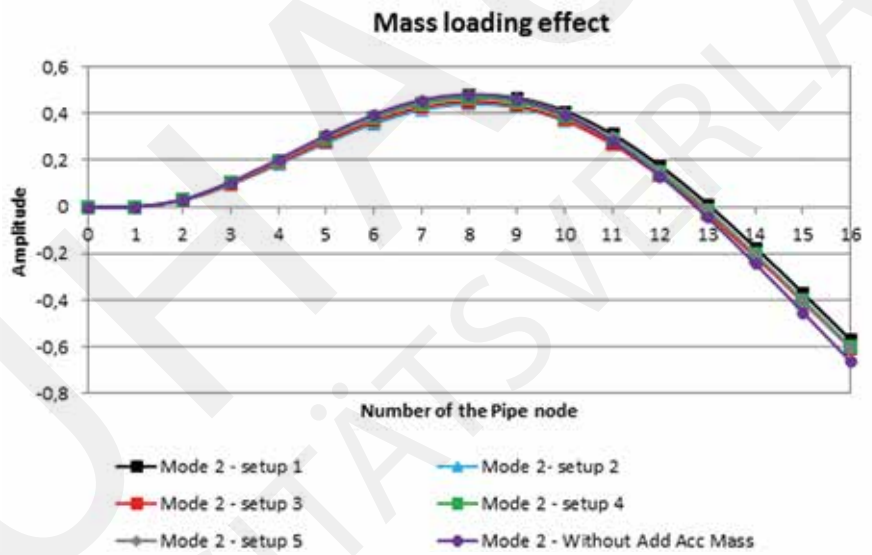


Figure 15 – Modeshapes of Mode 3
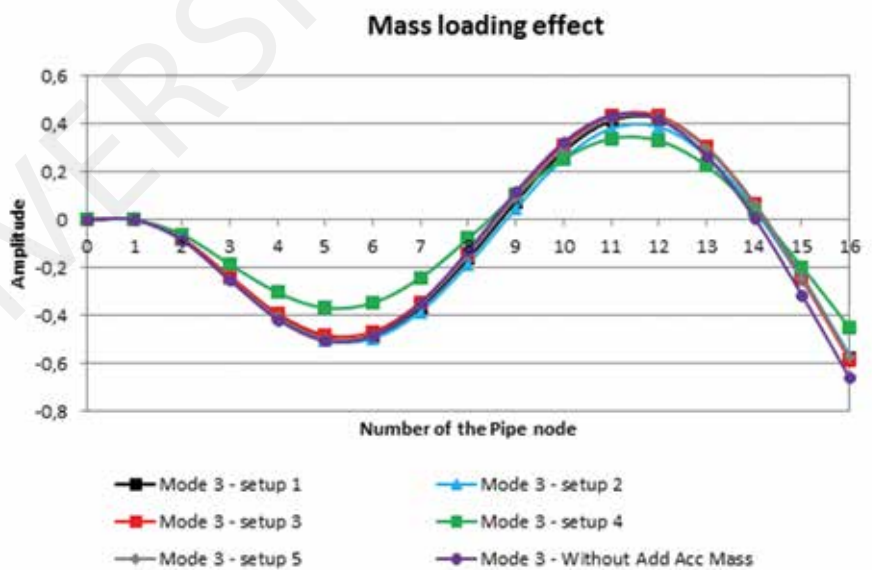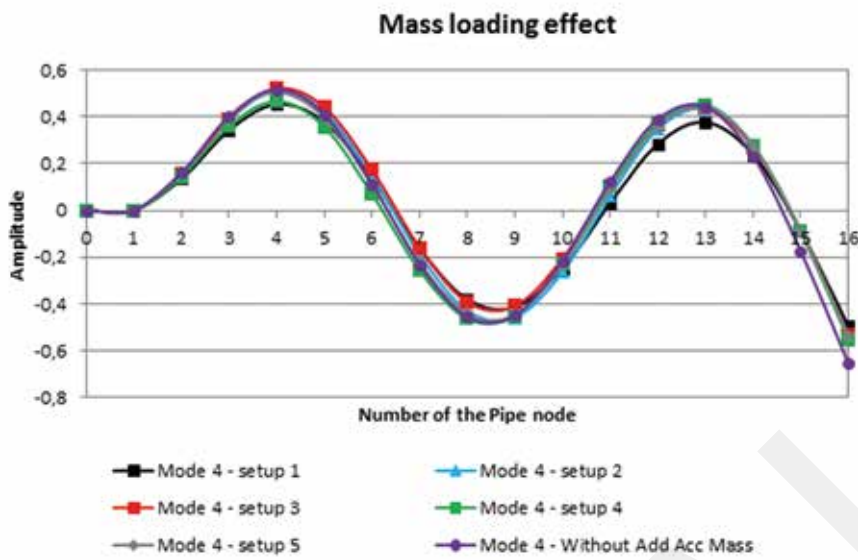
Figure 16 – Modeshapes of Mode 4
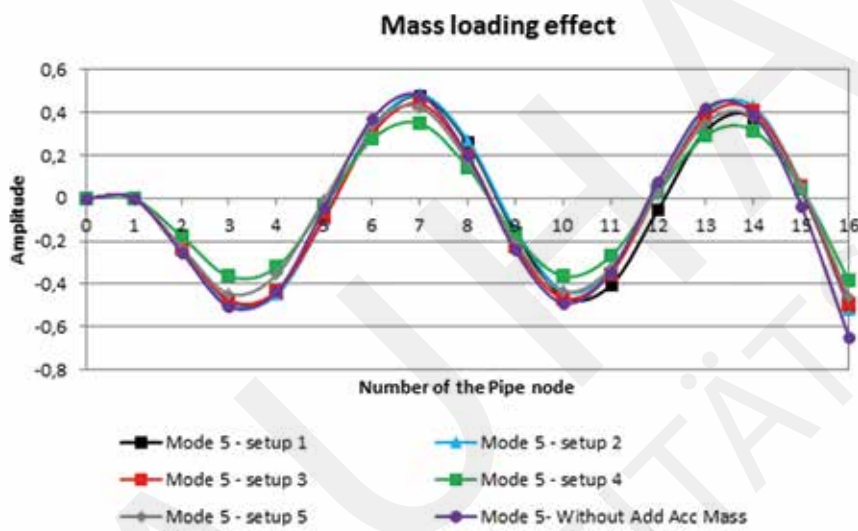


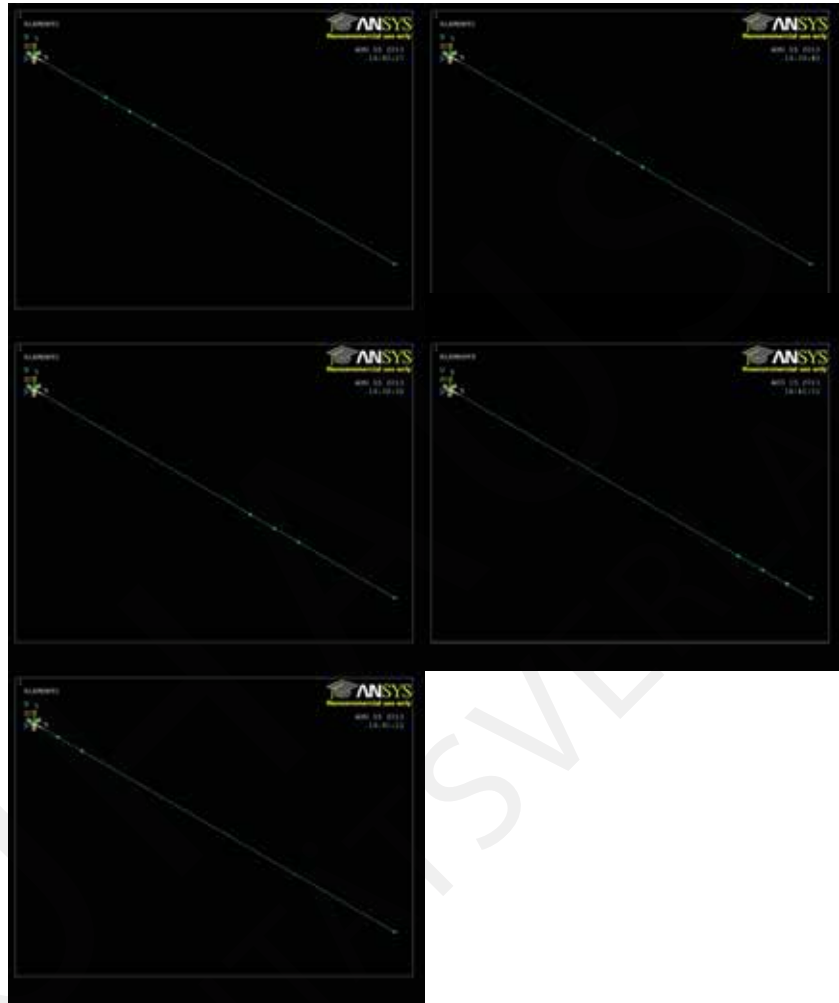Figure 17 – Modeshapes of Mode 5

## Optimisation of the FEA Model

To take care of the accelerometers masses in the simulation, additional point masses has been added to the FEA model as seen in Figure 18. A separate model for each setup has been created.

## Model updating – Optimisation

Following the experimental procedure described in the previous section. Suitable model updating was performed in order to resemble as best as possible the experimental conditions. Extracted results of the updated models used in both software packages were then compared and the respective objective functions were setup in order to proceed with the optimisation process.

## General considerations

Preliminary analysis of all finite element models entailed several assumptions regarding both material and mechanical properties of the structure. With regard to the material properties the following uncertainties need to be considered:

- Mass density (ρ) and stiffness. In terms of Young's modulus of elasticity (E) are both derived from the information sheet provided by the manufacturer.
- The added mass of the accelerometers and the installation rings and magnets is comparable to the reduced scale model of the pipe and may induce significant alterations to the total mass matrix that need to be accounted for. by adding point masses to the respective nodes.
- As a result of the previous consideration, the assumption of the evenly distributed mass may no longer be applicable and the effect of the added mass to the flexibility of the model must be investigated through successive analyses.
- Given that the model under consideration is composed by linear elements and the mass is assigned to the centroid of the pipe, allowance should be also made for the eccentricity of the installed sensors by inserting some rotational inertia. However, this factor is neglected for the sake of simplicity. since only translational uncoupled modes are considered.

With regard to mechanical properties and boundary conditions. the following considerations need to be made:

- Observed model imperfections. Which mainly involve deflections from the vertical axis. Were deemed negligible.
- The base was considered fully fixed in the initial model. Whereas the concrete block formulated to support the cantilever may allow for some base flexibility.
- The section widening near the top that is comprehensively described in the information sheet is considered too small to have a significant effect to the behaviour of the structure.

## Updating of the SLang Model

The assumptions mentioned above where applied to the two models created with SLang and ANSYS. In order to obtain an overview of the effect of these factors. The modal frequencies of successive analyses were compared. Starting from the first configuration of sensors. The added masses were placed at the three successive points below the top. Maintaining the same 0.20 m discretisation as in the initial model and the experiment. The masses were then moved as a group to the next points of interest corresponding to the sensor setups as described in the previous section. The results of the analyses are given in.

Table 7 – The influence
of the added mass on the
natural frequencies

| Setup | 1 | 2 | 3 | 4 | 5 |
|-------|---|---|---|---|---|
| Mode Nr | | | | | |
| 1 | 2.90160 | 3.06790 | 3.17540 | 3.21990 | 3.22780 |
| 2 | 19.94000 | 19.55600 | 18.69900 | 19.58600 | 20.32400 |
| 3 | 56.02200 | 54.40600 | 55.93800 | 52.80700 | 56.77800 |
| 4 | 108.56000 | 109.74000 | 107.40000 | 106.90000 | 110.23000 |
| 5 | 180.70000 | 179.38000 | 179.60000 | 179.24000 | 180.36000 |

It is obvious from the results presented above that the influence of the added masses to the frequencies is considerable. As a result. These models will be used for the optimisation process. A frequency matrix in the was formulated within SLang and the objective function was applied to both the above matrix and the one derived from the measured frequencies. In order to account for alterations in material properties two parameters were selected for the optimisation. Namely the mass density and the stiffness as expressed by the modulus of elasticity. The frequencies used for the optimisation were derived from each setup separately, while a combination of all setups was considered for the mode shapes. The optimisation follows a simple objective function described as follows:

$$f(\rho,E) = \sqrt{\sum_{m=1}^{5}\sum_{i=1}^{n}\left(\frac{f_{meas,i} - f_{num,i}}{f_{meas,i}}\right)^2} + \sqrt{\sum_{j=1}^{n}\sum_{k=1}^{n}\left(\phi_{meas,jk} - \phi_{num,jk}\right)^2}$$

The application of the optimisation code developed in MATLAB returned the optimum values for the considered parameters that will be used for the final simulation. The convergence of both parameter values and the objective value are given in the following diagrams.
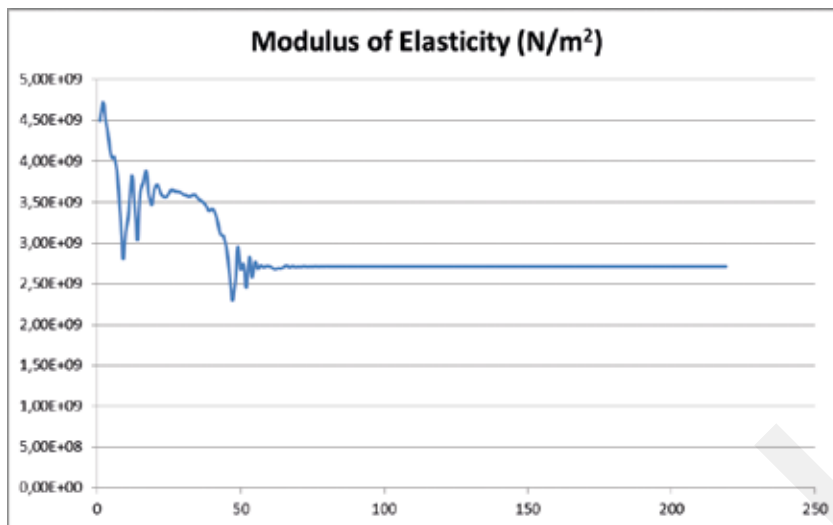
Figure 19 – Updating Modulus of Elasticity
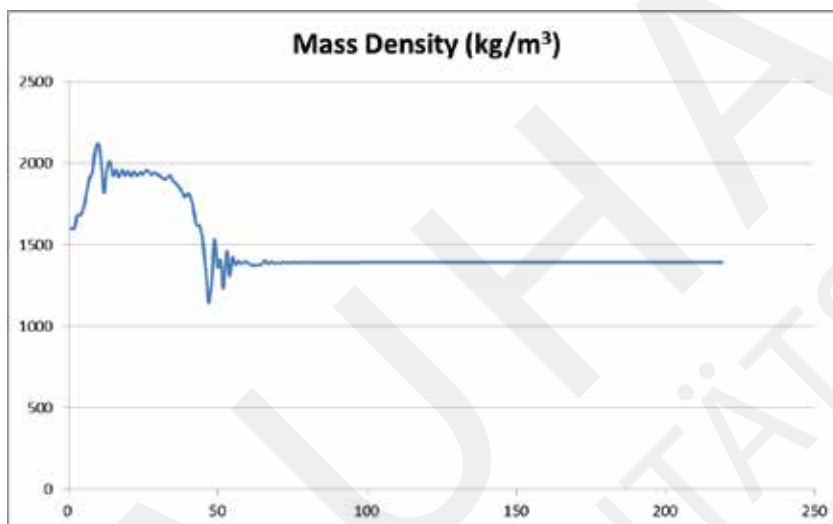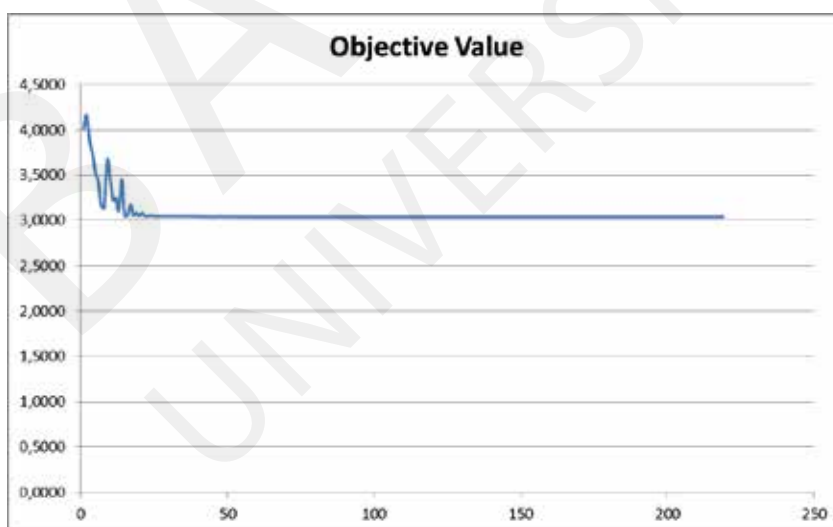


Figure 20 – Updating mass density



Figure 21 – The value of the considered objective function which used to update the mass density and Modulus of Elasticity

The acceleration time history results were obtained after applying the impulse load of the first setup at the top node of the model. Three different cases were considered corresponding to the initial model updated with the sensors' masses, the optimized model and the experimental records. The comparison of all three models shows that the response histories of all three models are quite similar. Moreover, the results of the frequencies of the optimized model and the experimental results show a small discrepancy between numerical and measured values.

Figure 22 – A comparison of the acceleration time history from the updated model and the measurement
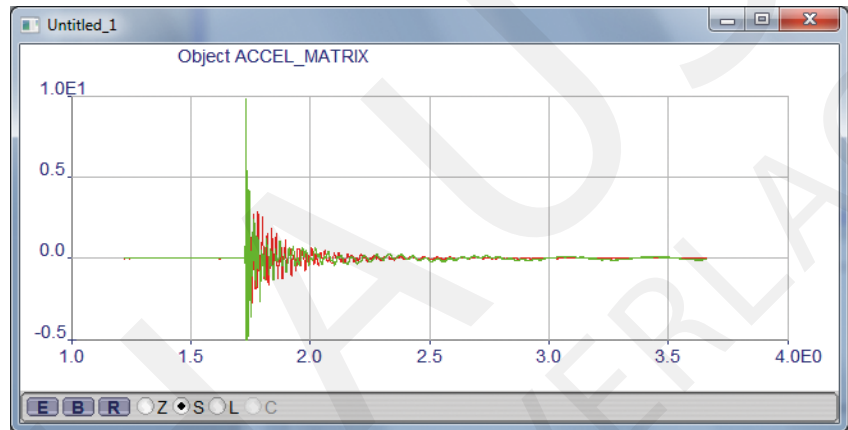


Table 8 – The A comparison of the natural frequencies of the studied structure before and after model updating with the measurement frequencies

| Setup Model | 1 Setup | | | 2 Setup | | | 3 Setup | | |
| --- | --- | --- | --- | --- | --- | --- | --- | --- | --- |
| | | Numerical Model | Optimised Model | | Numerical Model | Optimised Model | | Numerical Model | Optimised Model |
| 1 Mode | 2,74452 | 2,90160 | 2,76590 | 2,93815 | 3,06790 | 2,92520 | 30,06206 | 3,17540 | 3,02820 |
| 2 Mode | 19,62089 | 19,94000 | 19,01800 | 18,89437 | 19,55600 | 18,640800 | 17,86350 | 1869900 | 17,82700 |
| 3 Mode | 54,34921 | 56,02200 | 53,43000 | 52,49444 | 54,40600 | 51,88300 | 54,17411 | 55,93800 | 53,34900 |
| 4 Mode | 108,36550 | 108,56000 | 103,53000 | 104,95570 | 109,74000 | 104,66000 | 102,54130 | 107,4000 | 102,43000 |
| 5 Mode | 166,54150 | 180,70000 | 172,35000 | 165,59090 | 179,38000 | 171,08000 | 166,10790 | 179,60000 | 171,29000 |

| Setup Model | 4 Setup | | | 5 Setup | | |
| --- | --- | --- | --- | --- | --- | --- |
| | | Numerical Model | Optimised Model | | Numerical Model | Optimised Model |
| 1 Mode | 3,09724 | 3,21990 | 3,07100 | 3,10141 | 3,2278 | 3,0785 |
| 2 Mode | 18,96386 | 19,58600 | 18,67700 | 19,94362 | 20,324 | 19,386 |
| 3 Mode | 50,56787 | 52,80700 | 50,34900 | 54,99875 | 56,778 | 54,156 |
| 4 Mode | 101,81980 | 106,90000 | 101,95000 | 105,01310 | 110,23 | 105,13 |
| 5 Mode | 165,85560 | 179,74000 | 170,94000 | 165,45760 | 180,36 | 172,01 |

The generally non-linear cost-fuctions, as defined in the project as the sumed squared differences between meausrements and model responses, need to be minimized in an efficient manner. The students working in group V established an algorithmical framework providing tools for this optimization task. Before these tools have been applied to the optimization tasks of other groups during the summer academy, the methods have been intensively tested on academic examples, see e.g. [BAUHAUS SUMMER SCHOOL ,,MODEL VALIDATION AND SIMULATION, 2012 - Project 5, Report, pages 319 - 323)]

Two main classes of optimizers have been developed and tested, the optimal choice of them is mainly depending on the differentiability of the cost-function:

## Gradient and Newton Methods

Classical approaches in the field of nonlinear optimization are Gradient-based and Newton-type methods. These methods are motivated by studying necessary and sufficient conditions of optimality. These class of optimizers are generally supported by mathematical analysis concerning convergence and convergence rates. In this course gradient methods with line-search strategies and a so-called quasi-Newton method, where the Hessian matrix is approximated by a rank two update according to the BFGS approach are tested The latter approach allows to approximate Hessians and to use Newton directions in the optimizer instead of gradient directs, which depending on the topology of the optimizing problem may tend to zig-zagging leading to slow convergence.

## Direct Search Methods

As it is not always possible to calculate gradients in a satisfying manner, mainly due to missing differentiability of the cost functional, direct search methods are valuable tools. A very effective and well-proven method is the algorithm according to Nelder-Mead, which bases on simplex. A simplex is the connection of (n+1) points in the parameter space, where n is the number of parameters which need to be identified. Now, the strategy is to replace always the vertice which has the largest value in the cost function. The replacement is done by reflecting this point to the centroid of all other points. A series of expansion and contraction approximates a kind of line search. After finding a new point, the vertices are sorted again and the vertice with the worst cost function value is again replaced. Being close to an optimum, the simplices start to shrink.

## Conclusions

Within this project the dynamic behaviour of a cantilever structure with circular cross section was studied. The system was modelled numerically using different discretisations. Furthermore modal tests were performed at a physical model. The test results made mass loading effects of the used sensors and elements used to attach the sensors to the structure obvious. Since the different mass distributions have an effect on the dynamic structural behaviour it was decided to consider the systems resulting from different setups separately.

The results of the model updating process by means of a numerical optimization showed a relatively good agreement with the experimental results. It can be concluded that the decision to consider the different systems separately but within one optimization lead to a reduction of uncertainties which, in turn, contributed to an increase of the quality of the results.

ABADIAS, David
Polytechnic University of
Catalonia, Spain

BRANDIS, Denis
University Josip Juraj
Strossmayer, Crotia

DEHGHANIAN, Kaveh
Middle East Technical
University Ankara, Iran

DONAT, Daniel
Freie Universität Berlin,
Germany

EKR, Jan
Brno University of Technology,
Czech Republic

GOLDBERG, Paul
New Jersey Institute of
Technology, USA

KONTOZOGLOU, Evangelos
A.U.T.H., Greece

STUTZ, Henning
GRK 1462,
Bauhaus-Universität Weimar

BILAL, Mustafa
Bauhaus-Universität Weimar

# Project 2 – Bridge Soil-Structure-Interaction under Cyclic Loading: Simulation and Experimental Validation

## Abstract

The aim of this study is to simulate the static and cyclic behavior of a dry Hostun sand by the introduction of the model capable to incorporate SSI and compare the experimental results with those of a numerical analysis. A robust macroelement model is used to realize the SSI by the inclusion of the plastic soil behavior. The experimental result is validated with the existing finite element software and the macroelement model consisting of the nonlinear soil behavior coupled with the structural element.

## Introduction

This project anticipated the recreation of the Bender Elements test of a prescribed specimen of Hostun Sand in a controlled test environment here at the Bauhaus University. In general it should be noted that sand has a particle range in diameter from 0.0625 mm to 2 mm, however Hostun sand in particular has a particle range from 0.08 mm to 0.8 m placing it in a range between very fine and coarse particles.

## Experimental procedure

In accordance with the test procedure, an empty wooden box 98.13 cm in length by 47.83 cm in width was filled to a height of 38.73 cm with dry Hostun sand, the soil specimen type chosen for this experiment. The filling process was done in several steps and afterwards, compaction was done for each layer. Once filled the wooden box was referred to as the Test Sample. This Test Sample consumed 266.666,7 gm of sand giving the Test Sample a volume of 181.781.497.5 cm3 and a density of 1.467 gm/cm$^3$ with a specific gravity of solids of 2.65 g/cm$^3$.

The filling process was completed over the course of 2 days and was carried out with laboratory precision. Sample sand was provided by the Bauhaus University Weimar. This sand was measured and then meticulously transported near and placed into the test sample. Once the desired height was achieved, dictated by the present parameters of the test chamber, the test procedure was able to commence.

The test procedure involved a pair of ceramic piezoelectric transducers set 32.17 cm each from the edge of the long length of the test chamber. Within test chamber six Bender elements were planted, three elements on each side. Further, in the center of the test chamber was located the cyclic compression apparatus. This apparatus consisted of a steel plate, a ball barring and a compression shaft capable of inducing a static or cyclic load. This apparatus was further connected to control and data acquisition system.
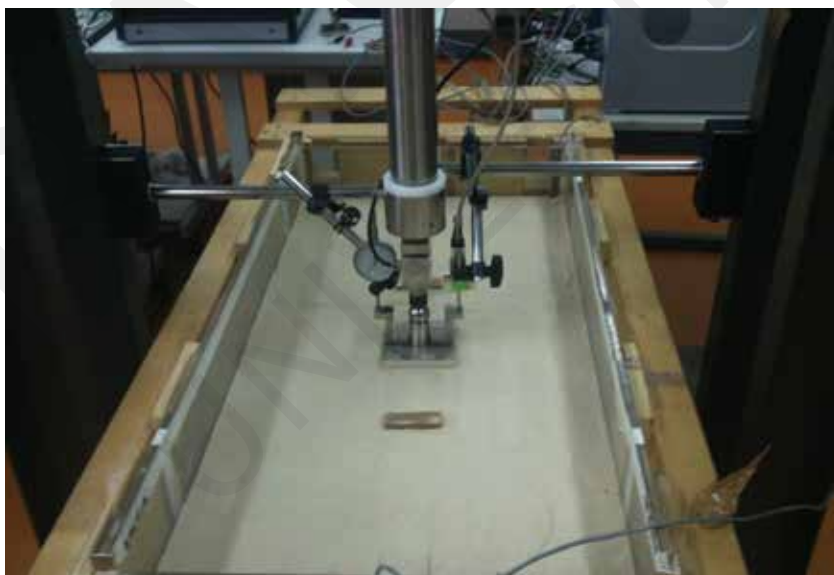
WUTTKE, Frank
Bauhaus-Universität Weimar

KAFLE, Binod
Bauhaus-Universität Weimar

MUYIWA, Alalade,
Bauhaus-Universität Weimar

NEPAL, Bisheswor
Bauhaus-Universität Weimar

ZABEL, Volkmar
Bauhaus-Universität Weimar

Figure 1 – Plate and gauges to monitor the vertical displacements
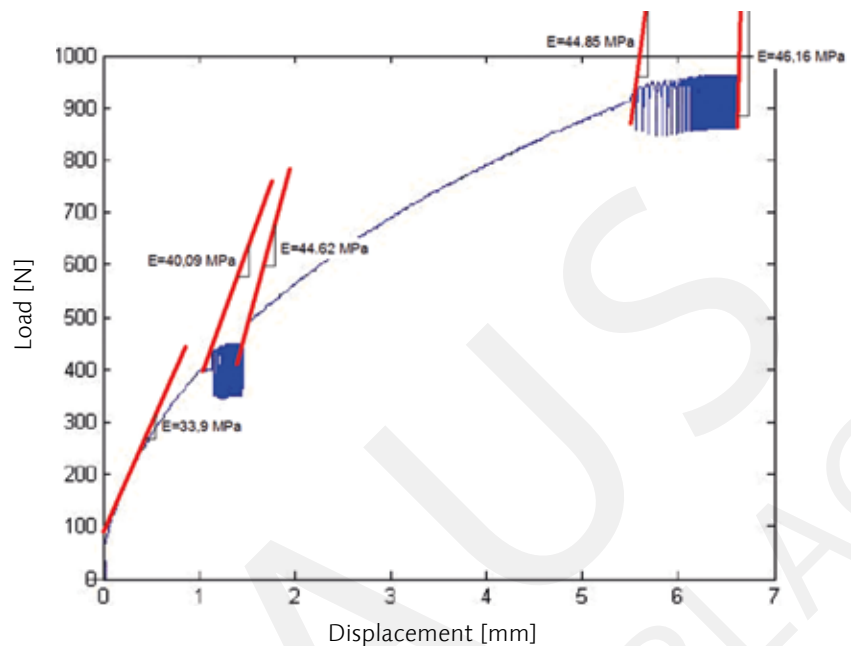
In this experiment, the Bender Element test method is being used to measure the shear wave velocity of laboratory soil specimen as: In this equation L is the distance between the transducer and t is the travel time of the shear wave, $\rho$ is the density and $G_{max}$ is the shear modulus. This particular Bender Elements test consisted of two steps with a consistent depression motion of 0.0015 mm/s.

In the first step of this test a 400 N compression load was applied to the test specimen and then cyclic load was employed at a frequency of 0.1Hz. Afterwards travel time between transducers were calculated and stored. In the second step, the load was increased up to 900 N, then load cycles of 100 N were applied to the specimen and shear wave velocity was calculated again for a predetermined duration. Apparatus were in place to insure the accuracy of the recorded data.

In the chart above it can be observed that during the first step the 400 N force displaced the soil specimen for a total of about 0.3 mm from an approximate initial displacement of 1.1 mm to a new approximate displacement of 1.4 mm employed at a frequency of 0.1Hz for aprox 25 cycles.

During the second step the 900 N force displaced the soil specimen for a total of about 1.5 mm from an initial displacement of 5.2 mm to a new approximate displacement of 6.7mm employed at a frequency of 0.1Hz for 104 cycles.  At a Total duration of the compression test procedure was approximately 182 minutes.

## Measurement of shear stiffness

The Bender Element Test allows measuring the shear wave velocity $V_s$ in soils, and consequently to determine the initial shear modulus ($G_{max}$) of a soil sample, thereby defining the stiffness of the soil. The $G_{max}$ is a key parameter in small strain dynamic analyses, such as those, which predict the soil behavior or the Soil-Structure-Interaction (SSI) during earthquakes. The shear modulus can be calculated by using the theory of wave propagation in an elastic body, from which we obtain the fundamental formula, which correlates the density $\rho$ and the shear wave velocity Vs to the aforementioned fundamental shear modulus (equation 2)

It has become conspicuous that the shear modulus heavily depends on the density and the shear wave velocity; the density due to the compaction incurred by the vertical load, changes during the experiment, which affects the magnitude of the shear modulus. Thus, before and after every cyclic loading the shear modulus was calculated to account for the fact that the volume underneath the footing was decreasing, thereby modifying the density. An idealized volume of soil extending for a distance of 1.5B, in which B is the dimension of the footing, was used to calculate the initial mass of the soil; the mass should remain constant during the experiment, so the calculation of the modified density is a rather straightforward procedure. The initial characteristics of the volume of interest are

$$\rho_0 = 1.467 \text{ kg/m}^3$$
$$V_0 = 8600 \text{ cm}^3$$
$$m_0 = 12733_H$$

It should be noted that the initial volume was extending just underneath the footing, but the final one extends 5 cm to both sides of the footing, something that was deemed desirable because the aforementioned volume was too small and the induced settlements increased tremendously the soil density. The settlements were taken from the force-displacement diagram. The results for every phase, which is defined just before and after every cyclic loading, are presented in the next table

Table 1 – Modified density for the soil sample during loading

| Heigth $H_i$ [cm] | Volume $V_i$ [cm³] | Modified Density $\rho_i$ [g/cm³] |
|---|---|---|
| 21.58 | 8632 | 1.475 |
| 21.53 | 19.05725 | 1.479 |
| 21.14 | 53.31688 | 1.506 |
| 21.03 | 68.1351 | 1.514 |

## Constitutive modeling

The Finite Element (FE) program PLAXIS v.12 was used to simulate and validate the behavior of the Hostun sand under cyclic loading.
One of the advantages of PLAXIS is that it encompasses many constitutive models to simulate the behavior of soils and rocks under static and cyclic loads. In this research there were 3 different models: the Mohr-Coulomb failure criterion, the hardening model, as well as a hypoplastic-sands model.
Information about these models was taken mainly from the material models manual accompanying the program.

### Mohr-Coulomb model

The Mohr-Coulomb is a linearly elastic-perfectly plastic criterion in which the accumulated strains are expressed as sum of an elastic part, as well as a plastic part, so as to say

$$\underline{\varepsilon} = \underline{\varepsilon}^e + \underline{\varepsilon}^p \quad (1)$$

The plastic strain rates according to the classical theory of plasticity can be represented as vectors which are perpendicular to the yield surface, something that has been proven to overestimate the dilatancy $\rho$. Using Hooke's law the stresses rates can be determined from the next equation. In the Mohr-Coulomb criterion the shear stresses are correlated with the cohesion and the normal effective stresses using the following equation

$$\tau = c + \sigma'_n \tan\phi' \quad (2)$$

In PLAXIS the user is required to define the Young's modulus E, the Poisson's ratio v, the cohesion c, and the friction angle $\rho$.

Figure 3 – Mohr-Coulomb failure criterion
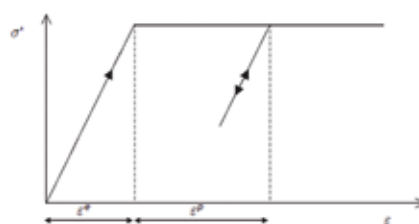


Figure 3.1  Basic idea of an elastic perfectly plastic model

## Hardening soil model

The Hardening soil model is used to simulate the behavior of both soft and stiff soils. Contrary to the Mohr-Coulomb criterion the yield surface is not fixed, and can harden under plastic strains. This model encompasses both shear and compressive hardening. The parameters PLAXIS requires the user to define are those of the failure, namely the effective cohesion c', effective angle $\varphi'$, and angle of dilatancy; the user must also define the parameters affecting the soil stiffness and cap, namely various values for the Young's modulus to consider its dependence on strain such as the $E_{SO}^{TOF}$, which is the secant stiffness in a standard drained triaxial test and the $E_{SO}^{TOF}$, which is the tangent stiffness for the primary oedometer loading.

## Hypoplastic soil model

The term Hypoplastic was first used by Dafalias in the context of incrementally nonlinear hardening plasticity so Hypoplastic models are special examples of incrementally non-linear models.
The following graph shows limiting void ratios for granular material (Gudehus, 1996).

In the mentioned graph, the term $e_i$ is the maximum void ratio (isotropic normal compression), $e_c$ is critical state void ratio (CSL) and $e_d$ is minimal void ratio at state of maximum density.

$$\frac{e_i}{e_{i0}} = \frac{e_c}{e_{c0}} = \frac{e_d}{e_{d0}} = \exp\left[ -\left( \frac{-tro}{h_s} \right)^n \right] \quad (3)$$

$h_s$, n, $e_{io}$, $e_{co}$ and $e_{do}$ are modal parameters (Bauer, 1996)
In fact, in any proportional compression (constant direction of strain rate), a normal compression line (NCL) is followed after reaching normally consolidated state. epo controls position of the given NCL with $e_{c0} < e_{p0} < e_{i0}$.

$$e_p = e_{p0} \exp\left[ \left( \frac{-3p}{h_s} \right)^n \right] \quad (4)$$
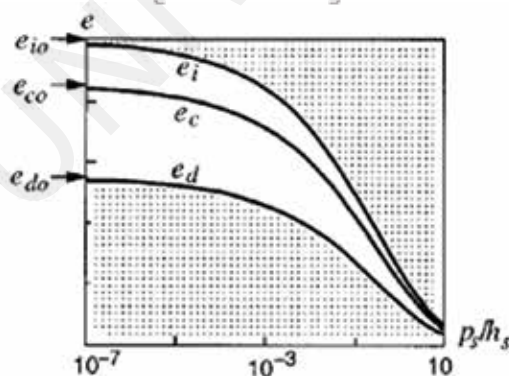


Table 4 – Limiting void ratios for granular materials (after Tejchman and Gorski 2008)
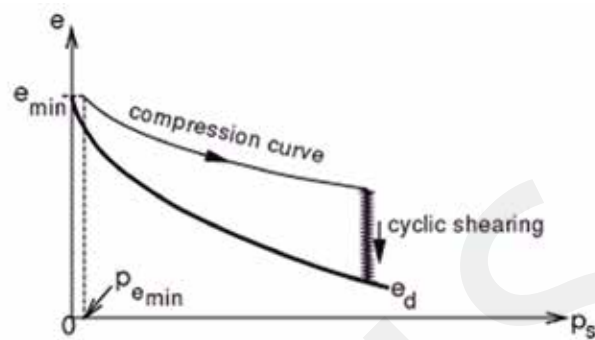
Any proportional compression test can thus be used for the determination of $h_s$ and n. It is not reccomended to calibrate $h_s$ and n by direct regression, but rather adopt the physical meaning of the parameters.

The parameter $e_{co}$ defines the position of the critical state line in the ln p vs. e space.

$$e_c = e_{c0} \exp\left[ \left( \frac{-3p}{h_s} \right)^n \right] \qquad (5)$$

$e_{io}$ can only be measured by the experiment done in low gravity situation. Parameter $e_{do}$ controls position of the minimum void ratio line. The best densification can be obtained by means of cyclic shearing with small amplitude at constant pressure.

$e_{do}$ can then be obtained by extrapolation using $h_s$ and n evaluated from oedometric experiments results.

## Macroelement modeling

Many variations can be found in nature of the cyclic loading (seismic actions, wind stroms, under currents and so on) which may affect civil engineering structures (chimmeny, towers, off-shore structures, etc). In such conditions, in the dynamic response of these structures, a crucial role is played by the mechanical response of the foundation-soil systems which is stressed by incline and eccentric cyclic loads. For these reason the Eurocode EC8 prescribes, the analysis of the non-linear mechanical behavior of the soil to calculate irreversible displacements due to seismic actions.

This can be done in various ways. For instance, an structure can be meshed with Finite Elements in order to analyze the whole dynamic problem. An alternative way consists of lumping the soil compliance in few discrete springs and dashpots that constrain the movement of the foundation. The later method is clearly much more economical, but has important limitations. The linear

behavior of the spring and dash pots implies the uncoupling of the effects of the external actions of the foundation displacement.
The concept of the macroelement shows that it is possible to overcome this difficulty by abandoning the conceptual framework of elasticity of springs. The system of spring will be therefore substituted by a macroelement Nova and Montrasio (1991) connecting generalized stresses (force and overturning moment acting on the foundation) and the corresponding (in the work equation) generalized strains (displacement and rotations).

The mathematical model

A short description of the mathematical model will be now given. See Nova and Montrasio (1991a) for a detailed presentation.
The model was formulated on the basics of two basics hypotheses.

a.) The foundation and the soil can be considered as a macro-element for which the loadings act as generalized stress variables while the displacements and rotations of the foundation (only rigid strip foundations were consi dered) are the corresponding generalized strain variables
b.) The constitutive law of the macro element i.e. the re-lationship between generalized stress and strain rates, is rigid-plastic strain-hardening with a non-associative flow

rule.

Formally this can be expressed as
dq = CdQ
Where Q is the vector of the generalized non-dimensional stress variables, defined as

$$Q = \begin{Bmatrix} \xi \\ \lambda \\ m \end{Bmatrix} = \frac{1}{V_M} \begin{Bmatrix} V \\ H/\mu \\ M/\psi B \end{Bmatrix} \quad (6)$$

And q is the vector of the generalized strain variables

$$q = \begin{Bmatrix} \eta \\ \varepsilon \\ \varsigma \end{Bmatrix} = - \begin{Bmatrix} \nu \\ \mu u \\ \psi B \Theta \end{Bmatrix} \quad (7)$$

## Numerical modeling with PLAXIS

PLAXIS is a finite element computer program used to perform deformation and stability analysis in geotechnical engineering. Actual geotechnical structures and phenomena can be modeled in plane strain or axisymmetric model. Produced mesh elements
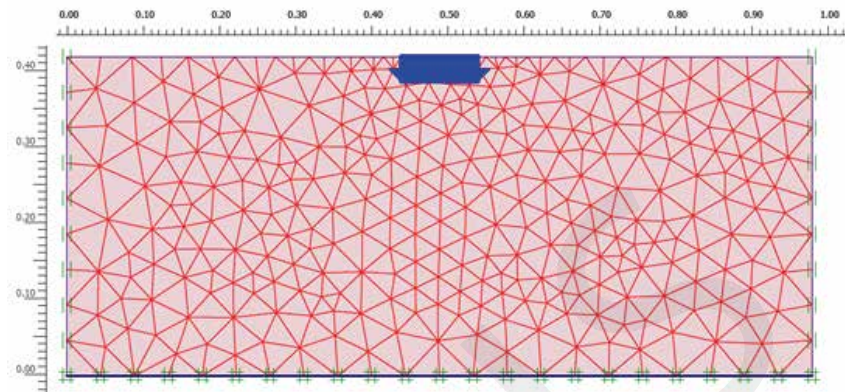
are always triangular elements which can be 6-node or 15- node. PLAXIS has the ability to model several constitutive models such as Mohr-Coulomb, Hardening soil model, jointed rock model, Soft Soil creep model and soft soil model for the simulation of the nonlinear, time dependent and anisotropic behavior of soil/rock.

## Simulation

The process steps in PLAXIS are the following. First, a model should be defined. Geometry, material properties and structural elements should be specified. Then boundary conditions and load should be applied to the model. In the next step mesh is being generated. In this project, we used plane strain model with 15-noded triangular elements. A 10×10 cm rigid plate supposing as a shallow foundation was modeled on the soil. The properties of Hostun sand which was used in laboratory is demonstrated in Table 2.

Analyses were performed   using a Mohr-Coulomb model, a hardening soil model as well as  hypoplastic model. After several iterations the results obtained were compared with the experimental results.

Table 2 – Hostun sand properties used in simulation

| | |
|---|---|
| Initial void ratio | 0.76 |
| Dry density | 1.47  g/cm$^3$ |
| Particle density | 2.65  g/cm$^3$ |
| Friction angle | 42 $^0$ |
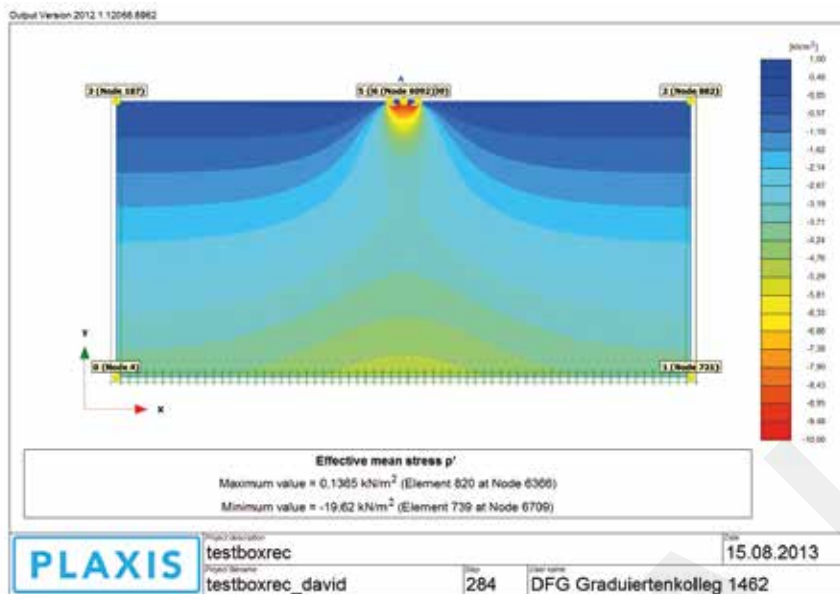
## Results

The results of the experimental, as well as the numerical simulation of the cyclic response of soil will be presented.

### Experimental

The aforementioned curve with due regard in defining the various strain-depending Young's modulis is presented in Figure 8. It can be observed that the settlements induced by the static and cyclic loading densify the loose sandy material, which affects subsequently the value of the initial shear modulus $G_0$. The Young's modulus is directly related to the shear modulus with known constitutive equation;

$$E_{max} = G_{max} \cdot 2 \cdot (1+v) \qquad (8)$$

Furthermore, a plot of the change of shear wave velocity with depth (Figure 9) visualizes the effect of the static and cyclic loading on soil stiffness with the depth. The shear wave velocity $V_s$ will be computed at various depths, below the footing. The average velocity will be calculated, so as to have a clearer depiction on the modification of the shear modulus in the entire specimen.

Figure 8 – Young's modulus for different parts of the loading curve
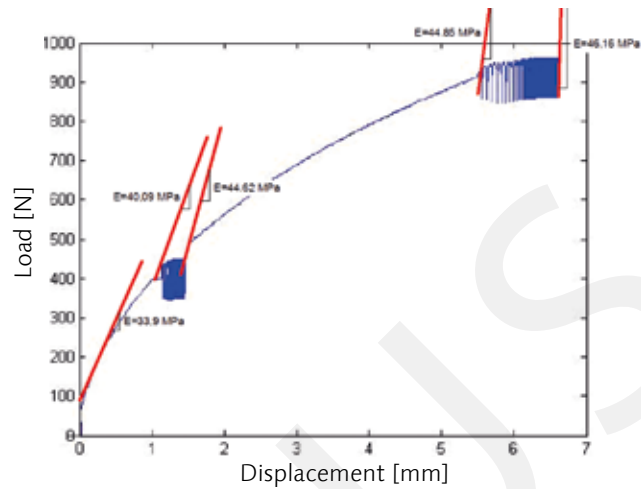


Figure 9 – Change of shear modulus with the depth
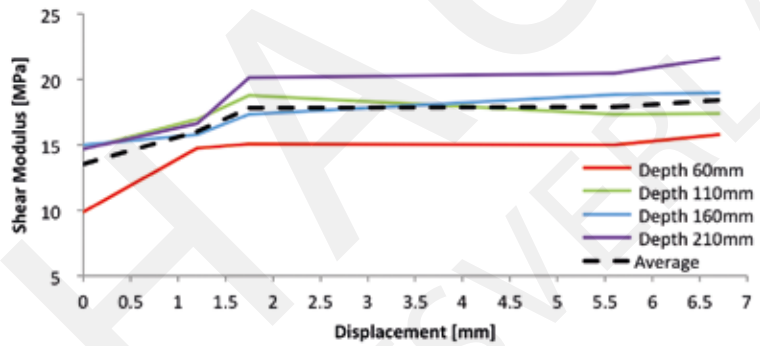


## Numerical simulation-PLAXIS

The results from PLAXIS are presented in Figure 10. The three different constitutive models namely, Mohr-Columb, Hardening Soil and Hypoplastic models were used in PLAXIS to model the cyclic response of the soil with different load history. From the following Figure 10, the hypoplastic model closely resembles the static loading of the soil, but it has been difficult to reproduce the cyclic response of the soil.

Figure 10 – Numerical simulation in PLAXIS using different constitutive models

## Macroelement model

The results of the macroelement model is presented in Figure 11. The numerical response is close to the experimental results. The high number of cycles is reproduced by the macroelement model. Macroelement model thus serves as an important model for the soil response under cyclic loading, which by not being very complex can predict accurately, the response of the soil under complex loading.

## Conclusions

The purpose of the project 2 in the University of Weimar was to determine the static and cyclic behavior of dry sand. An experimental procedure was performed to determine the shear modulus and the Young's modulus of the sand, as well as define the load-displacement curve of the behavior of sand.

The shear wave velocity was computed at various depths to illustrate the effect the load-induced settlements on the shear stiffness of the soil. The numerical models in PLAXIS were not as accurate as we wanted them to be, due to the insufficient time to understand completely the rudiments of both the FE program, as well as the constitutive models.

Furthermore, the response of the macroelement model was quite close to the experimental results. This serves to illustrate the advantages of such models, which become pronounced in cyclic loadings with a substantial number of cycles.

## Bibliography

Das, B. (2008). Advanced Soil Mechanics (éd. 3rd). New York: Taylor and Francis.

Gudehus, G. (2011), Physical soil Mechanics, Springer.

Gudehus. G. (1996), Comprehensive Constitutive Equation for Granular Material, Soils and Foundations, 36(1) : pp 1-12

Kramer, S. L. (1996). Geotechnical Earthquake Engineering. Prentice Hall.

Masin, D. (2012). Hypoplasticity for Practical Applications. Prague, Czech Republic.

Nova, R., & Montrasio, L. (1991). Analysis of Settlements of Shallow Foundations on Sand. International Conference on Soil Mechanics and Foundation Engineering, (pp. 505-509). Florence.

PLAXIS Corporation. (2012). Material Models Manual. Consulté le 8 16, 2013, sur PLAXIS Corporation Web site: http://www.plaxis.nl/plaxis2d/manuals/

Santamarina, J., & Lee, J.-S. (2006, September). Bender Elements: Performance and Signal Interpretation. Journal of Geotechnical and Geoenvironmental Engineering, 1063-1070.

Tejchman, J. & Gorski (2008), Computations of size effects in granualr bodies within micro-polar hypoplasticity during plane strain compression, International Journal of Solids and Structures, Vol 45, PP. 1546-1569.

KAMPENHUBER, David
Unit of Applied Mechanics,
University of Innsbruck,
Innsbruck, Austria

MOSCHEN, Lukas
Unit of Applied Mechanics,
University of Innsbruck,
Innsbruck, Austria

PAVEL, Florin
Department of Reinforced
Concrete Structures,
Technical University of Civil
Engineering Bucharest,
Bucharest, Romania

SINKOVIC, Klemen
The Institute of Structural
Engineering, Earthquake
Engineering and
Construction IT, University
of Ljubljana, Ljubljana,
Slovenia

RADOSLAV, Orlinov
RC Department, UACEG-
Sofia, Sofia, Bulgaria

FELJA, Ivona
Faculty of Civil Engineering
in Osijek, Josip Juraj

# Project 3 – Damage assessment of a commercial building due to the main shock and after shock from the Van-Ercis earthquake 2011

## Introduction

This report is the outcome of the project group number 3 during the summer school in Weimar 2013. Scope of this report is the damage assessment of a commercial building located in eastern Turkey especially in Erciş. To get an overview of the project the general situation will be discussed.

The building was under construction during the mainshock as well as during the aftershocks. A research-team from the Zirve University in collaboration with a team from the Mustafa Kemal University applied measurement instruments in several floors after the main and several aftershocks. The outcome are velocity data-sets as an result of ambient excitation.

However, content of this report are different aims. First of all, project group number 3 was separated into several sub-teams:
- GMPE group
- Dealing with the ground motion data from mainshock and aftershock. The primary goal is to define the acceleration response spectrum for the specific site and support further groups with acceleration series.
- Modelling group
- Two different software packages are used to define the structural model. The goal of this group is to estimate the damage using different numerical methods.
- System Identification group
- This group deals with the velocity data recorded from the research team after the aftershocks. Aim of this group is to figure out the damaged period of the structure and identify the soil conditions.

## Ground motion prediction

### Introduction

The Van-Ercis earthquake occurred on October 23, 2011 close to the city of Van, near Lake Van in Eastern Turkey. The magnitude of the seismic event was initially estimated at $M_W = 7.2$, later on the value was revised to $M_W = 7.0$.

The earthquake was produced by an unknown WSW-ENE reverse fault with north-dipping fault plane [3]. The epicentre is situated at 38.689° latitude and 43.4657° longitude at a depth of 19 km. The earthquake claimed 604 lives, with most of the deaths occurring in the city of Erciş situated at about 40 km from the epicentre (EERI, 2012).

191 buildings collapsed totally or partially in Erciş and only 6 buildings collapsed in Van, although Van was situated at about 20 km from the epicentre. 3713 buildings were declared not safe for occupation (heavily damaged), while 2209 were declared as possibly safe for occupation after the seismic event. The mainshock had 5 after shocks having Magnitude $M \geq 5.5$ (3 of which occurred in the same day as the mainshock) and 12 after shocks measuring more than $M \geq 5.0$ (the last after shock with $M \geq 5.0$ was recorded on November 30).

The most important after shock took place on November 9, 2011 at a distance of about 10 km from Van and had a magnitude $M_L = 5.6$. 40 people lost their lives as a result of this earthquake when 2 hotels in Van collapsed. A total of 25 buildings collapsed in Van, most of which were seriously damaged by the mainshock.

This event was produced on a strike-slip fault previously unidentified (like the case of the mainshock). Akyüz et al. [2] also note the predominance of strike-slip mechanisms to the NE and

HOXHA, Marjus
Civil Engineering Department, Zirve University, Gaziantep, Turkey

VELCHEV, Vanya
UACEG-Sofia

GYORKO, Zoltan
Budapest University of Technology and Economics, Budapest, Hungary

CELIK, Tahir Burak
Mustafa Kemal University, Antakya, Turkey

SCHWARZ, Jochen
Earthquake Damage Analysis Center (EDAC), Bauhaus-Universität Weimar

SW of the rupture area, while reverse mechanisms predominate to the Western part of the source. Other significant earthquakes [2] in the region near Van took place in 1903 (MS = 6.7), 1941 (MS = 5.9) and 1976 (MS = 7.3). The last earthquake of 1976 produced over 3000 deaths and over 9000 damaged buildings. Another important earthquake which has hit the region occurred in 1646 [2].

## Strong ground motion data

Unfortunately, no strong ground motion data were recorded in the epicentral region of the mainshock. The seismic station at Van did not record the main shock due to a malfunction (EERI, 2012). The closest seismic station (no. 6503) which recorded the main shock was situated at Muradiye (epicentral distance of about 40 km). A total of 22 records were obtained from the October 23, 2011 seismic event (although only 2 were recorded at epicentral distances smaller than 100 km - Muradiye and Bitlis). Nevertheless, the strong ground motion from Muradiye exhibits peak ground accelerations (PGA) of 0.18 g (NS component), 0.17 g (EW component) and 0.08 g (vertical component). The after shocks, with the exception of the November 9 event did not produce significant strong ground motions. The November 9, 2011 earthquakes was recorded in Van (seismic station no. 6501) at an epicentral distance of 14 km with peak ground accelerations of 0.15 g (NS component), 0.25 g (EW component) and 0.15 g (vertical component). The time-histories of the two strong ground motions are shown in Figure 1 and Figure 2. The response spectra for the two seismic stations are compared with the design spectra from the Turkish seismic design code in Figure 3 and Figure 4.

It is clear from Figures 3 and 4 that the recorded spectra are below the design spectra. In the case of the Muradiye seismic station the absolute acceleration response spectrum of the recorded strong ground motion is about half of the design spectrum. It is also visible that the strong ground motion recorded at Van station during the November 9, 2011 after shock produced a stronger shaking than the strong ground motion recorded at Muradiye during the mainshock. The severity of the strong ground motion from Van explains the level of damage produced during this after shock.
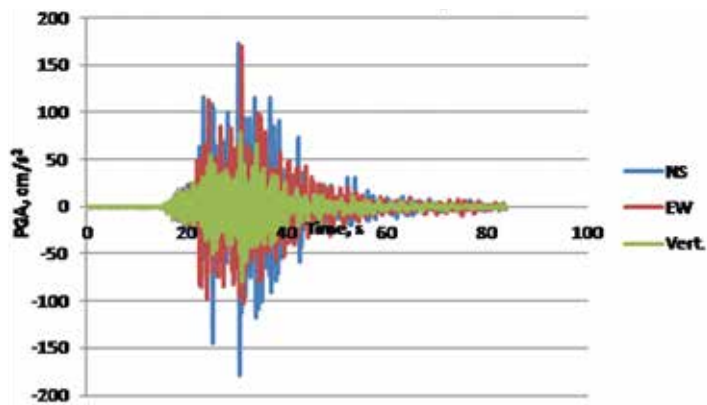
Figure 1 – Acceleration time-history of the mainshock for Muradiye seismic station
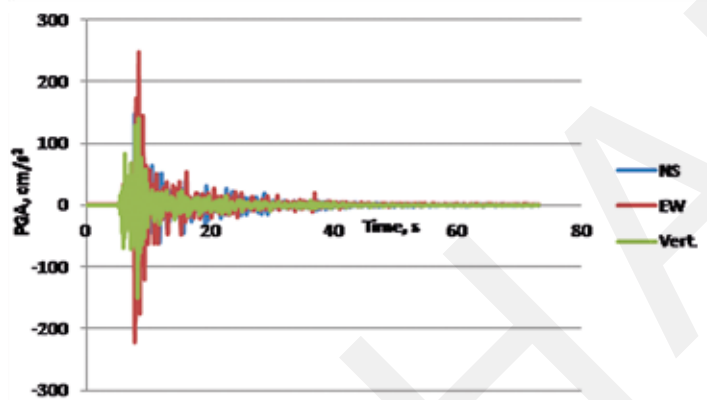


Figure 2 – Acceleration time-history of the Nov. 9, 2011 after shock for Van seismic station
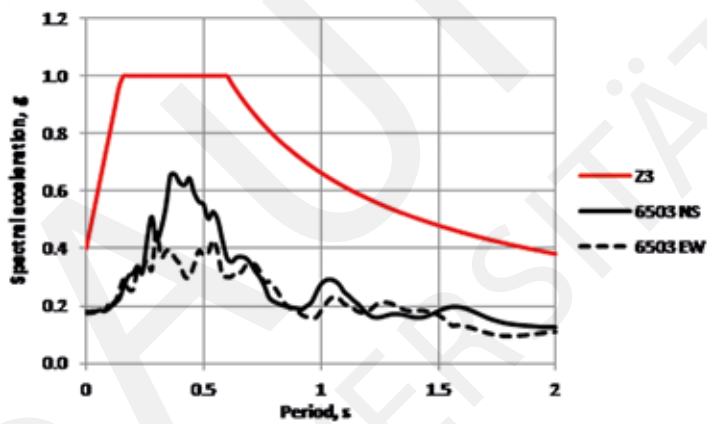


Figure 3 – Comparison of recorded absolute acceleration response spectra with the design spectra for Muradiye seismic
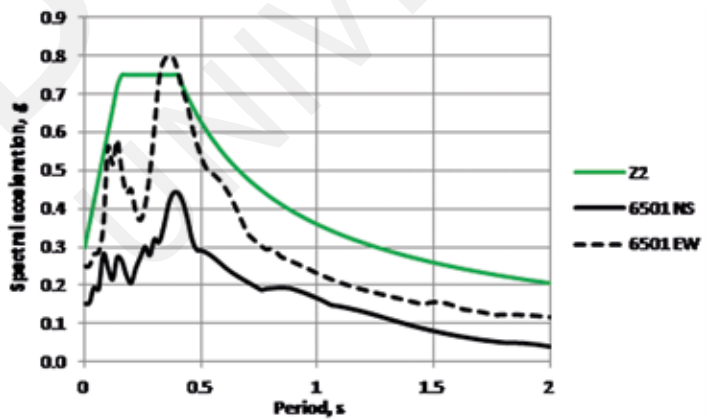


Figure 4 – Comparison of recorded absolute acceleration response spectra with the design spectra for Van seismic

## Comparison with GMPEs

The recorded strong ground motions of the main shock (October 23, 2011) are compared with several GMPEs (ground motion prediction equations) given in the literature [1, 4, 5] in Figure 5, Figure 6 and Figure 7.



Figure 5 – Comparison of Kalkan and Gülkan [4] GMPE with the recorded data of the mainshock
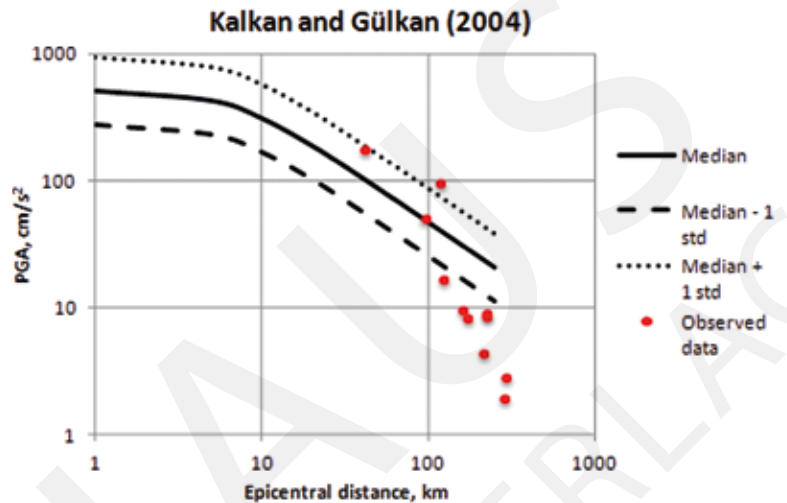


Figure 6 – Comparison of Akkar and Çağnan [1] GMPE with the recorded data of the mainshock
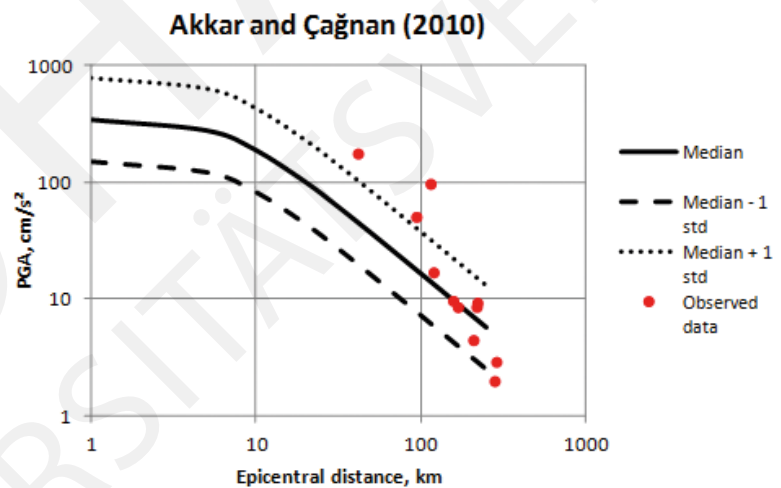


Figure 7 – Comparison of Schwarz et al. GMPE [5] with the recorded data of the main shock
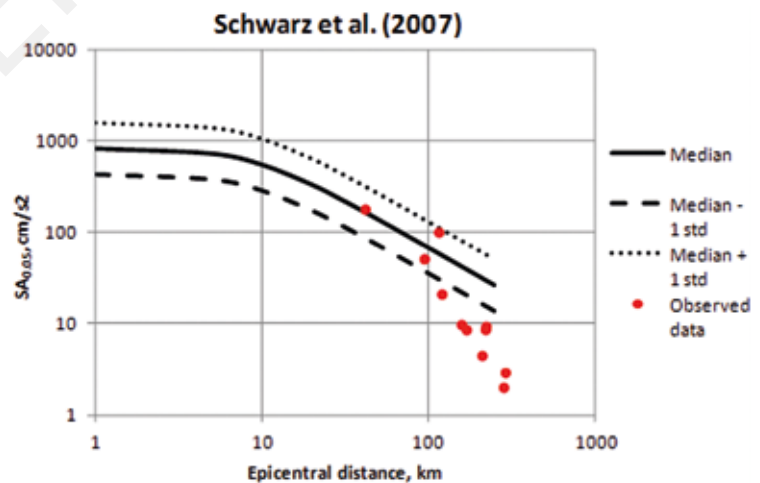
Unfortunately, as mentioned before no strong ground motion was obtained in the epicentral region during the main shock, so the values of the amplitudes given by the GMPE can't be assessed for small epicentral distances. However, from the 3 above figures it is clear that 2 GMPEs [2, 5] overestimate the observed strong ground motions for epicentral distances in excess of 100 km, while the other GMPE (Akkar and Çağnan [1]) performs very well for epcientral distances in excess of 100 km. The Schwarz et al. GMPE [5] appears to fit very well with the data recorded below 100 km. Moreover, the very large differences between the strong ground motion amplitudes given by the 3 GMPEs are also visible.

## Ground motion estimation for Erciş and influence of aftershocks

The selected building in the city of Erciş is situated at an epicentral distance of roughly 39 km from the epicentre of the main shock. So, from this point of view the distance is similar to that between the epicentre of the earthquake and the seismic station at Muradiye. But it is believed that the level of shaking at Erciş was greater than that at Muradiye (EERI, 2012). The level of damage in the city of Erciş supports this observation. Among the main parameters which may affect the level of shaking at a particular site are the focal mechanism, the directivity or the local soil conditions. Because both sites (Muradiye and Erciş) are situated on the hanging-wall side and far away from the fault trace, it appears that the local soil response is responsible for the amplifications of the strong ground motions. A site response analysis performed by Siyahi *et al*. [6] shows that the local soil conditions in Erciş can amplify the bedrock ground motion by over than 50%. Moreover, liquefactions and liquefaction induced lateral spreading and settlements were also observed in Erciş region. The peak ground acceleration expected for Erciş is according to the analyzed GMPE in the range 0.18 - 0.30 $g$, values below the design value of the PGA of 0.4 g. However, the frequency content of the strong ground motion can't be assessed with the available data.

The influence of the aftershocks on the analyzed building appears not to be very important. The epicentral distances between the building and the after shock with magnitudes M ≥ 5.5 are in the range 23–65 km, with 3 events having epicentral distances smaller than 30 km. The median expected level of ground motion in the region of the building is in the range 0.05–0.10 $g$. However, due to the local soil conditions the ground motion might have been amplified.
The level of amplifications in the case of the after shocks is in our opinion smaller than in the case of the main shock especially due to the smaller earthquake rupture duration. Due to the reduced

duration of shaking the nonlinear soil response is not as important as in the case of the mainshock.

## Structural Analysis using the OpenSEES interpreter

### Introduction

This subsection deals with the estimation of damage using the open software for earthquake engineering (acronym OpenSees, [21]) interpreter. This section is subdivided into subsection given in the list below:
- modeling linear structural behavior
- taking nonlinearities into account
- mass assessment
- modal and pushover analysis
- presentation of results
- conclusions
- references

### Modeling of linear structural behavior

First of all the load-bearing structure is a reinforced concrete frame (RC frame) with a total number of 6 stories and a basement, where the basement is not part of this structural model. Concrete slabs sever for load-bearing elements between the girders of each floor. Thus, the cross section of the girders include the geometric properties of the beam itself as well as the effective width of the concrete slab of to the bending shape due to earthquake excitation respectively due to lateral forces. Vertical members are simply modeled with the cross section shown in the drawings. Boundary conditions are defined as fixed supports, this means all degrees of freedoms (DOFs) are fixed – displacement DOFs as well as rotational DOFs.

### Modeling of nonlinearities

Internal forces are determined on the deformed structural system, in other words due to gravity loads the system is pre-stressed and additional bending moments due to the deflected shape are considered (P$\Delta$-effect). Material nonlinearities are defined at begin and end of each structural member using concentrated plasticity models [7]. The shape of the backbone curve depends on several parameters, e.g. reinforcement, strength of concrete, axial loading, etc. [8]. Therefore, the analysis package automatically calculates the backbone curve after definition of the rebar layers [9] according to the European standard [10, 11].
Finally the implementation in OpenSees requires the definition of hysteretic material behavior. Scope of this study is damage

assessment using nonlinear static methods (SPO), respectively the N2 method [12]. Hence, definition of cyclic deterioration and a simple backbone curve can be used. For this cases OpenSees provides hysteretic material developed by Scott and Filippou [13] where a trilinear capacity curve can be defined, see Figure 8.

## Mass assessment

Generally, masses are defined as lumped masses. The dead-load of each story is approximately 193 tons. Lumped masses are estimated by the influence area of each column.

## Modal and push over analysis

Modal analysis is performed to figure out the periods as well as the mode shapes of the undamaged structure. It is important to note, that the periods are the outcome of an rough estimation, because material properties are not well defined, mass assessment is not exact respectively unknown. The capacity curve is determined performing pushover analysis. Therefore, different load-pattern with respect to the first and second mode-shapes are applied to the structure separately in global X- and Y-direction to figure out the static-response of the building respectively the lateral strength in those directions, see Figure 9.
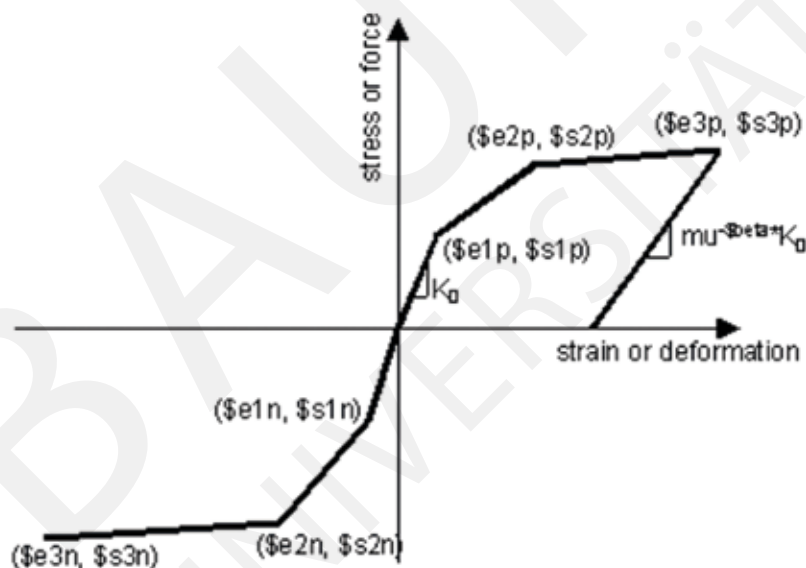
Figure 8 – Hysteretic Material

Figure 9 – Pushover curves
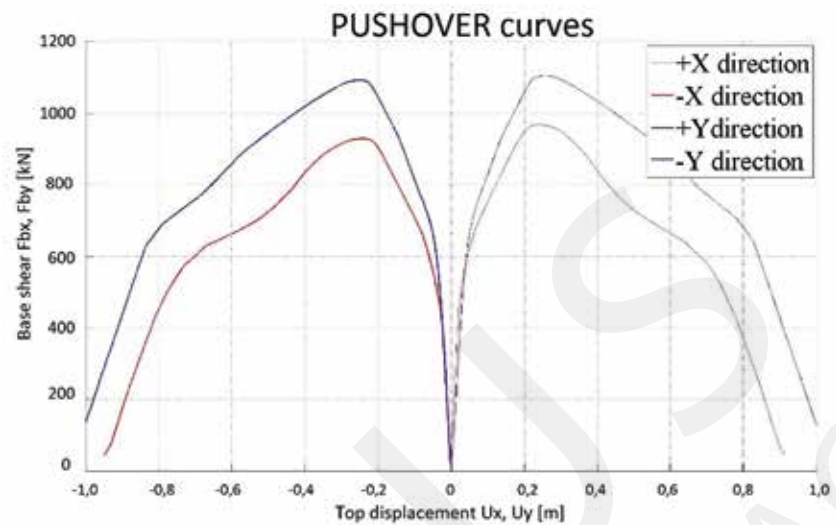


Figure 10 – Target Displacement in X-Direction
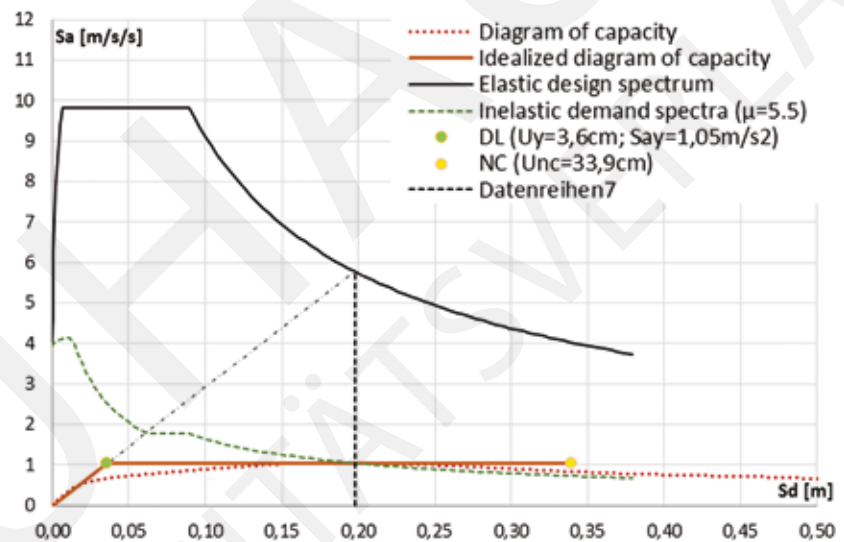


## Presentation of results

Finally, the N2 method is used to estimate the performance point of the structure. Therefore, the following steps are required:
- Performing the pushover analysis for X and Y direction.
- Converting the multi degree of freedom system (MDOF) into an equivalent single degree of freedom (SDOF) system.
- Bi-linearization of the pushover curve.
- Mapping back the pushover curve from base shear – displacement coordinates into capacity coordinates (spectral acceleration/displacement).
- Definition of the inelastic demand spectrum based on ductility demand.
- Determination of the performance point respectively for X and Y direction (Figure 10 and 11).

The outcome is that damage can be detected in the columns of the basement as well in the girders, see Figures 12 to 15. Generally, it makes sense to determine pushover curves in several directions (because the ground-motion does not care about the orientation of the building with respect to the fault). Hence, the capacity (respectively the target displacement) is illustrated in Figures 10 and 11.
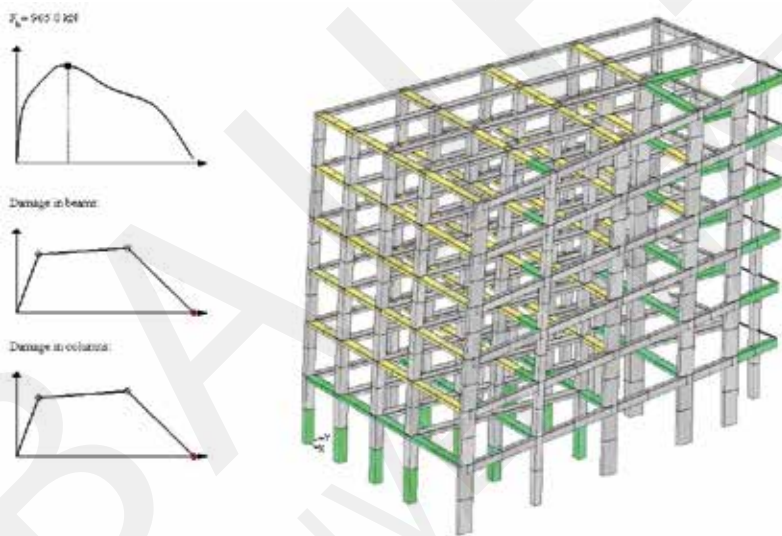
Figure 13 – Damage due to load-pattern with respect to mode shape 2 in Y direction (bottom view)
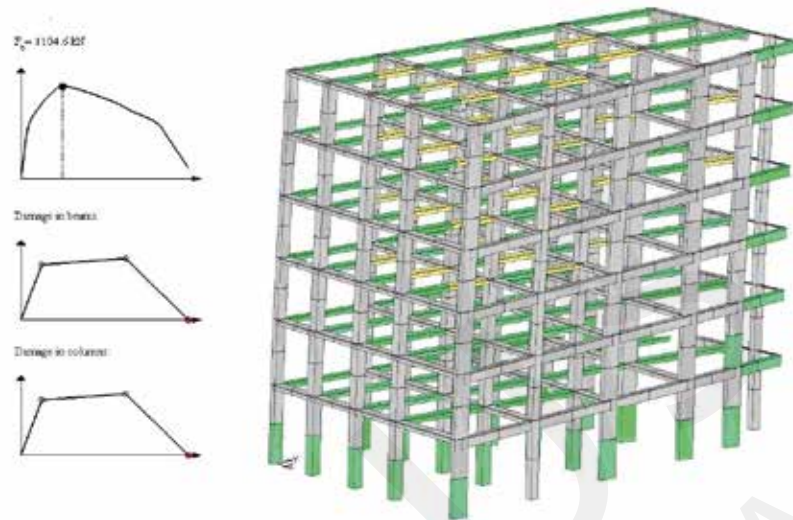


## Conclusions

The results differ in comparison to the real (after inspection) damage. Probably, results could be more accurate if a modal pushover analysis is performed taking more modes into account [14, 15] or by performing modal adaptive pushover analysis [16]. However, when talking about a first try of damage assessment this study leads to adequate results, because many epistemic uncertainties e.g. material properties, the way of manufacturing, etc. are not taking into account. An extended study using nonlinear dynamic methods seen through incremental dynamic analysis [17] would be an interesting aspect in terms of assessing damage due to the main shock as well as collapse prevention due to an aftershock.

## Structural Analysis using SAP2000

### Modeling

The building is 6-storey a R. C. frame structure with one basemant for bearing. Storey height is from 3.65 m to 4.20 m. For the project work only one section of the building is studied (in red). The building is seperated by an expansion joint.
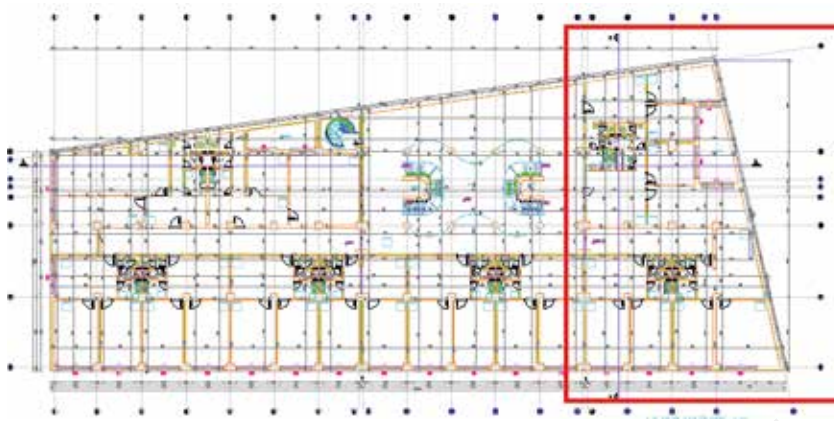
Figure 14 – Normal plan of the building

There are two openings at the slab at the following slab elevations: +8.91m; +13.04m; +16.17m and +19.80m. A console starts from the second floor but it is considered not contribute to the pushover analysis.
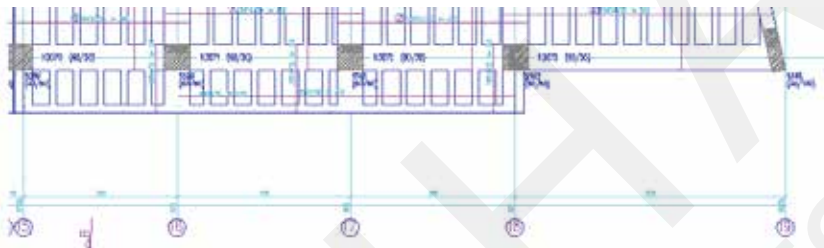


Figure 15 – Console starting from the second floor (neglected in analsyis)



Figure 16 – View of the building during conctruction*

* Prof. Dr. M.C. Genes

Figure 17 – Damage of a column



## Overview

Columns section size varies from 30cm/70cm to 60cm/100cm. Two shear walls are part of the bloadbearing structure with dimensions of 30cm/420cm respectively 30cm/210cm. Sectional properties of all beams 30cm/60cm. The slab is ribbed with a thickness of 7cm, respectively the height of the ribs is 30 cm.

| Loading | Member | specific weight [kN/m²] |
|---|---|---|
| | slab | 1.75 |
| | ribbs | 1.88 |
| | hollow-tile floor slab | 1.00 |
| | floor covering | 0.55 |
| | leveling | 1.10 |
| | plaster | 0.40 |
| | Total | 6.68 |
| | Member | specific weight [kN/m²] |
| | inner walls | 1.00 |
| | cladding | 0.50 |

Note: Cladding is presented by linear load on the outer beams. All the loads are transformed in linear distributed load over the beam elements. All loadbearing structural elements are modeled by linear frame elements. The columns are restrained by fixed supports. The basement consist of two slabs and suteren walls. It is considered to be rigid box basement, so its behavior to the RC frame is irrelevant.
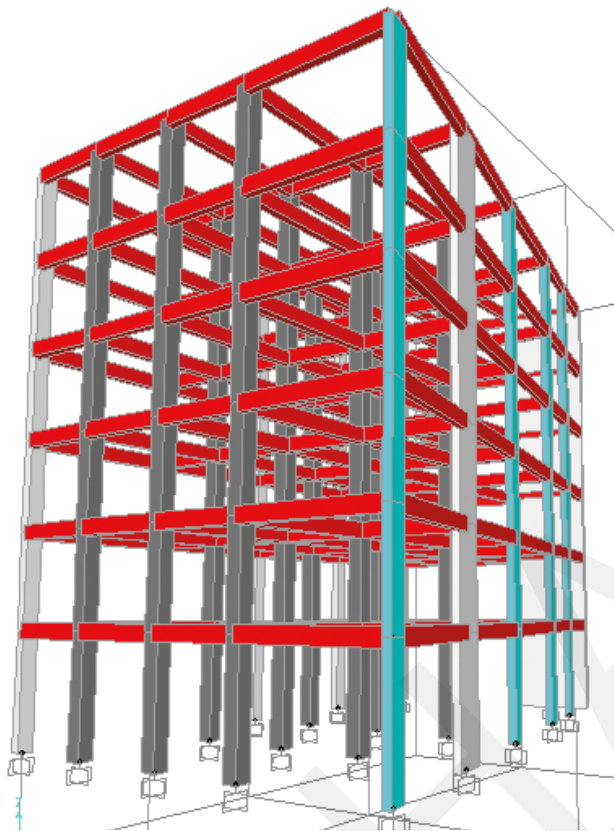
Figure 18 – FE model

## Modal analysis

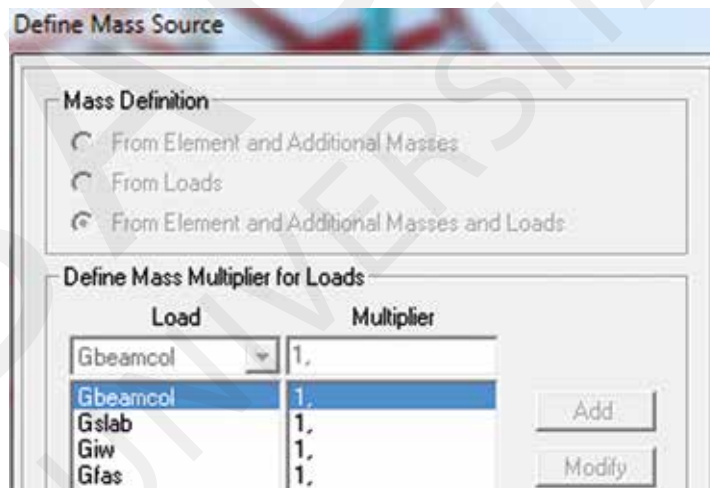The masses for modal analysis are automaticly obtained by the load cases.



Figure 19 – Defining the mass source

A modal analysis is caried out. The fittest three modal shapes are shown in Figure 20, 21 and 22.
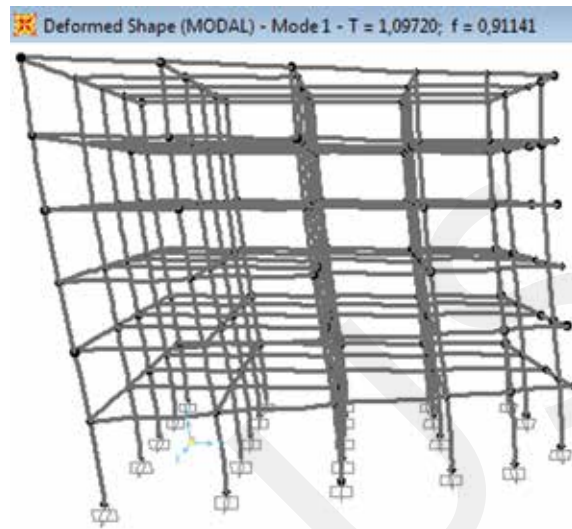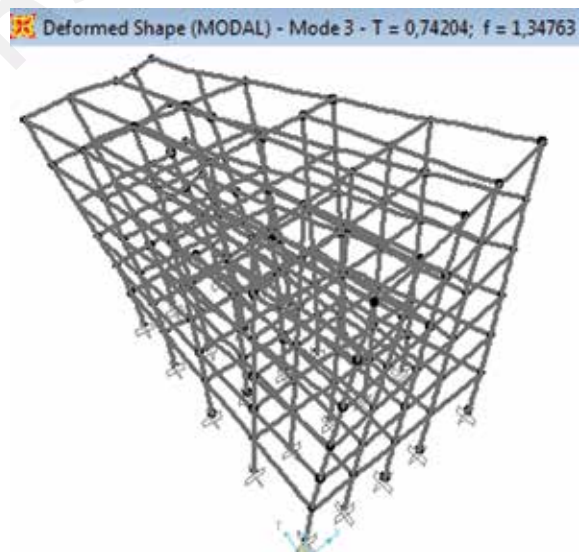
Figure 20 – Mode 1



Figure 21 – Mode 2



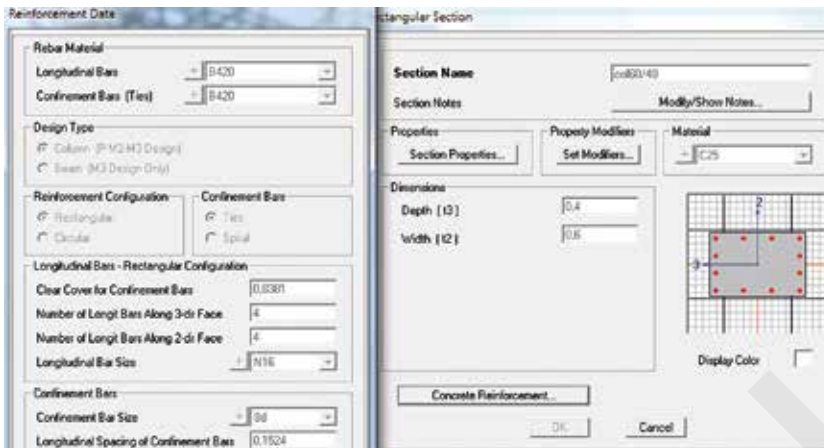Figure 22 – Mode 3

## Push over analysis



Figure 23 – Reinforcement properties
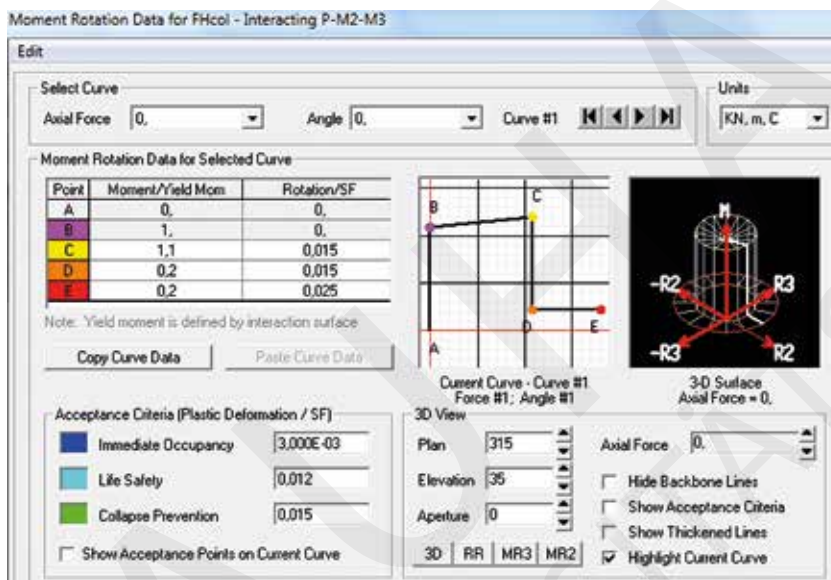


Figure 24 – Moment rotation data

All reinforcement properties are entered as shown on column and beam application details.

Hinges with different properties are assigned to beams and columns:

- For columns – hinges with axial force and two bending moments P-M2-M3
- For beams – hinges with bending moment for the major axe M3
- For shear walls – hinges with shear force V2

First part of push over analysis is solution for vertical loads. The results are saved and horizontal loading is applied on steps. The load pattern may be defined manually or by eigenmode. For the two main directions in plan horizontal loadings are from the first and second mode shapes.

Figure 25 – The displacements in X direction are obtained by second mode
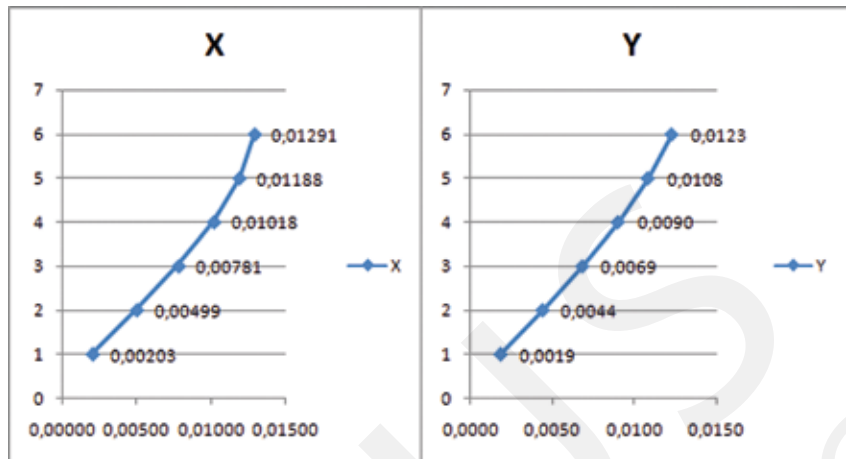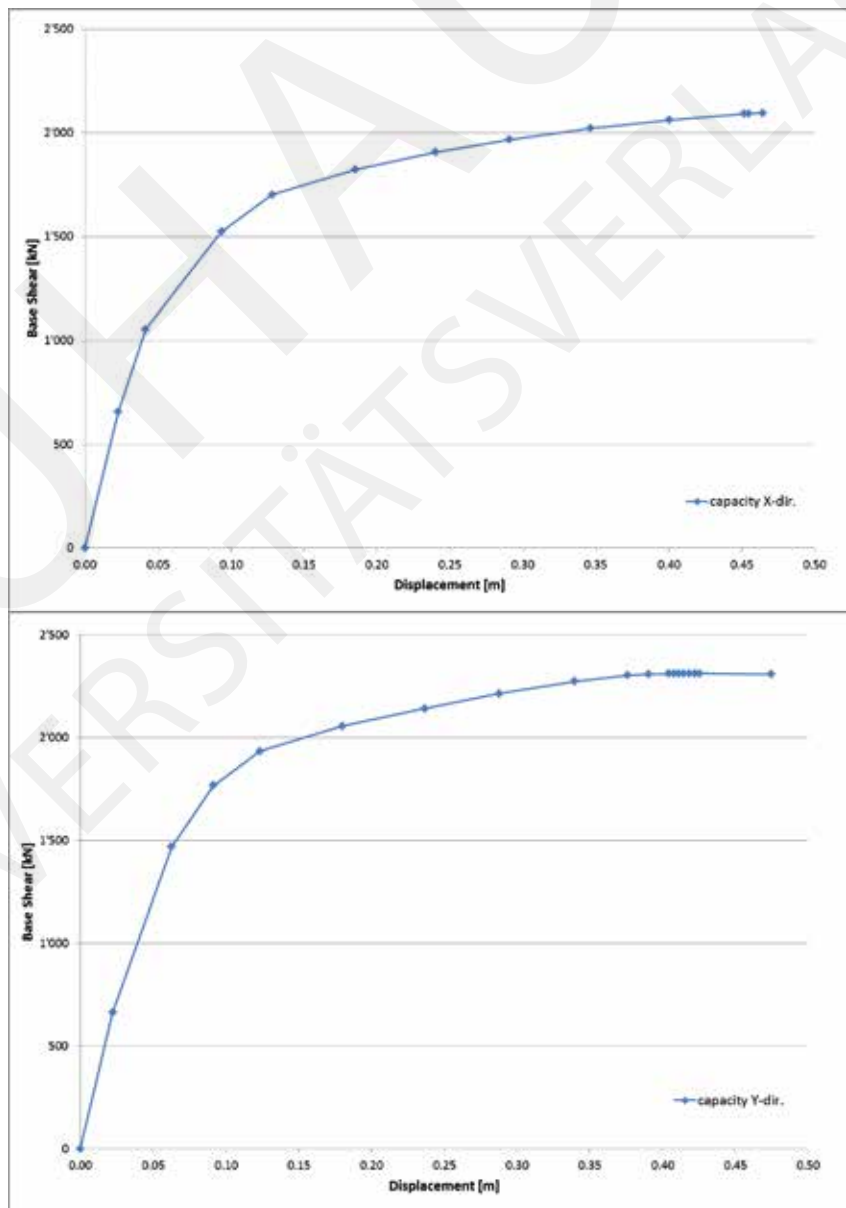


Figure 26 – Results from the push over analysis for each direction

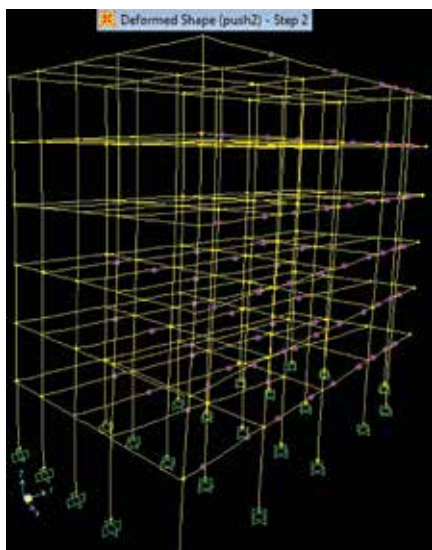Plastic hinges appear in the beam elements:



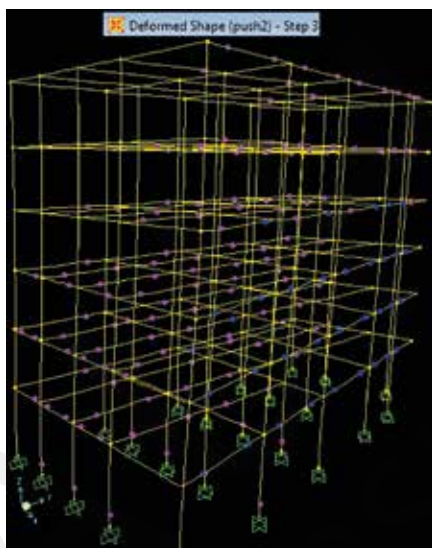Figure 27 – Deformed Shape 1
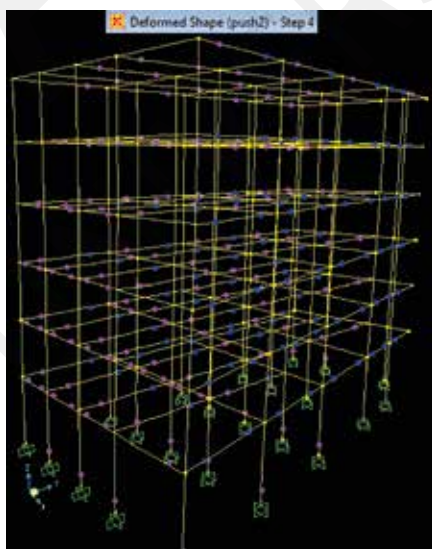


Figure 28 – Deformed Shape 2



Figure 29 – Deformed Shape 3

In order to transform the frame into a single degree of freedom system (SDOF) a correctional coefficient r has been used:

$$r = \frac{\sum \overline{F_i}}{\sum \frac{\overline{F_i^2}}{m_i}}$$

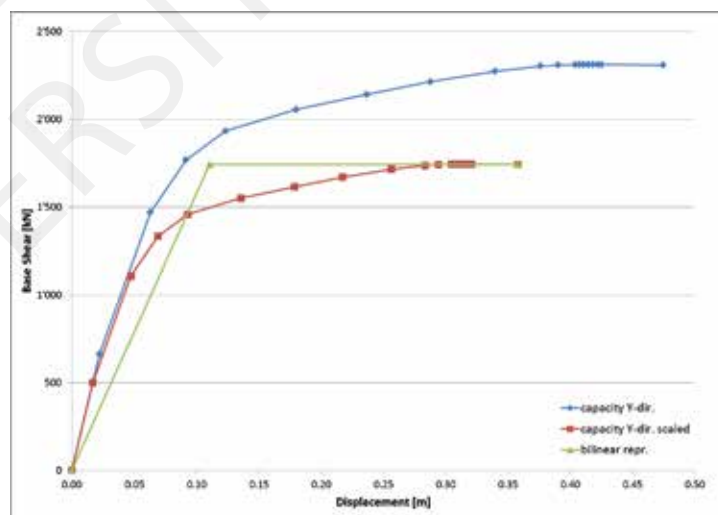$F_i$ – inertia force;  $m_i$ – mass of each level

The behavior is represented by bilinear force-displacement graphic, which has the same area as the push over curve (see Figure 31 & 32)

Figure 30 – Force-displacement graphic 1
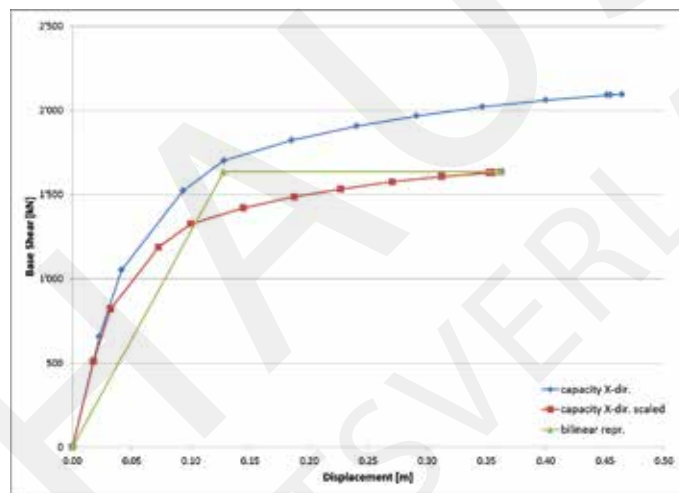


$$T_x = 2pi = \sqrt{\frac{m^* \, d_y^*}{F^*}} \, 2pi = \sqrt{\frac{1776,7 \cdot 0.128}{1634.5}} \, 2.34[s]$$

Figure 31 – Force-displacement graphic 2



$$T_x = 2pi = \sqrt{\frac{m^* \, d_y^*}{F^*}} \, 2pi = \sqrt{\frac{1776,7 \cdot 0.128}{1634.5}} \, 2.34[s]$$

## Conclusions

The first period of vibration of the undamaged structure is 1.25s. The observed damage on the building is caused by torsional mode. The outer columns have damage due to rotation. Plastic hinges arise on the first floor in the beams and there was shear failure in the shear wall. Similar mechanism is observed in push over analysis.

As the result of the analysis we can conclude that the building was not properly designed for an earthquake with this magnitude. Due to the residual deformations the section of the building was demolished.

## System Identification

### Instrument locations

Five sensors were positioned on, and one sensor beside the building. The exact position can be taken from Figure 33. These sensors recorded the velocity response of the building in all three directions (x, y and z). The measurement was performed on October 29, 2011. All records were sampled with 100Hz and lasted approximately one minute. Different sensors recorded different number of single records (MR1:79, MR2:79, MR3:56, MR4:79, MR4:79, MR6:80).
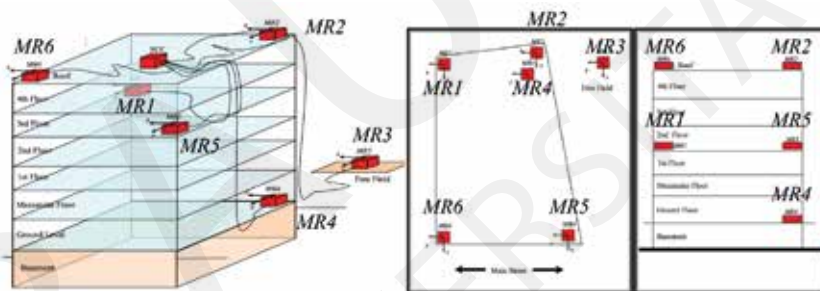


Figure 32 – Instrument locations on the building

Peak picking

In order to identify the vibration periods of the damaged building classical peak-picking method was applied. Therefore the median-velocity spectra of each sensor were used. Before transforming the data into the frequency domain, a Butterworth filter was applied to get rid of frequencies below 0.2Hz and above 30Hz. The resulting spectra in x, y and z direction from sensor 1, 2 and 4-6 are presented in Figure 34. The spectra from sensor 3 are not shown, because it's results only correspond to the soil response and not to the building itself.

The highlighted areas in Figure 34 are exactly the same in each graph and correspond to the bandwidths of 0.60–0.69Hz, 0.71–0.80Hz, 0.81–0.93Hz, 1.08–1.25Hz, 1.40–1.70Hz, 1.80–2.05Hz and 2.70–3.40Hz. Analyzing the peaks from left to right result in an approximation of the vibration periods and the mechanism" of the corresponding modeshape. The first mode period probably can be identified between 0.60Hz and 0.69Hz which results approximately in $T_1 = 1.53$s. The corresponding modeshape seems to be dominated by a movement in y-direction. Nevertheless the identified vibration periods seems to have both, a component in x and y direction. This leads to the conclusions, that the damaged building principal moves in a torsional manner. On the other hand the gray line in Figure 35 (which corresponds to the sensor in the base level) has no significant peak at this frequency. Summarized can be said, the first mode of vibration probably is a combination of a translational movement of the whole building (including basement) in y direction and a torsional movement resulting of the building above the basement.

The next peak in the velocity spectra between 0.71Hz and 0.80Hz maybe describes the second vibration period of the building which could be calculated to approximately $T_2 = 1.33$s. It seems, that there is the same energy input according to this frequency in both, x- and y direction, maybe a little bit dominated in x-direction. Looking at the corresponding frequency of sensor number 4 (ground floor) leads to the conclusions, that the second mode of vibration is a classical torsional mode of higher levels, without any movement of the basement. The third peak between 0.81Hz and 0.93Hz also is present in both, x- an y direction spectra off all sensors (including the basement). The modeshape corresponding to $T_3 = 1.03$s seems to be again a torsional mode but including the basement too.
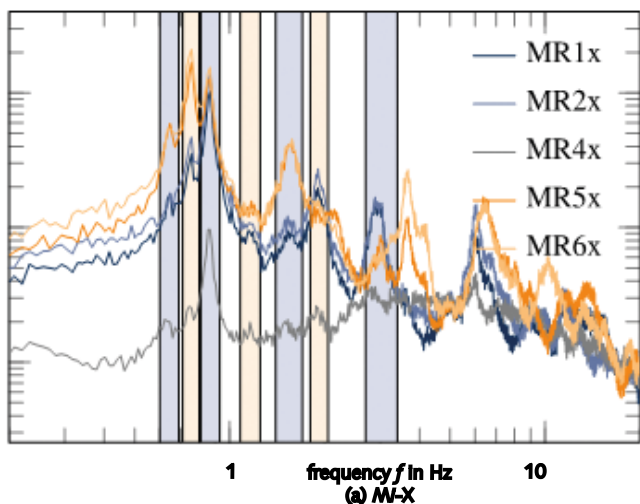
Figure 33 – Median velocity spectra for sensors 1,2,4,5 and 6 separate in (a) x (b) y and (c) z direction
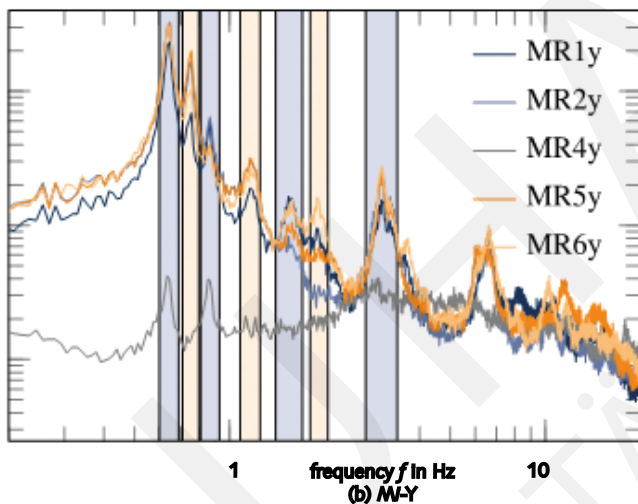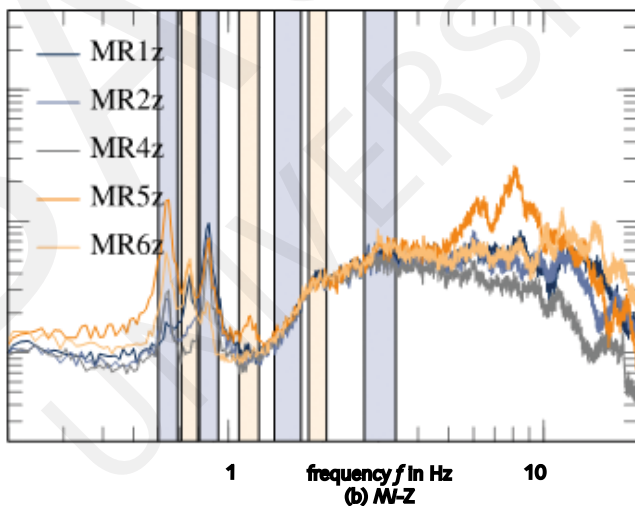
Figure 33 – (b)

Figure 33 – (c)

## H/V Ratios – site classification

The applied site classification method is based on the spectral H/V-ratios of microtremor data recorded at the ground surface [19]. These ratios represent the quasi-transfer function of the underlying soil profile, and therefore a quick site classification can be carried out by comparing the shape of H/V-ratio with the transfer function of a complying theoretical model profile or by simply arranging the H/V-peak into ranges of possible peak locations. Such a site classification scheme contains more information about the site than the commonly used average shear-wave velocity in the upper 30m. The scheme involves the total thickness of sedimentary layers over geological bedrock in addition to the shear-wave velocities. Similar schemes have been proposed before Bray and Rodriguez-Marek [18] and are incorporated in several international seismic code provisions, e.g. of Germany (DIN 4149:2005) [19].

According to Figure 37 the prevailing soil conditions can be classified as B – S according to DIN4149:2005. Note that B–S is not considered in the present draft of DIN 4149, but detailed information can be found in [20].

Figure 34 – H/V ratio - soile classification
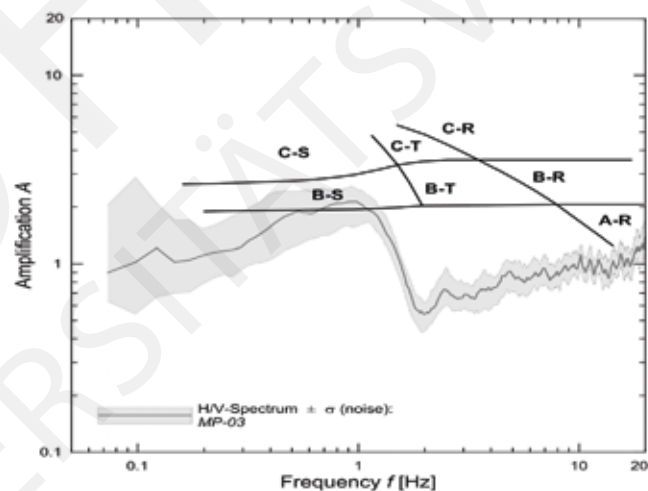
## Final Conclusions

An analysis of seismic excitation, structural analysis of a reinforced concrete building (RC building) and processing of measured data of the damaged structure is shown.
The hazard analysis shows that the variability of the predicted strong ground motion parameter is large. The reason of the damage for the analyzed building is related both to the size of the main shock and to the nonlinear soil response in Erciş. It is also clear that the recorded strong ground motion at Muradiye can't be extrapolated for Erciş due to the local soil response, which has probably increased the strong ground motion amplitudes in the medium periods range.

Nevertheless, the influence of the following aftershocks is considered as limited, due to their size (maximum magnitude M = 5.8), epicentral distance to the building (the smallest distance is 23 km) and rupture duration (which is smaller than in the case of the main shock, leading thus to a decreased nonlinear soil response).

A first issue in prediction of the base acceleration as well as the damage using nonlinear static analysis (static pushover Method SPO) is performed. In structural analysis two different software packages are used to build an mathematical/physical model. The two models leads to different results, because of the different assumptions.

A more accurate damage prognosis is too time consuming, respectively nonlinear dynamic analysis would probably lead to more successful damage prediction. Finally, the predicted periods of the damaged structure (measured) could not be compared with the calculated ones (modal analysis after SPO), because this would blow up the framework of this study.

# References

[1] Akkar, S. and Çağnan, Z. (2010). A local ground-motion predictive model for Turkey, and its comparison with other regional and global ground-motion models. Bulletin of the Seismological Society of America 100(6): 2978-2995.

[2] Akyüz, S., Zabci, C. and Sançar, T. (2011). Preliminary report on the 23 October 2011 Van Earthquake. Istanbul Technical University, Istanbul.

[3] EERI Special Earthquake Report (2012). Learning from earth-quakes - The MW 7.1 Erciş-Van, Turkey earthquake of Octber 23, 2011. Earthquake Engineering Research Institute.

[4] Kalkan, E. and Gülkan, P. (2004). Site-dependent spectra derived from ground motion records in Turkey. Earthquake Spectra 20(4): 1111-1138.

[5] Schwarz, J., Lang, D.H., Kaufmann, C. and Ende, C. (2007). Empirical ground-motion relations for Californian strong-motion data based on instrumental subsoil classification. Proceedings of the 9th Canadian Conference on earth-quake Engineering, Ottawa, Canada, Paper no. 1359.

[6] Siyahi, B., Cetin, K.O., Unutmaz, B., Uckan, E., Karabulut, H., Akbas, B., Fahjan, Y. and Altunel, E. (2012). The effects of site and soil conditions to the earthquake damage: October 23, 2011 Van-Tabanli earthquake (MW = 7.2). Proceedings of the 15th World Conference on Earthquake Engineering, Lisbon, Portugal, Paper no. 3504.

[7] Ibarra, L.F., Medina, R.A. and Krawinkler, H. (2005). Hysteretic models that incorporate strength and stiffness deterioration. Earthquake Engineering and Structural Dynamics 34: 1489-1511.

[8] Haselton, C.B. and Deierlein, G.G. (2007). Assessing Seismic Collapse Safety of Modern Reinforced Concrete Moment Resisting Frame Buildings. Report No. 156. The John A. Blume Earthquake Engineering Center, Department of Civil and Environmental Engineering, Stanford University.

[9] Dolšek, M., (2010). PBEE Toolbox. The Institute of Structural Engineering, Earthquake Engineering and Construction IT (IKPIR).

[10] EN 1998-1 (2011). Design of structures for earthquake resistance – Part 1: General rules, seismic actions and rules for buildings. European Committee for Standardization.

[11] EN 1992-1-1 (2005). Design of Concrete Structures – Part 1: General rules and rules for buildings.

[12] Fajfar, P., 2000. A nonlinear analysis method for performance-based seismic design. Earthquake Spectra, 16, 3: 573–592.

[13] Scott M. and Filippou F., Effects of Hysteretic-Material Parameters. http://opensees.berkeley.edu/OpenSees/manuals/usermanual/4052.htm

[14] Chopra, A.K. and Goe, R.K (2002). A modal pushover analysis procedure for estimating seismic demands for buildings. Earthquake Engineering and Structural Dynamics 31: 561–582.

[15] Chopra, A.K. and Goe, R.K (2004). A modal pushover analysis procedure to estimate seismic demands for unsymmetric-plan buildings. Earthquake Engineering and Structural Dynamics 33: 903–927.

[16] Gupta, B. and Kunnath S.K. (2002). Adaptive spectra-based pushover procedure for seismic evaluation of structures. Earthquake Spectra 16:367–392.

[17] Vamvatsikos, D. and Cornell, C. A. (2002). Incremental Dynamic Analysis. Earthquake Engineering and Structural Dynamics 31: 1097–1117.

[18] Bray, J. and Rodriguez-Marek, A. (1997). Geotechnical site categories. In: Proceedings of the First PEER PG&E Workshop on Seismic Reliability of Utility Lifelines; San Francisco, California

[19] Lang, D. and Schwarz, J. (2006). Instrumental subsoil classification of Californian strong motion sites based on single-station measurements. In: Eighth U.S. National Conference on Earthquake Engineering; Apr. 18–22, 2006, San Francisco, California.

[20] Lang, D. (2004). Damage Potential of Seismic Ground Motion Considering Local Site Effects.

[21] McKenna, F., Fenves, G. and Scott, M. (2013) OpenSees (Version 2.4.1): Open System for Earthquake Engineering Simulation. url: http://opensees.berkeley.edu/

AKANSEL, Vesile Hatun
METU University, Turkey

BLAGOEVA, Biliana
University of Architucture,
Civil Engineering and
Geodesy, Bulgaria

NISHI, Ryosuke
University of Japan

PANAGIOTOPOULOS,
Dionysios
Aristotle University of
Thessaloniki, Greece

RUGGERINI, Andrea Walter
University of Bologna, Italy

BULUT, Ozeren
Mustafa Kemal Universitesi,
Turkey

WITTOR, Björn
MOTRA, Hem Bahadur
HILDEBRAND, Jörg
Bauhaus-Universität Weimar

# Project 4 – Special aspects of steel bridge structures

## Abstract

In this Project, techniques for strengthening steel bridge in Jena (Thuringia, Germany) have been employed using carbon fiber reinforced polymers (CFRP). The CFRP plates were selected due to their outstanding mechanical characteristics, non-corrosive nature, and relative ease of application. The need for economical and fast rehabilitation solutions reflects the importance of using CFRP as a repair material. This Bridge was strengthened by installing CFRP plates to the bottom flange of steel girders in the positive moment regions. The strengthening system consists of preparation of the bonding surface and installing the CFRP plates to the beam surface with a high strength epoxy adhesive for the transfer of force to the high strength CFRP plates. Nonlinear finite element analysis software, ANSYS, and software optiSLang were used to verify and evaluate of the rehabilitation technique.

## Introduction

There are thousands of steel bridges that are at various levels of advanced deterioration due to many years of service and exposure to the environment. Rehabilitation can involve various strategies

and application methods. These strategies include adding steel plates to the girders in order to increase the girder capacity, adding new girders between the old ones or replacing the whole bridge [1]. Nowodays, retrofitting has become the dominant use of the material in civil engineering, and applications include increasing the load capacity of old structures (such as bridges) that were designed to tolerate lower service loads than they are experiencing today, as well as repair of damaged structures. In the construction of older steel bridges, conventional rehabilitation, such as welding steel plates to the outer face of the flange where the flange is in tension has been the traditional method for a long time but induces high thermal stresses in the steel members [2]. Since crack initiation from the weld of cover plate ends was recognized as potentially causing catastrophic failure of the steel girders it has become important to improve this situation.

The proposed rehabilitation and strengthening methodology for steel girder bridges is to install CFRP plates to the bottom flange of the girders. There are a number of important advantages offered by this type of strengthening technique. First, CFRP components are light, and can be easily positioned and then attached using epoxy adhesives. They are also resistant to corrosion, and thus they do not need extensive maintenance. CFRP laminates added to the tension flange of steel girders will enhance their flexural capacity [3].

### Case study

Corresponding to this project, it has been tried to include sufficient strengthening of the footbridge to cross the federal road B88 in Jena (Thuringia, Germany, Figure 1). According to the documents the girder has a length L= 25.500 mm. The hollow box, composed of a trapezoidal cross section and a cantilever panel, consists of a carbon steel material with grade St37 or S235. Since no further testing information regarding S235 exist, therefore S460 has been used in conformance with this project.



Figure 1 – Footbridge in Jena*

* Prof. J. Hildebrand

## Evaluation of materials

There are a number of components as materials that must be taken into account to better perception in this project. They are broken down in three groups as following:

Steel

The steel grade used for this project is S460 and to describe steel behaviour, four different material models have been grouped into the tensile test, linear elastic, bilinear isotropic hardening, and multi-linear isotropic hardening.

Tensile test

It is important to underline that direct tensile test is one of the most common test that could be done for ductile steels to plot stress-strain curve [2]. As a matter of fact tensile strength can be described by stress-strain graphs. Stress-strain curves provide a fundamental engineering description of the mechanical behaviour of materials. From the stress-strain curve descriptions, there is an important manifestation that is known as neck. This phenomenon is more for decreasing in the area cross section. Accordingly, two curves can be considered for each material (Figure 4).

Figure 2 – Effect of neck on stress-strain curve for ductile steel, A: Engineering stress, B: True stressTrue stress
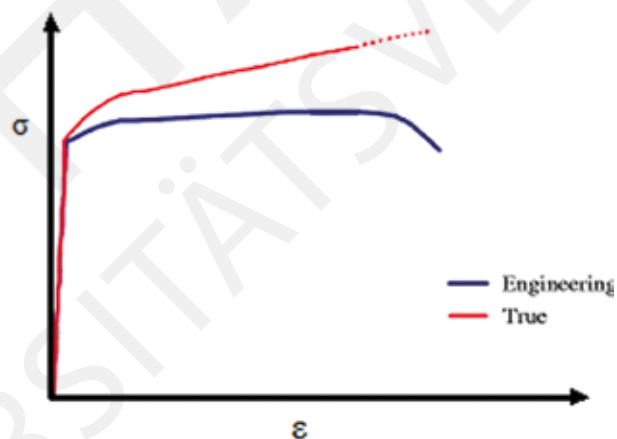


Therefore to determine true stress and true strain equations, there will be:

$$F = P/A0 \qquad (1)$$
$$F_t = P/A \qquad (2) \qquad A_0$$
$$g = */L0 \qquad (3)$$
$$g_t = Ln\,(1+g) \qquad (4) \qquad L_0$$

Where $\sigma$ (N/mm2) is engineering stress, $\sigma_t$ is true stress, A0 is area cross section of member and A is area cross section which changes during the time, $\varepsilon$ is engineering strain which is a dimensionless number, $\varepsilon_t$ is true strain L0 is original length. The stress-strain curve associated with this test is depicted in Figure 5.
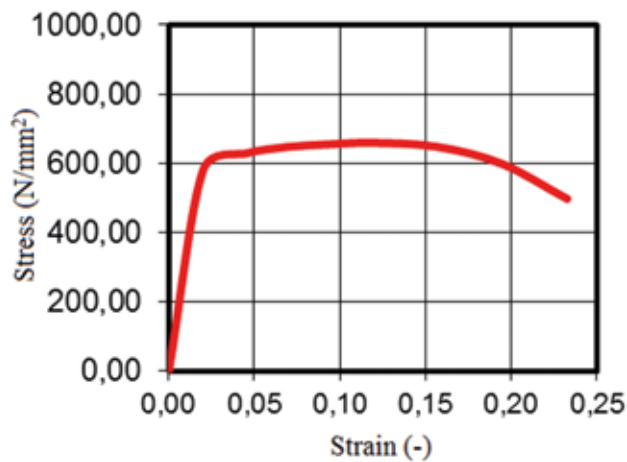
### Linear elastic

A linear elastic material as shown in Figure 4 has a linear relationship between how hard it has been squished and how much it deforms. It also returns to its original shape when squishing is stopped. The "Young's modulus, E" which tells how much a material will stretch or shrink along an axis when it is pushed or pulled is $2*10^5$ N/mm$^2$ and a Poisson's ratio ($\upsilon$) which tells how much a material shrinks along its cross-section when it is pulled along an axis is 0.3. The stress level at which a metal or other materials ceases to behave elasticity (Yield stress) is 460 N/mm$^2$ and 595 N/mm$^2$ was taken into account for ulimate stress.

### Bilinear isotropic hardening

After yielding occurs, the yield point may increase due to strain hardening. This changes the yield surface, and the way in which it evolves in simulation is determined by isotropic hardening assumption. The stress-strain curve can be represented by bilinear or multilinear curve (Figure 5). Isotropic hardening states that the yield surface expands uniformly during plastic flow. The term 'isotropic' refers to the uniform dilatation of the yield surface and is different from an isotropic yield criterion.
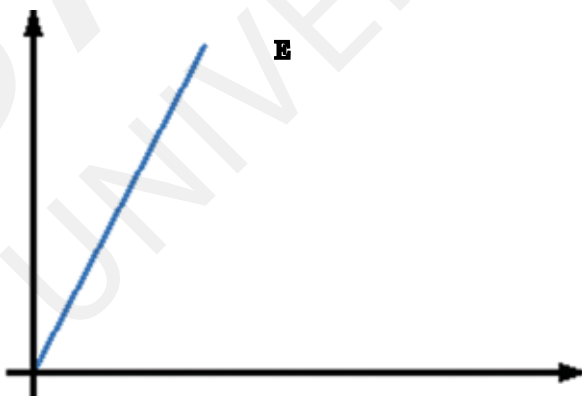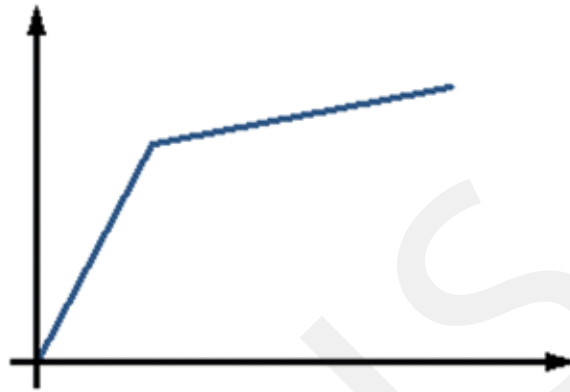
The properties of bilinear isotropic hardening material have been brought in Table 1.
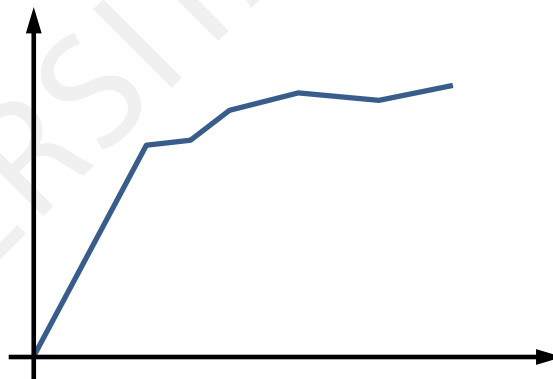
**Multi-linear isotropic hardening**
As it has been mentioned in part (b) regarding bilinear and multi-linear curves (Figure 6); the main parameters are modulus of elasticity in tension and strain at the proportional elastic limit point in tension.

|  | Yield stress | Young's modulus | Poisson's ratio | Ultimate stress | Tangent modulus |
|---|---|---|---|---|---|
| Bilinear isotropic hardening | 460 N/mm2 | 2*105 N/mm2 | 0.3 | 595 N/mm2 | 950 N/mm2 |

The values recorded in this test in terms of plastic area have been shown in Table 2.

| Multi-linear isotropic hardening | Point 1 | Point 2 | Point 3 | Point 4 | Point 5 |
|---|---|---|---|---|---|
| Stress (N/mm2) | 460 | 462 | 530 | 575 | 595 |
| Plastic strain (-) | 0.0 | 0.002 | 0.0075 | 0.015 | 0.025 |

Table 2 – Multi-linear iso-tropic hardening properties

### Carbon

Over the past two decades Fiber reinforced plastic (FRP), also known as fiber reinforced polymer materials have made a rapid transition from being subjects of academic research to being increasingly considered for use in the renewal of civil infrastructure. FRP is a composite material consisting of a polymer matrix reinforced with fibers. Fibers are usually aramid, fiberglass, or carbon, while the polymer is usually a vinylester, polyester thermosetting plastic, or epoxy [1]. Figure 7 shows a stress-strain comparison between steel and various FRPs. It shows that CFRP have similar stiffness to steel, while AFRP and GFRP have lower stiffness compared to steel. Both CFRP and AFRP have high strength compared to GFRP. Comparing the FRP modes of failure against steel, it is clear that all FRP have a brittle failure mode, while steel has its well-known ductile behavior.

Carbon fiber reinforced polymer (CFRP) is a kind of polymer matrix composite material reinforced by carbon fibers. The reinforcing dispersed phase may be in the form of either continuous or discontinuous carbon fibers. Carbon fibers are expensive but they possess the highest specific mechanical properties per weight, such as modulus of elasticity and ultimate strength. Carbon fibers are used for reinforcing the polymer matrix due to their following properties:

- very high modulus of elasticity, exceeding that of steel.
- high tensile strength.
- low density.

Nevertheless, the linear stress-strain characteristics of CFRP up to the failure and lack of yield point have a negative impact on the overall ductility of the strengthened element.
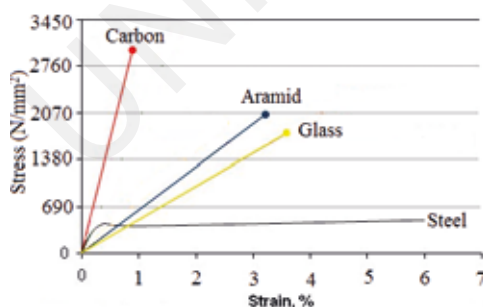


Figure 7 – Comparison of stress-strain behavior of steel and FRPs

Table 3 – Properties of linear and bilinear carbon

|  | Yield stress | Young's modulus | Poisson's ratio | Ultimate stress | Tangent modulus |
|---|---|---|---|---|---|
| Linear elastic carbon | 3600 N/mm2 | 2.4*105 N/mm2 | 0.2 | 1.7 kg/m3 | – |
| Bilinear isotropic hardening carbon | 3600 N/mm2 | 2.4*105 N/mm2 | 0.2 | 1.7 kg/m3 | 0 MPa |

All in all, when total replacement is not an option and traditional retrofit methods are uneconomical and time consuming, an alternative retrofit method using CFRP composite material provide engineers with an effective solution that can increase the life cycle of these bridges. The characteristic for both linear elastic carbon and bilinear isotropic hardening carbon was depicted in Table 3.
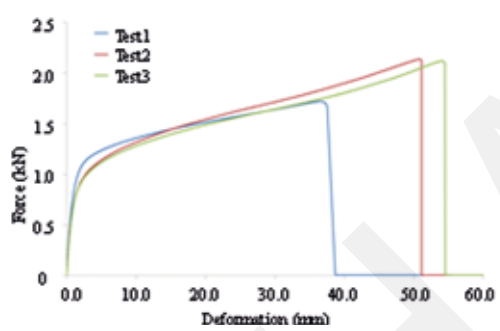
### Glue

Adhesive material (epoxy) was defined in the model to connect the CFRP laminate to the bottom flange of the steel beam. Glue is basically inorganic adhesives. It is a suitable means can join different materials together that may differ in composition, moduli, coefficients of expansion, or thickness. Since bonding does not need high temperatures then it can be the best means for joining heat sensitive materials together [2]. Usually it can be found as a liquid or semi-liquid. This means that their mechanical and viscoelastic properties will be affected by changes in temperature. This effect will largely be dependent on whether the adhesive is a thermoset or a thermoplastic. A successful installation is highly dependent upon careful surface preparation and maintenance of adequate bond conditions.

### Elongation/Strain

As temperature is increased, the tendency is for adhesives to have higher elongation or strain to failure. This is due to the increased mobility of the polymer chains. In this project two kinds of glue were taken into account in terms of short time and long time for three tests. As depicted in following Figure 8 the first glue is named hard glue while the second one is soft glue.
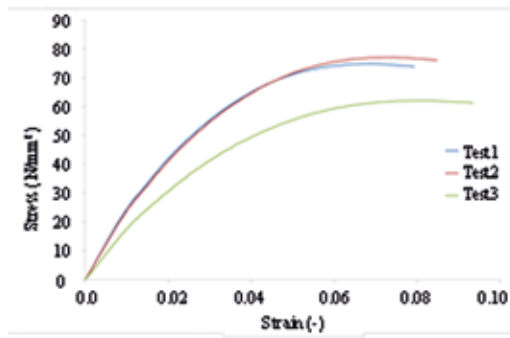
Glue 1-short time test


Glue 2-short time test
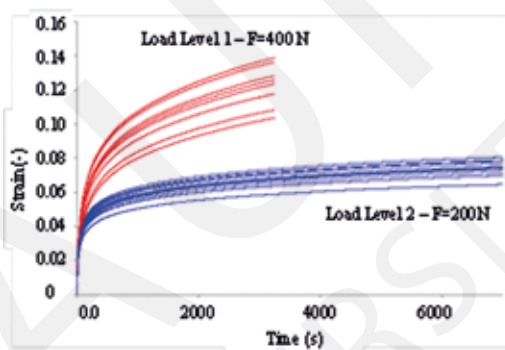

Glue 1-long time test


Glue 2-long time test

Figure 8 – A review of two kinds of glue

In order to correctly evaluate the behavior of glues as incompressible materials there can be used computational models such as Mooney-Rivlin model a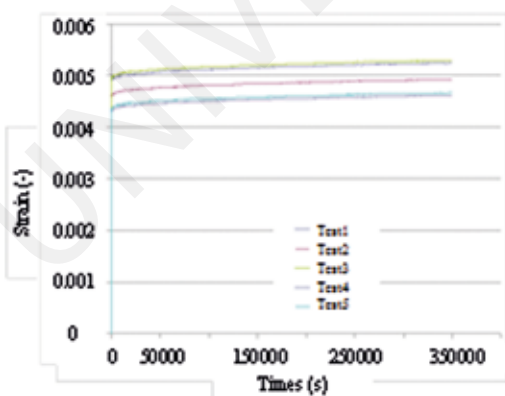nd Ogden model which are the most adequate [5]. Based on the finite element tests parameters for Mooney-Rivlin model were determined. As it has been shown in Figure 9 t he Mooney-Rivlin (3 parameters) was used for glue one while it was nine parameters for glue two. It describes the hyperelastic materials behavior which can endure large elastic deformations. It allows a more accurate examination of the stress distribution throughout the fiber during loading, including the effect of geometric changes.

Figure 9 – Hyper-elastic models for glue 1 and 2
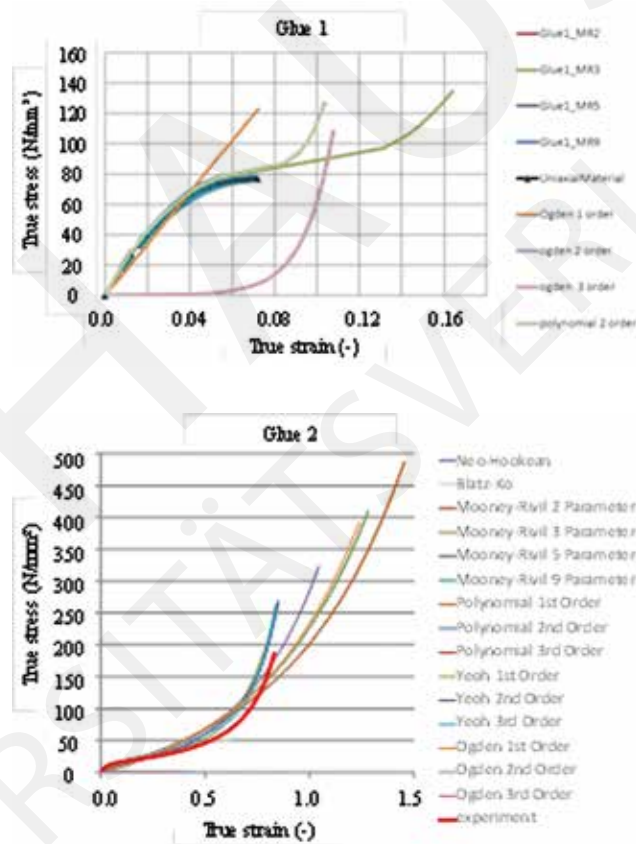
## Analysis of the mode

This study is carried out to analyse the effect of various mentioned materials applied in the bridge on its structural behaviour. FE model (Figure 10) was developed using ANSYS. A total of four and eight CFRP strips were tested as part of the numerical study for estimating of saving cost.



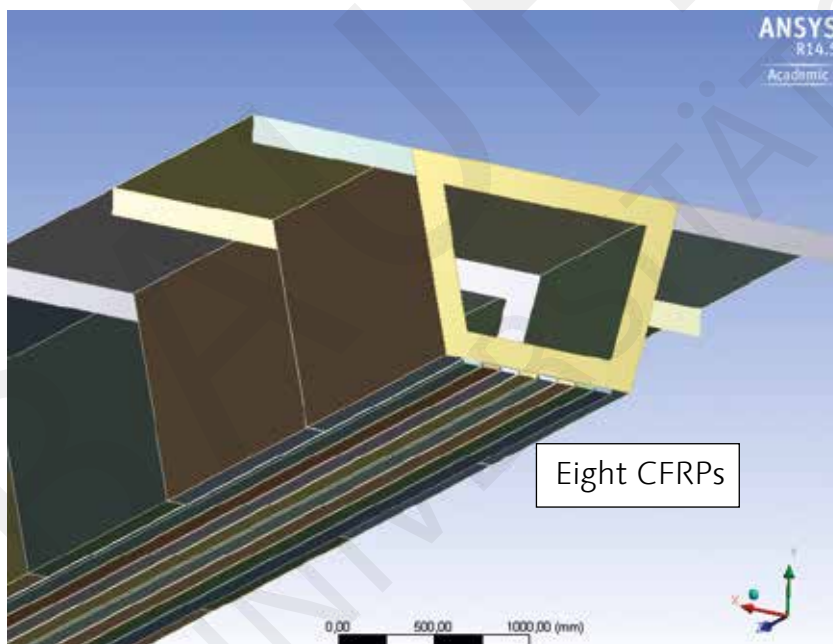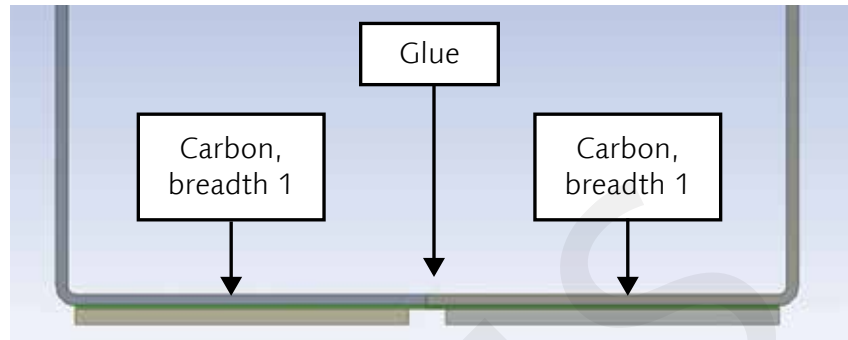Figure 10 – Case study footbridge in Jena and its FE model*



Figure 10 – continuation

Figure 11– Applying materials for optimisation of the model



Reliability analysis have been conducted on a design example to optimize the geometry parameters. The design is mainly considered to meet a deflection. Details of the CFRP strengthening coupled with Glue were shown in Figure 11 and summarized as a Table number 4. All input parameters were optimized to determine their behavior in accordance with output parameters.

An extensive parametric study using the FE model was performed to determine the sensitive parameters affecting the CFRP rehabilitation process. The information in Table number 4 also show that the design methodology used that was based on materials compatibility and laws of the constituent material is effective in predicting the strength and deformation of the bridges. The following table summarizes key output response data based on the input parameters. In other words, design variables optimization and its improvement of materials was used optiSLang process.

Table 4 – Sensitivity analysis between input and output parameters
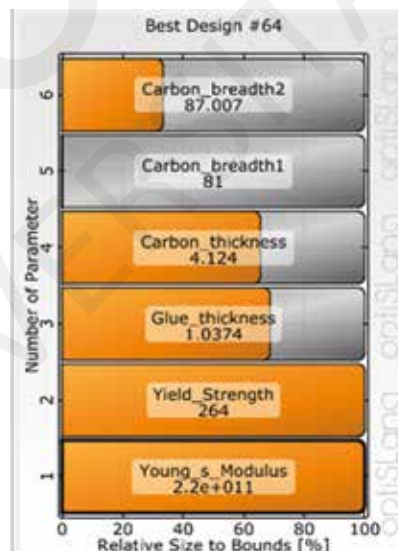


Relative Size to Bounds[%]-
Input Parameters
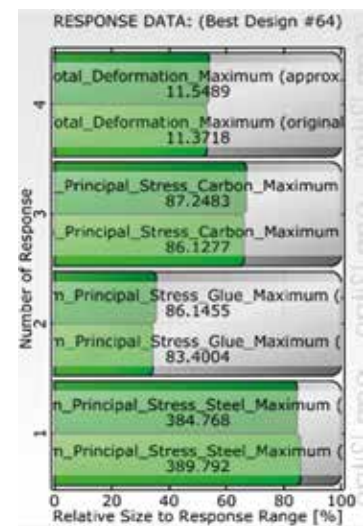
Relative Size to Response Range[%]-
Output parameters

Objective function:
Maximum principle stress,
Maximum deflection

↓

Parameterization of problem-
Defining design materials

↓

Design variables: Young's
modulus, Yield stress, breadth

↓

Solving the problem for
optimization using optiSLang
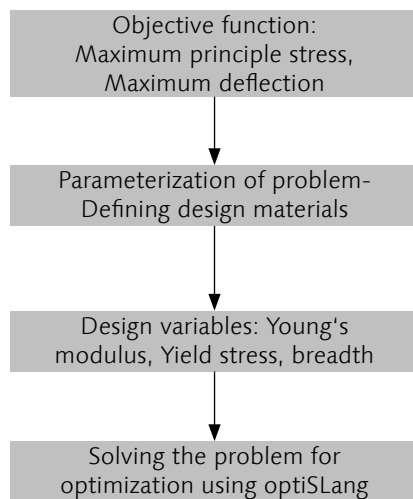
Figure 12 – Materials optimization process

The objective is to minimize the deformation of the bridge keeping it structurally safe under the sever loading.

From an optimization standpoint the Figure 12 shows clearly the process of this project.

## Load models

In general, the load combination is done using dead and live loads to be applied in the design of bridge. In other words for simulating, the actual condition and achieved accurate response, loading pattern is presented. The model was analysed under sever load combination (Table 5) to the characteristics in Table 2 in order to investigate the bridge behaviour in terms of deflection.

| Load | LC1 | LC2 | LC3 | LC4 | LC5 |
|------|-----|-----|-----|-----|-----|
| Dead | * | * | * | * | * |
| People-all (0.01 Mpa) | * | | | * | |
| People-one side | | | * | | |
| Snow (0.0012 MPa) | | * | | | * |
| Wind (0.000391 MPa) | * | | * | | * |
|  | * | | * | | |
| +50 | | | | * | |
| -30 | | * | | | * |

Table 5 – Load combinations

The most critical load combination is the one which subjected to high environmental temperature due to the different thermal expansion coefficient of the materials involved. Utilizing above tables and results of displacement due to presence of carbon and glue in steel bridge it was suggested that bonding of the composite materials have been divided by four and eight carbon strips as developed in Table 6 and 7.

Table 6 – Reinforcement with four carbon strips (%) in Y direction

| Reducing bridge deflection | LC1 | LC2 | LC3 | LC4 | LC5 |
|---|---|---|---|---|---|
| Short term Glue 1 | 21 | 16 | 17 | 34 | 14 |
| Short term Glue 2 | 20 | 13 | 8 | 34 | 12 |
|  | 20 | -30 | 20 | 50 | -30 |

Table 7 – Reinforcement with eight carbon strips (%) in Y direction

| Reducing bridge deflection | LC1 | LC2 | LC3 | LC4 | LC5 |
|---|---|---|---|---|---|
| Short term Glue 1 | 25 | 18 | 22 | 39 | 15 |
| Short term Glue 2 | 24 | 17 | 21 | 39 | 15 |
|  | 20 | -30 | 20 | 50 | -30 |

With respect to above tables reduction of total deformation for four carbon strips in terms of sever loading has been achieved by about 34%. The percentage of the maximum reduction deflection for eight carbon strips was 39%. Therefore, the reduction range from 34% in terms of four strips to 39% for eight strips is not considerable since the materials have been used twice.

Figure 13 depicts deflections at mid-point of the bridge in vertical direction under load combinations due to the high temperature.

Figure 13 – Short term comparison for
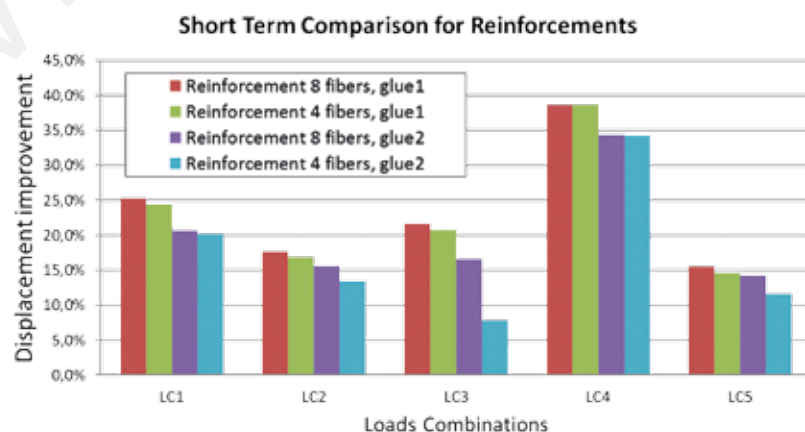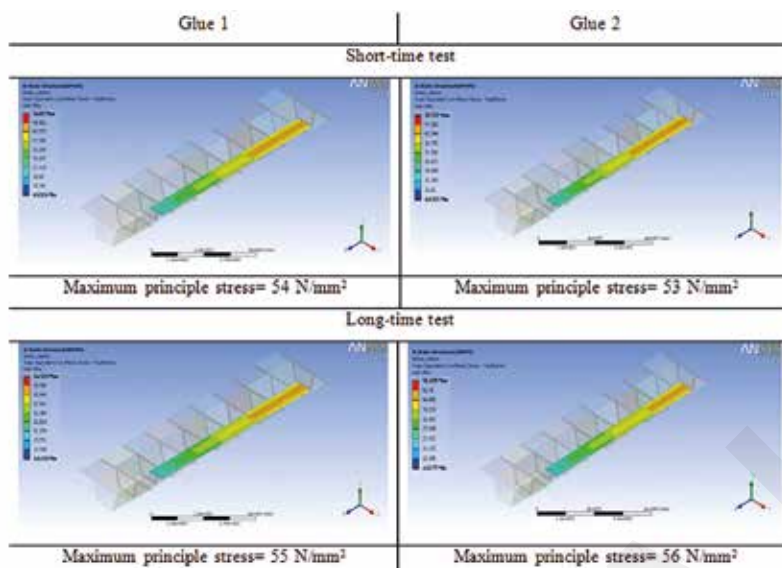


**Short Term Comparison for Reinforcements**

Maximum principle stress with respect to the different glues along the outer surface of the CFRP strips were measured as observed in Figure 14 where composite materials have been used.

## Concluding remarks

The report describes the tasks performed and the design process of steel beam strengthened using CFRP. Discussion of the FE models built to simulate the experimental beams is also presented. Figure 15 shows an isometric view of the three dimensional FE model developed, where each part was meshed separately. This report discussed two topics: first, simulation work of a steel bridge using FE model, and the second part was to evaluate the strengthening of steel girder bridges using CFRP plates. This includes the gain in strength, section modulus, and stiffness of the bridge girders.

data show that the proposed FE model is a good representation in terms of the number of elements, structural details, and in providing reasonably accurate results. Multilinear isotropic hardenin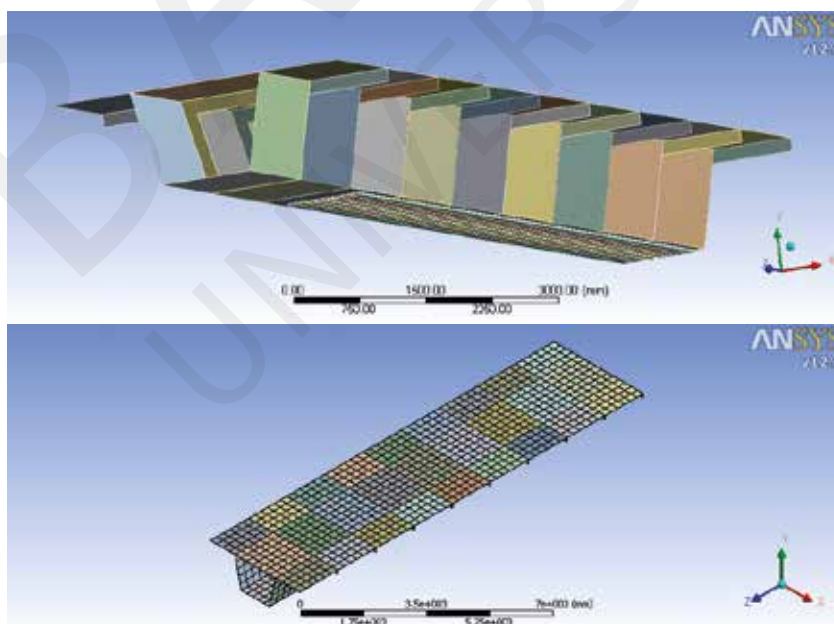g material model preferred due to having similar trend with steel material model. In terms of glue hyperelastic material models has been used to check the responses. The steel bridge was retrofitted using bilinear CFRP with an effective solution which can increase the life cycle of the bridge. Based on the results of this numerical investigation and the abovementioned highlights, the following conclusions can be remarked:

- The steel girder bridge can be improved by using CFRP composite materials which enhanced its behavior.
- Composite materials have shown a long service life, which is considerably longer than that of the primary bridge.
- From the foregoing it can be seen in the results increasing the number of layers improved the maximum moment at failure; however, the reducing of the deflection in eight strips was not increased noticeably (5%) compared with four strips.
- Since the glue yielded quickly as the CFRP strips were loaded; thus, a large ductility in the adhesive for glues was required to achieve a high strain in order to reduce deflection in the CFRP strips.
- The results also indicated that increasing the modulus of elasticity of the CFRP by about 20% could reduce the deflection by as much as 39%.

## References

Salama, T., Abd-El-Meguid, A. (2010). Strengthening steel bridge girders using CFRP. University transportation center for Alabama (UTCA).

Tawfik, Q.H., Karunasena, W. (2010). Use of CFRP for rehabilitation of steel structures: a Review. Southern Region Engineering Conference, 11-12 November 2010, Toowoomba, Australia.

Shield, C., Hajjar, J., Nozaka, K. (2004). Repair of fatigued steel bridge girders with CFRP strips.
University of Minnesota, USA.

Bouafia, Y., Kachi, M.A. (2011). Study of mechanical behavior of concrete in direct tensile fiber chips. ICSAAM 2011, September 7-11, 2011, Bucharest, Romania.

Vlasceanu, D., Gheorghiu, H., Pastrama, S.D. (2011). Experimental determination of the Mooney-Rivlin parameters for hyperelastic materials like rubber. University politechnica of Bucharest, Romania.

BAUMGARTNER, Laurenz
LFU, Innsbruck, Austria

KULIKOFF, Rodrigo de
Oliveira Bresser
EESC-USP School of
Engineering of Sao Carlos
University of Sao Paulo

JÁGER, Bence
BME, Budapest, Hungary

LI, Ke
Tongji Universit, China

MA, Tingting
SLDRCE, Tongji University,
China

ZHIVKO, Nikolov
Risk Engineering Ltd.,
Bulgaria

SHANMUGAM, Narayanan
Bauhaus-Universität Weimar

GEBREMARIAM, Kibreab
Bauhaus-Universität Weimar

HABTEMARIAM, Abinet
Bauhaus-Universität Weimar

# Project 6 – Wind-induced Vibrations of Long-span Bridges

## Abstract

The project will deal with the structural modelling and dynamic analysis of long-span cable-supported bridges under wind excitation.

· Numerical modelling techniques for long-span cable-supported bridges
· Simulation of dynamic structural behaviour
· Models for Predicting Wind-induced Vibrations of Long-span Bridges
· Numerical (CFD) analysis of bridge aerodynamics and dynamic response to wind
· Optimising aerodynamic performance

In the course we will first look at methods of modelling the structural behaviour of such bridges, specifically cable-stayed and suspension bridges, in commercial Finite Element software. The specific focus will be on determining the dynamic properties, like natural frequencies and corresponding mode shapes.

In the next step, various phenomena of dynamic wind excitation will be introduced. These include turbulence-induced buffeting, vortex-induced vibrations and instabilities like flutter.

A Computational Fluid Dynamics (CFD) software will be introduced and applied to determine the aerodynamic properties of bridge decks. These results will be used to assess the wind excitation phenomena using various analytical and numerical methods. Also fully coupled numerical fluid-structure interaction analyses are performed.

Finally, we will look at optimising the structural response through aerodynamic optimisation as well as additional structural damping measures.

MA, Tingting
SLDRCE, Tongji University,
China

ZHIVKO, Nikolov
Risk Engineering Ltd.,
Bulgaria

GEBREMARIAM, Kibreab
NHRE, Bauhaus-Universität
Weimar

# Group 1 – Buffeting Response of the Queensferry Crossing During Construction StageBridge in Construction Stage

## Abstract

The buffeting response of a double-main-span cable-stayed bridge during the longest double cantilever construction stage is analysed. The commercial software SOFiSTiK is adopted in developing the Finite Element (FE) model of the bridge and for subsequent buffeting analysis. The effects of geometric non-linearity and additive attack angle produced by aerostatic loads are included. The research firstly reckoned the instantaneous change in wind attack angle, and modified the aerostatic forces, self-excited forces and buffeting forces. The static wind coefficients used in buffeting analysis are obtained from VXFlow; a code based on vortex particle method.

## Introduction

Nowadays, cable-stayed bridge construction is developing into an extra long-span and flexible phase. The nonlinear time domain

analysis method has therefore become a necessary choice and a developing trend for the refined analysis of bridge buffeting and flutter. For long-span cable-supported bridges, wind-induced vibrations of a bridge deck are classified mainly as buffeting due to wind turbulence and self-excited vibration which depends on the motion of the deck. Buffeting is a kind of stochastic forced vibration and caused by the turbulence existing inherently in natural wind in conjunction with the so-called structural-induced signature turbulence. Hence buffeting is inevitable for any bridge exposed to the natural wind. Cable-stayed bridges, usually applied to cross long spans, are vulnerable to wind loads, especially during the construction stages due to lack of overall structural stiffness. The cantilever construction method is usually employed for the construction of cable-stayed bridges. With the increase of the cantilever length, the structure becomes more and more flexible, which will result in more significant wind-induced vibration. The notable displacement will be dangerous to the staff and machines during construction. Hence, the longest single cantilever and the longest double cantilever are always the most dangerous to wind effects during construction process.

The Qweensferry Crossing is a cable-stayed bridge with three single column towers, wind shielding and a single deck carrying two general lanes of traffic. The lengths of both main spans are 650m. Fig.1 illustrates the general arrangement of the bridge. The most dangerous construction stage for the bridge is the longest double cantilever construction stage, as shown in Fig.2. Therefore the buffeting responses including the displacements and forces are numerically analysed for this construction stage in SOFiSTik.
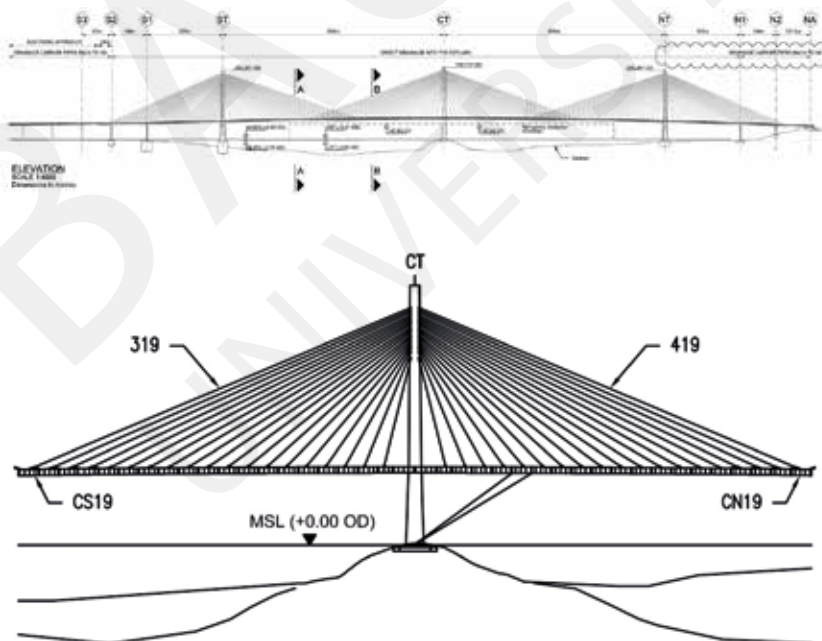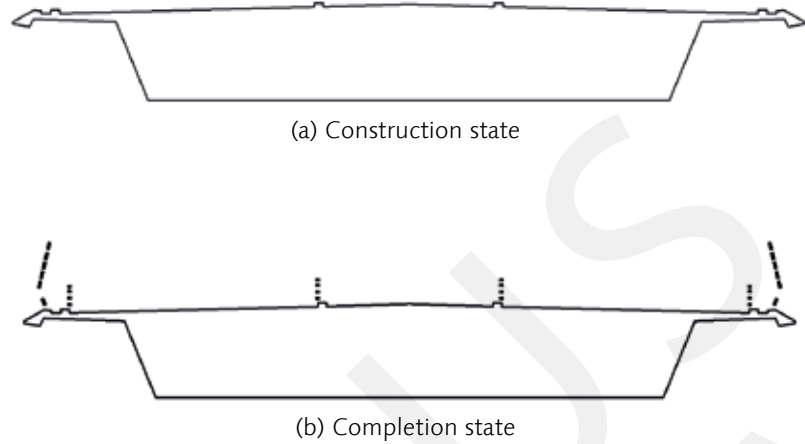


Figure 1 – General layout of the Queensferry Crossing



Figure 2 – Longest double cantilever construction stage of the central tower of the Queensferry Crossing

## Static Wind Coefficients

(a) Construction state



(b) Completion state

$$C_D = \frac{F_D}{\frac{1}{2}\rho U^2 D} \qquad C_L = \frac{F_L}{\frac{1}{2}\rho U^2 B} \qquad C_M = \frac{F_M}{\frac{1}{2}\rho U^2 B^2} \tag{1}$$

Buffeting analysis in SOFiSTiK utilizes the static wind coefficients of the deck section, which are usually obtained from wind tunnel tests or CFD simulation. In this paper, a particle-based CFD code named VXFlow is used to identify the coefficients of the deck section. Static wind coefficients of deck sections for both construction state (without windshields) and the completion state (with windshields) are identified. The configurations of both sections are shown in Fig.3. The mean wind speed in simulation is 10m/s.

The static wind coefficients, including the drag component, lift component and pitching moment component, can be expressed as:

$$C_D = \frac{F_D}{\frac{1}{2}\rho U^2 D} \qquad C_L = \frac{F_L}{\frac{1}{2}\rho U^2 B} \qquad C_M = \frac{F_M}{\frac{1}{2}\rho U^2 B^2} \tag{1}$$

where B and D are the deck width and deck depth, respectively. The static coefficients from VXFlow simulation are shown in Fig.4.

The results are compared with wind tunnel results as well, as shown in Fig.5. The parameters of B and D in Eq.(1) are 4.864m and 39.82m, respectively.

Figure 4. Static wind coefficients of the deck sections
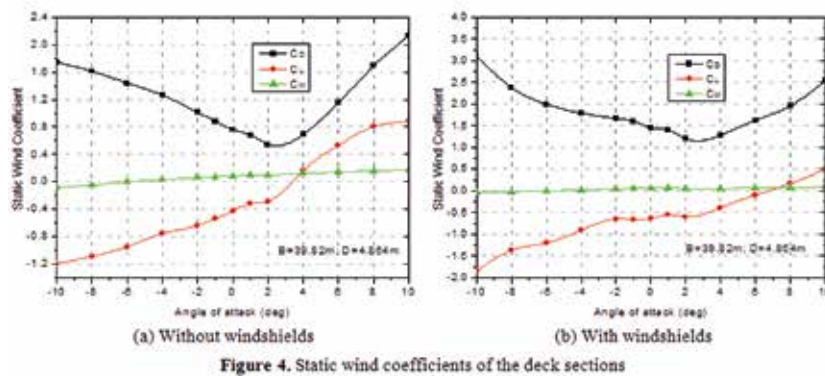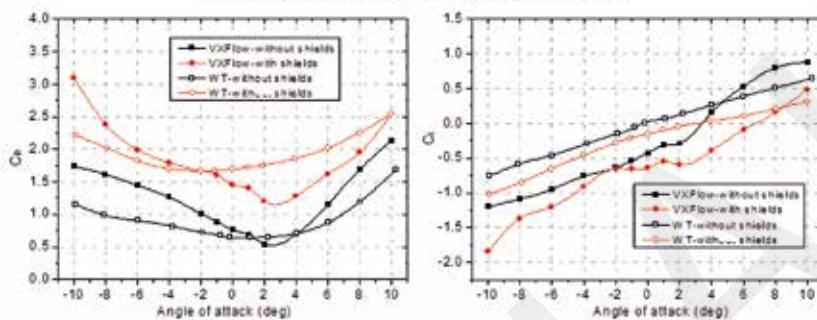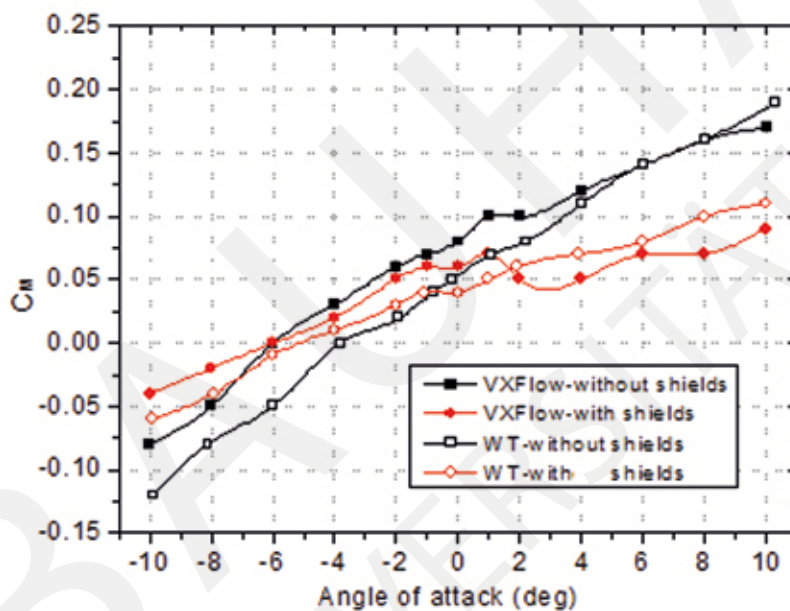
## Buffeting Analysis Results

Based on the static wind coefficients identified in VXFlow, the buffeting response of the longest double-cantilever construction state is analysed. Fig.6 shows the FEM constructed in SOFiSTiK.

Figure 6 – FEM of the longest double cantilever construction state
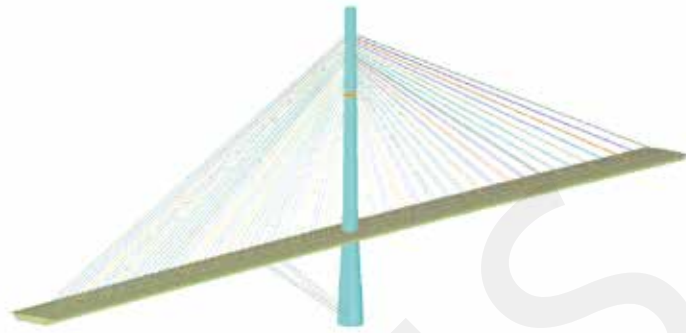


The time history of turbulent wind is simulated in SOFiSTiK based on the von Karman spectrum. The time length is 600s with the time interval of 0.2s. However, considering the unstable state in the beginning of the analysis, a time length of 620s is set for analysis. The mean wind speed of the deck position is 37.9m/s, with turbulence intensity of 10.9%. The effective wave lengths of longitudinal and vertical turbulence are 351m and 29m, respectively. The generated time histories of wind turbulence at the tip of the cantilever are shown in Fig.7 and the corresponding turbulence spectra are compared with von Karman spectrum in Fig.8. The spectrums of corresponding turbulence time history match well with the theoretical ones, which indicates the validity of the simulation.

Figure 7 – Generated time history of wind turbulence
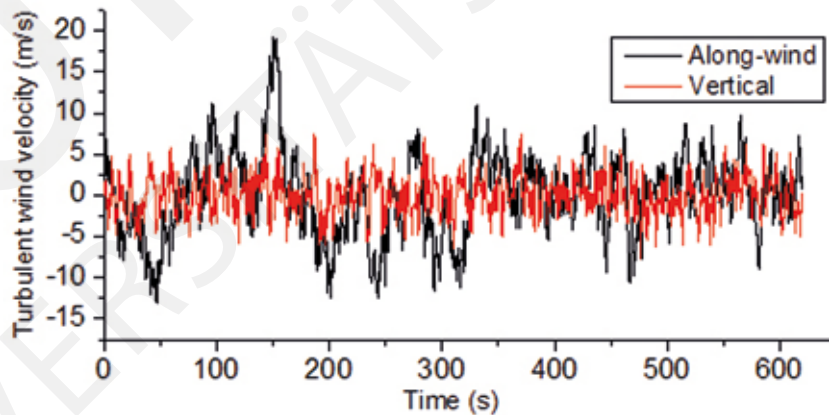


Figure 8 – Comparison of the turbulence spectrums
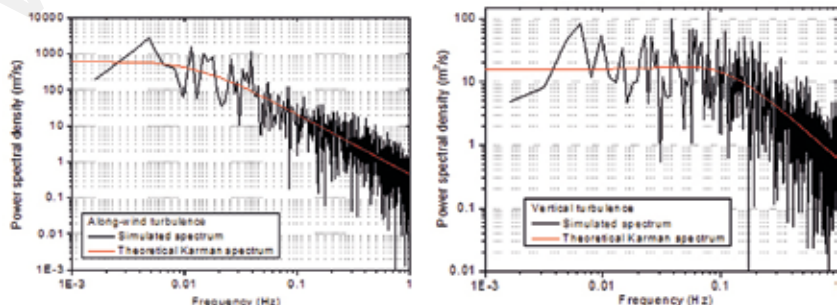
The maximum buffeting displacements of the cantilever are listed in Table 1 and the time histories are shown in Fig.9. In Fig.10. the force histories at the base of the tower are presented and corresponding peak values can be found in Table 2.
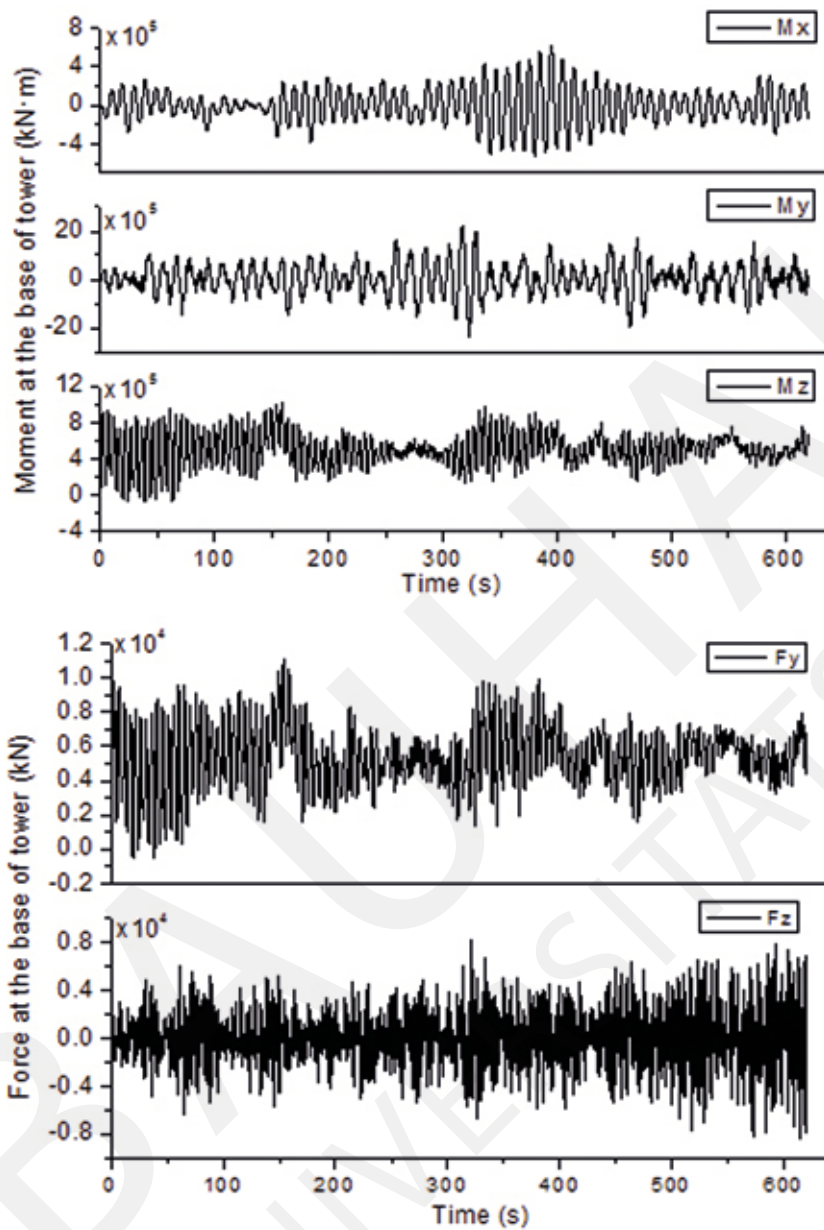


Figure 9 – Time history of the forces at the base of the tower

| Fy (kN) | Fz (kN) | Mx (kN•m) | My (kN•m) | Mz (kN•m) |
|---|---|---|---|---|
| 11060.1 | 8268.8 | 608987.3 | 2403560 | 1019870 |

Table 1 – Peak values of forces

Figure 10 – Time history of the displacement at the tip of the cantilever
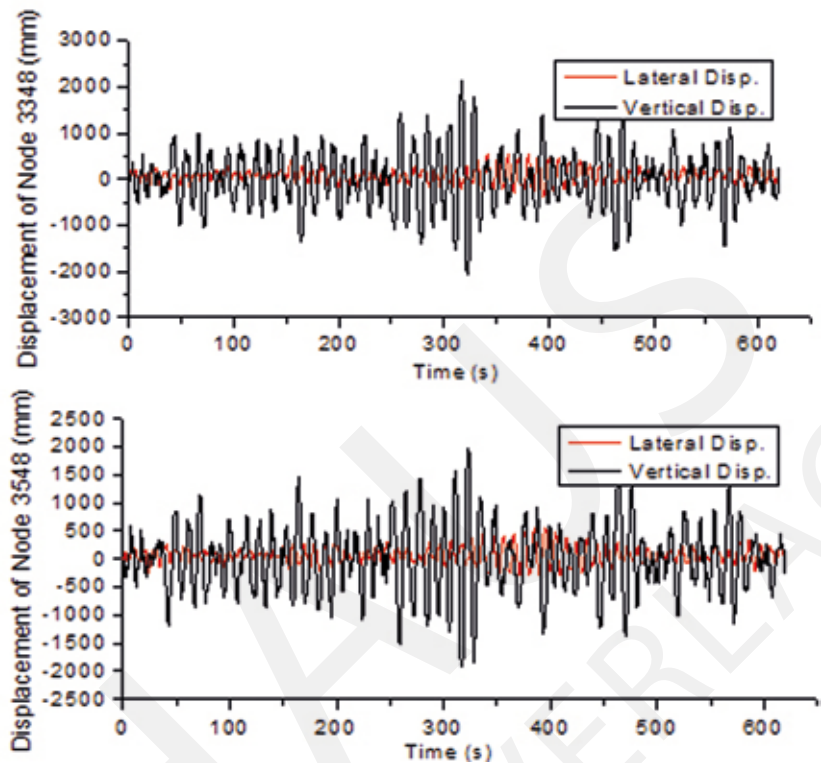


Table 2 – Peak values of displacements at the tip of the cantilever (units: mm)

|  | North tip |  | South tip |  |
|---|---|---|---|---|
|  | Uy | Uz | Uy | Uz |
|  | 556.9 | 2124.9 | 564.7 | 1948.3 |

## Conclusions

Static simulation results indicate that the windshields result in significant increase in drag coefficient, but in general a decrease in lift and moment coefficients. However, the effects of windshields on structural aerodynamics need further investigation. Besides, the static coefficients present similar variation trends toward angle of attack with results from wind tunnel test, which demonstrates the validity of VXFlow in static simulation to some extent.

Although some cables are employed for buffeting control, the buffeting response at the tip of cantilever reaches larger than 2m in vertical. Maybe more effective buffeting control method, such as the temporary piers or tuned mass dampers (TMD), is needed.

## References

Chen X.Z., Kareem A. (2002): Advances in Modeling of Aerodynamic Forces on Bridge Decks[J]. Journal Of Engineering Mechanics,  2002 :1193-1205.

Livesey F.M. Larose G.L. (1996): The Pont de Normandie during construction, aeroelastic modelling of behavior.
Journal of Wind Engineering and Industrial Aerodynamics, 1996, 65: 203-215.

Morgenthal, G. (2012): "VXflow Primer" version 0.994, Weimar, Germany.

Morgenthal, G. (2002): "Aerodynamic Analysis of Structures Using High-resolution, Vortex Particle Methods", PhD Dissertation, Departament of Engineering, University of Cambridge, UK.

Zhu L.D., Wang M., Wang D.L. (2007): Flutter and Buffeting performances of Third Nanjing Bridge over Yangtze River under yaw wind via aeroelastic model test[J]. Journal of Wind Engineering and Industrial Aerodynamics, 2007, 95: 1579-1606.

LI, Ke
Tongji Universit, China

HABTEMARIAM, Abinet
Bauhaus-Universität Weimar

SHANMUGAM, Narayanan
Bauhaus-Universität Weimar

# Group 2 – Flutter Analysis of the Proposed Runyang Bridge

## Abstract

The aim of this paper is to investigate the flutter behaviour of the proposed Runyang Bridge by analytical calculation and CFD model (VXflow). Also the analytical and CFD results are compared with the experimental wind tunnel test to validate the computational results. These kind of aerodynamic studies are essential for slender bridges. The flutter and aerodynamic properties can be improved by modifying the original section geometry.

Figure 1 – The Runyang suspension Bridge in china

## Introduction

The proposed bridge for the study is a suspension bridge with a main span of 3000m. The height of the tower is 400m. The width of the main girder is 35m and the depth of the main girder is 3m. The cross section of the bridge is adopted from the Runyang Bridge which is in China.

Flutter is a self-excited oscillatory instability, which is caused when aerodynamic forces supply energy to the oscillating structure and amplitude of the motion progressively increases. This behaves as "negative damping" and it occurs at any wind speed higher than a critical value, which is known as flutter limit. Classical flutter is an aerodynamic phenomenon in which rotation and vertical translation couple together in a flow-driven, unstable oscillation. In this case the negative aerodynamic damping occurs and deformations reach such a level that failure happens.

## Wind Tunnel Test

For the determination flutter derivatives wind tunnel test is carried out on the scaled (1:75) cross section of Runyang Bridge. During the wind tunnel test the critical wind speed is measured as 15m/s. The flutter derivatives obtained from the test were compared with the CFD analysis.
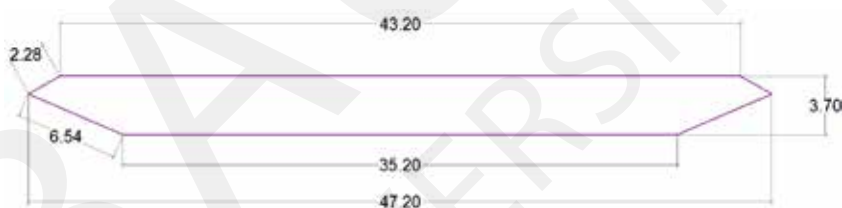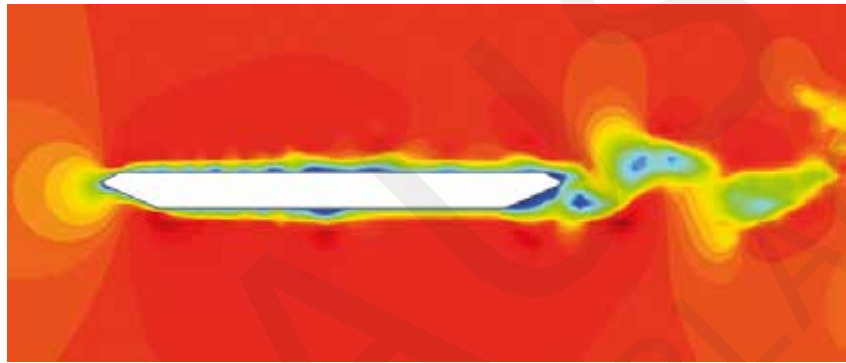


Figure 3 – The cross sectional dimension of the bridge used during the wind tunnel test (cm)

## Static Analysis

Table 1 – Static wind
coefficient results

| Coefficient | |
|---|---|
| CL | 0.002 |
| CD | 0.361 |
| CM | 0.016 |

Figure 4 – Visualization of
static analysis with VXflow



The aim of this paper is to investigate the flutter behaviour of the proposed Runyang Bridge by analytical calculation and CFD model (VXflow). Also the analytical and CFD results are compared with the experimental wind tunnel test to validate the computational results. These kind of aerodynamic studies are essential for slender bridges. The flutter and aerodynamic properties can be improved by modifying the original section geometry.

## Flutter Stability Analysis

In order to check the flutter stability of the bridge, forced vibration test is used to get the eight flutter derivatives ( in Eq. 1) of the cross section $H_1{}^*$~$H_4{}^*$ and $A_1{}^*$~$A_4{}^*$                                                  .

$$F_{se} = \begin{cases} L_{se} = \frac{1}{2}\ piU^2B \left( KH_1{}^*(K)\frac{h}{U} + KH_2{}^*(K)\frac{Ba}{U} + K^2H_3{}^*(K)alpha + K^2H_4{}^*(K)\frac{h}{B} \right) \\ M_{se} = \frac{1}{2}\ piU^2B^2 \left( KA_1{}^*(K)\frac{h}{U} + KA_2{}^*(K)\frac{Ba}{U} + K^2A_3{}^*(K)alpha + K^2A_4{}^*(K)\frac{h}{B} \right) \end{cases} \tag{1}$$

The oscillations in vertical and torsional direction have been simulated in VXflow separately (Details are shown in Tab. 2). Vortex particle method has been adopted and the results are compared with flutter derivatives which are got in theoretical solution of flat plate (solution of Theodorsen expression) and in wind tunnel test (details are shown in Fig. 5 and 6).

| | Amount of vortex particle | Flutter derivatives in Scanlan expression | | | | | | | |
|---|---|---|---|---|---|---|---|---|---|
| | | Vertical forced vibration | | | | Torsional forced vibration | | | |
| | | $H_1^*$ | $H_4^*$ | $A_1^*$ | $A_4^*$ | $H_2^*$ | $H_3^*$ | $A_2^*$ | $A_3^*$ |
| 2 | | -0.72 | 1.22 | 0.30 | -0.02 | -0.53 | -0.40 | -0.05 | 0.12 |
| 6 | | -3.79 | 0.18 | 0.88 | 0.18 | -1.70 | -3.56 | -0.34 | 0.96 |
| 10 | $2.1 \times 10^5$ | -7.24 | -1.02 | 1.69 | 0.45 | -2.49 | -10.51 | -0.80 | 2.94 |
| 15 | | -10.89 | -1.47 | 2.68 | 0.59 | -2.43 | -23.35 | -1.35 | 6.53 |
| 20 | | -11.58 | -2.72 | 3.76 | 0.60 | -2.87 | -41.55 | -2.50 | 11.99 |
| 22 | | -16.23 | -2.39 | 4.40 | 0.89 | -1.97 | -50.23 | 14.97 | -2.98 |

Although there are some differences between the data from CFD and wind tunnel test, the simulation of the most important $H_1^*$ and $A_2^*$ is good and the tendency of the computed flutter derivatives fit well with the wind tunnel test. Since the cross section is similar to flat plate and the vibration mode near flutter critical wind speed would be in two degree, coupled flutter analysis is adopted in the latter content.

Table 2 – CFD simulation result of flutter derivatives
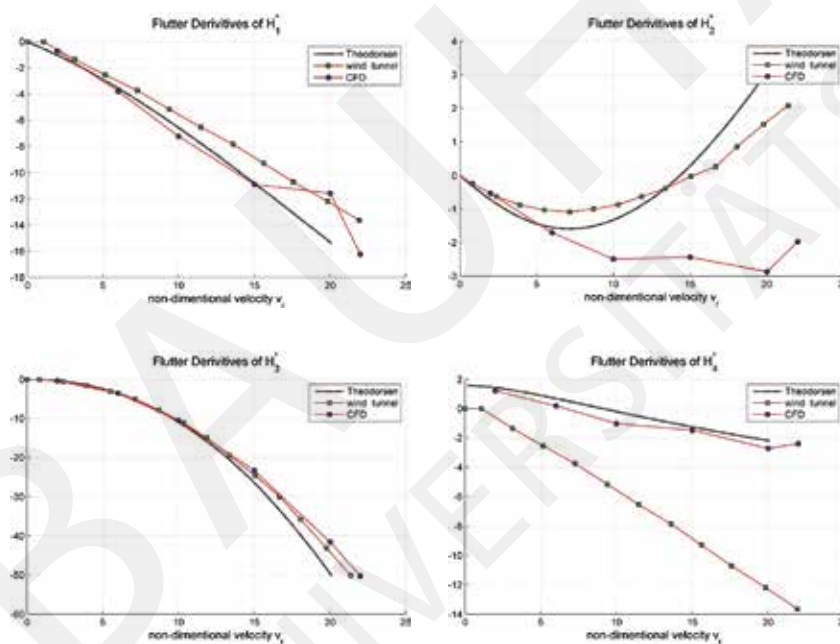
Figure 5 – $H_1^*$, $H_2^*$, $H_3^*$, $H_4^*$ comparison

Figure 6 – $A_1^*$, $A_2^*$, $A_3^*$, $A_4^*$
comparison
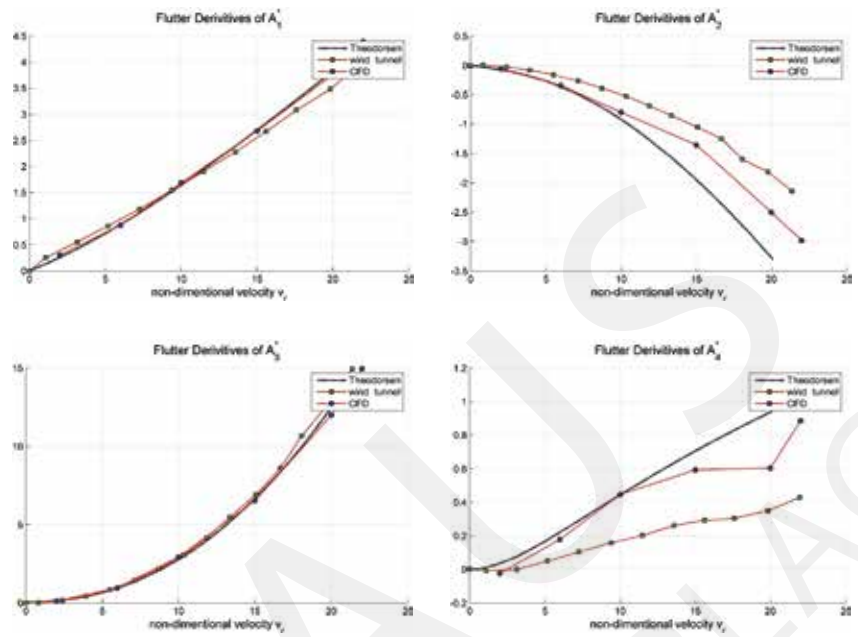


To get the flutter critical wind speed of this bridge, both of the structural dynamic characteristics of the bridge (details in Tab. 3) and the aerodynamic characteristics of the girder are needed.

As the wind speed increases, the modal characteristics change (details in fig. 7). When one of the modal damping ratios turns negative, this mode becomes instable. It will lead a diverging oscillation and the bridge will be in great danger. In this case, the cross section is streamlined and the diverging mode will be in coupled state which means the bridge will collapse, if no countermeasures are utilized when the wind velocity reaches the flutter critical wind speed, after a period of strong vibration in both heaving and pitching directions.

Table 3 – Structural dynamic
characteristics of the bridge

| Mode type | Modal damping ratio | Modal frequency | Modal mass / mass of inertia |
|---|---|---|---|
| 1st vertical mode | 0.5% | 0.071Hz | 40.09t/m |

Figure 7 – Modal damping ratio and frequency change along wind speed

Simulations of the girder vibration near flutter critical wind speed are also completed (details in Fig. 8, 9 and 10).
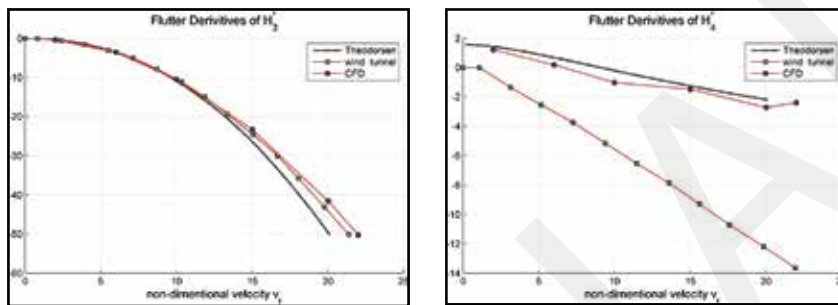


Figure 8 – Torsional and vertical vibration when U =
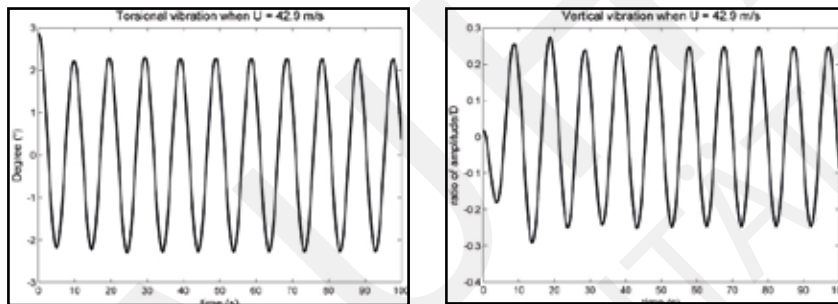


Figure 9 – Torsional and vertical vibration when U = 42.9m/s



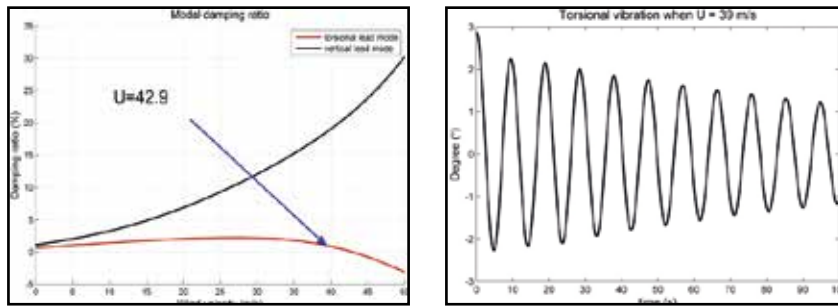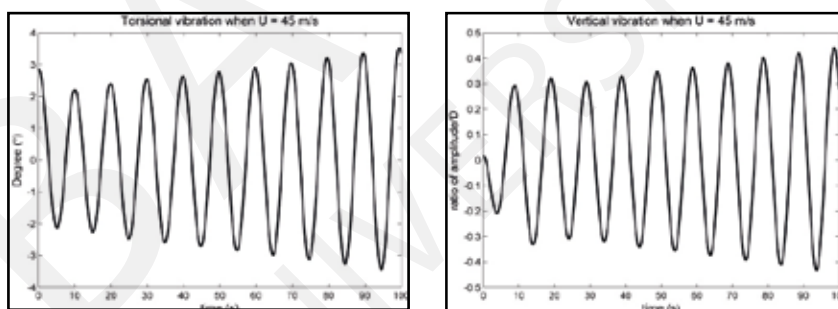Figure 10 – Torsional and vertical vibration when U = 45m/s

## Dynamic Analysis

For the dynamic analysis, we had used the sliced cross section of scaled wind tunnel model (of the Runyang bridge) which is shown in Fig.3 to determine the critical flutter wind speed using VXFlow. Appropriate scale factors are used to obtain the mass and stiffness matrix for the scaled wind tunnel model to scale down from the real bridge.

Table 4 – Critical wind speed associated to flutter instability

| Wind speed m/s | Bridge Depth Ratio | Stability phenomenon |
|---|---|---|
| 6 | 0.62 | Stable |
| 8 | 1.03 | stable |
| 9 | 1.16 | stable |
| 10 | 2.35 | stable |
| 12 | 3.03 | Instable (flutter wind speed) |
| 13 | 5.49 | instable |
| 15 | 6.11 | inst |

## Flutter Stability Analysis

In order to check the flutter stability of the bridge, forced vibration test is used to get the eight flutter derivatives ( in Eq. 1) of the cross section                                   .

The critical flutter wind speed limit of scaled bridge model is determined based on the vertical displacements for the given wind speed. The critical flutter wind speed is determined to 9 m/s, as the displacements are small at the initial time steps and it increases with the increase in time for this wind speed. Using the corresponding scale factor, the critical flutter wind speed for the real bridge is determined as 45 m/s.

Figure 11 – Vertical displacements (for U=12
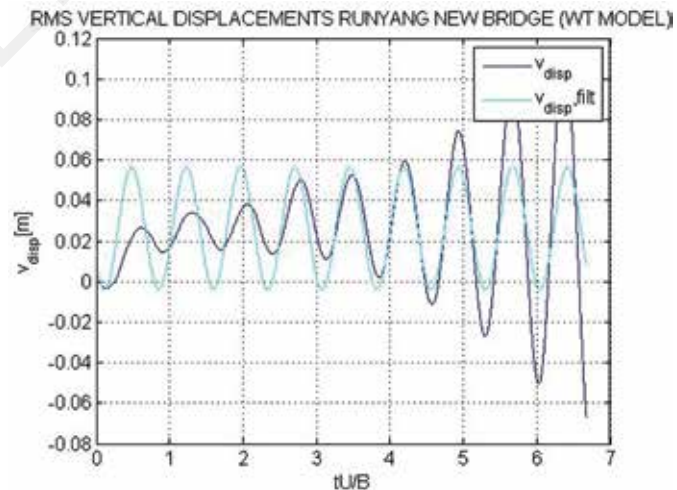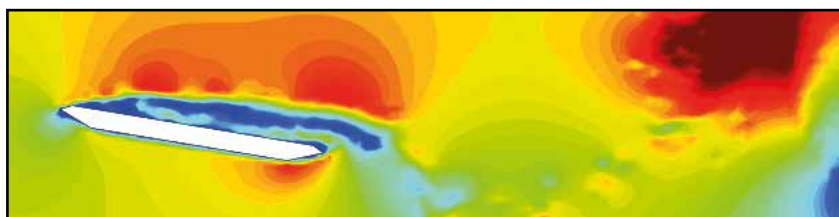
Figure 12 – Visualization of dynamic simulation for wind tunnel model with VXFlow

| Method of analysis (for real bridge) | Critical flutter wind speed (in m/s) |
|---|---|
| Theodorsen flat plate analysis | 43.8 |
| Forced vibration analysis - VXflow | 41.4 |
| Wind tunnel test (WTT) | 40.9 |
| Dynamic analysis – Real bridge | 45.0 |

Table 5 – Comparison between Critical wind speeds obtained from different analysis.

## Conclusions

The Bridge model had been analysed for the phenomenon of flutter instability with VXFlow by Forced Vibration and dynamic analysis. From the static analysis coefficients of drag, lift and moment are determined. Also the critical flutter wind speed for the real bridge and scaled wind tunnel model was determined and in following table critical flutter wind speed from forced vibration and dynamic analysis are tabulated:

From the above results, it can be concluded that critical flutter wind speed obtained from VXFlow & wind tunnel test are almost similar and the critical flutter wind speed obtained from dynamic analysis is comparatively higher.

## References

Abbas, T., Flutter analysis of suspension bridges using a two-stage numerical approach & flutter derivatives, Masters Thesis, 2011

Morgenthal, G. "VXflow Primer" version 0.994, Weimar, Germany, May 2012

Morgenthal, G. "Aerodynamic Analysis of Structures Using High-resolution Vortex Particle Methods" PhD Dissertation, Departament of Engineering, University of Cambridge, UK, Oct. 2002.

Scanlan R.H. Airfoil and bridge deck flutter derivatives. J. Eng. Mesh. Div.

Xiang H F, Ge Y J. On aerodynamic limit to suspension bridges. In: Proceeding of the 11th International Conference on Wind Engineering, Texas, USA: 2003.

BAUMGARTNER, Laurenz
LFU, Innsbruck, Austria

JÁGER, Bence
BME, Budapest, Hungary

KULIKOFF, Rodrigo
USP, São Carlos, Brazil

# Group 3 – Analysis of the Vortex Shedding Effect on the Alconétar Bridge in Construction Stage

## Abstract

In the frame of the Project Work our task was to analyse the vortex shedding effect on the Alconétar bridge in construction stage by using VXFlow. The main problem of this topic is that during the construction stage, when the arches were implemented without any vertical pillars on it, the second eigenmode was observed as vibration of the arches caused by a certain wind speed.

Figure 1 – Alconétar bridge

The aim of this study is to determine this certain wind velocity in which this vibration mode occurs. For the determination of the wind velocity related to this oscillation we have used a numerical method called Vortex Partial Method.

The analysis of the effect of the deflectors, which were applied on the structure against oscillation, will be performed after the determination of this certain wind speed. Using numerical calculation we can compare the results receiving from these two numerical models and also we can compare the results with the measured values.

## Introduction

Arcos de Alconétar is a bridge over the river Tagus located at a region of Spain called Alcantara Reservoir. It is a steel deck arch bridge with 220 meters span consisting of two arches formed by longitudinal box sectioned parts connected with a bracing system.

During the construction heavy harmonic oscillations occurred due to constant but low wind speed. The measured vertical displacement was about 40 centimetres.
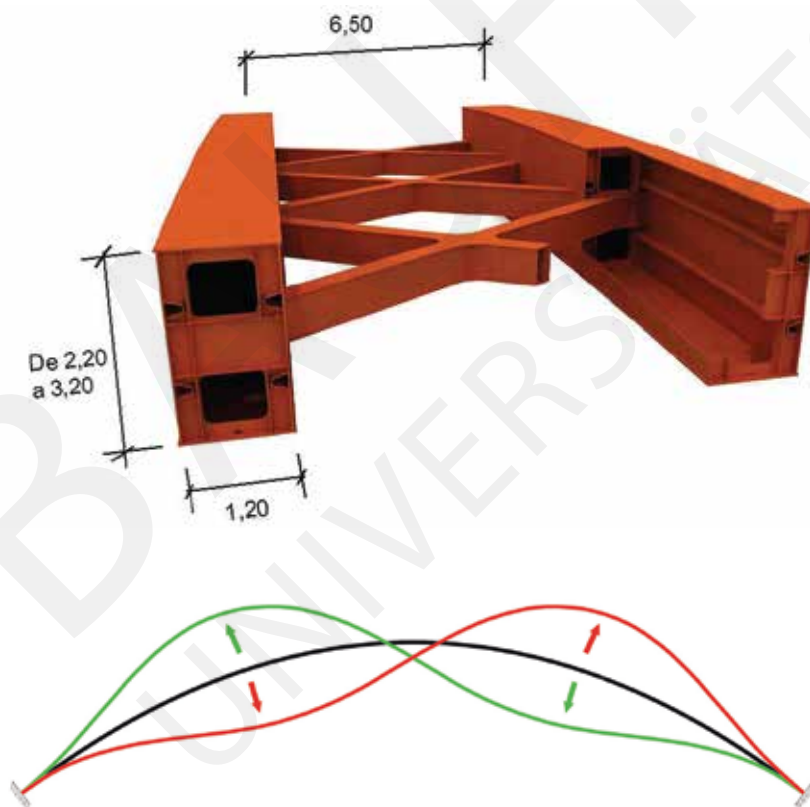


Figure 2 – Cross section of the arch



Figure 3 – Second vibration mode

Later studies showed that the vibration was caused by vortex shedding whose period coincided with the structure's second mode. To avoid such oscillation in the construction phase wind deflectors were applied on the steel structure to change the air flow's trajectory and suitably channel it to prevent vortex formin.

Figure 4 – Deflectors on the Alconétar bridge



Figure 5 – Detail of Deflectors

## Vortex-Shedding Excitation

The natural vibration frequency of the bridge depends on several factors for example mass, stiffness and damping. The vortex shedding frequency is a function of the height of cross section (D) and wind speed (U∞).

$$f_v = (0.8 - 1.2) f_n \quad (1)$$

If the vortex shedding frequency is close to one of the natural frequencies of the structure then lock-in phenomenon can happen. This phenomenon can cause resonance in a narrow range of wind speed. The Strouhal number is defined as follows:

$$St = \frac{fD}{U} \quad (2)$$

The vortex vibration phenomenon is caused by eddies on the "leeward side" of the cross section. This phenomenon is a self-limited phenomenon because the amplitude of the resonance can reach a limited value which could be between D and D/2 where D is the depth of the cross-section but it can be very dangerous from serviceability and from fatigue points of view.

## Numerical Mode

Vortex Particle Method is a Lagrangian Method and the program to perform the simulations is VXFlow. This program allows very efficient simulations of two-dimensional flows around bodies of arbitrarily complex geometry and arrangements

Cross Sections:
The cross section model does not have any braces. The cross sections models are shown in the Figure 4 and Figure 5.
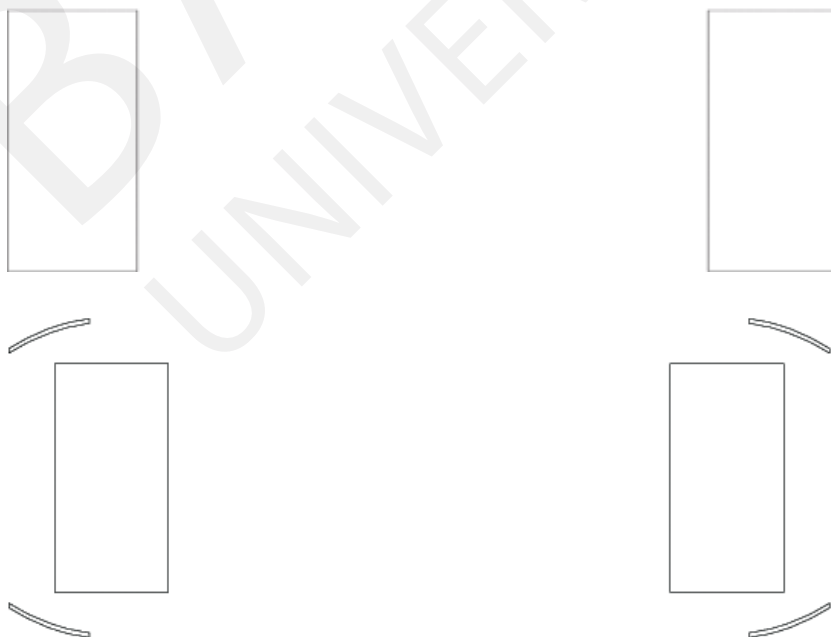


Figure 4 – Cross section (A)

Figure 4 – Cross section with deflectors (B)

## Analysis

**Static Simulations:**
Firstly the static simulation has been performed with cross section (A) in order to determine the dominant vortex shedding frequency. In this case the section is fixed. The flow interacts with the structure and it generates the vortex. The dominant vortex shedding frequency must be identified in order to determinate the critical wind speed for lock-in phenomenon. As shown in Figure 6 the maximum lift coefficient CL occurs with a Strouhal number of                .

Figure 6 – Spectral density of CL for static simulation, cross section (A)
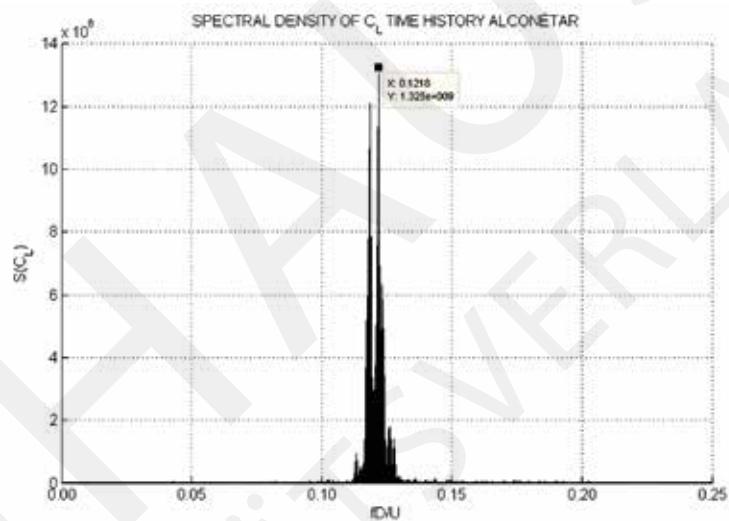


By using the definition of the Strouhal number the critical wind speed for the lock-in phenomenon can be determined. With the knowledge of the approximated critical wind speed dynamic analysis can be performed.

$$St = \frac{fD}{U} => 0{,}1218 \, \frac{0{,}7 * 2{,}41}{U} <=> U = 13{,}85 \text{ m/s} \quad (3)$$

**Dynamic Simulations:**
For dynamic simulation the range of wind speed was set from 8 to 18 m/s. For each wind velocity parameters were calculated for cross section (A). The Figure 7 shows the arrangement of vortex particles for a wind speed of 15 m/s.

Figure 8 shows the lift coefficient of cross section (A) at the critical wind speed of 15 m/s. It is easy to distinguish that the lift coefficient for the bare cross section is very regular and therefore the bridge can be easily excited due to low wind speed. The reason for this behaviour depends on the simple shape of the cross section.
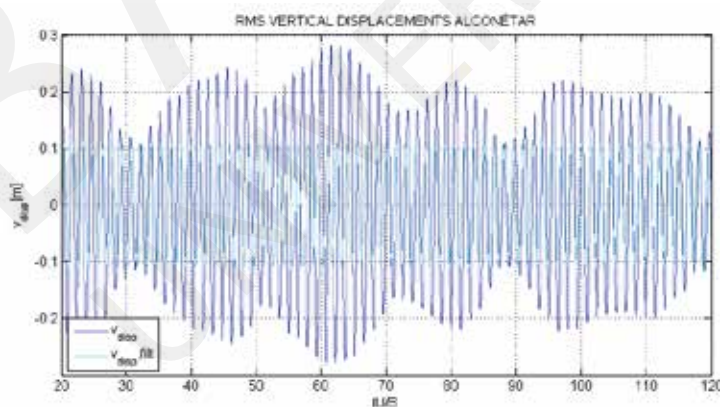
The results of vertical displacement are presented in Figure 9. The dark line stands for displacement time history by using several frequencies. The line in light blue is the RMS displacements time history, which is obtained by filtering the displacements time history by using the natural frequency of the bridge. For this cross section the average vertical displacement is around 20 cm.

## Simulations of improved cross section:

### Static Simulations:
To reduce the oscillation due to vortex shedding the proposed solution is applying deflectors on the girders. Therefore static and dynamic analysis was performed for cross section (B).

Figure 10 – Spectral density of CL for static simulation, cross section (B)
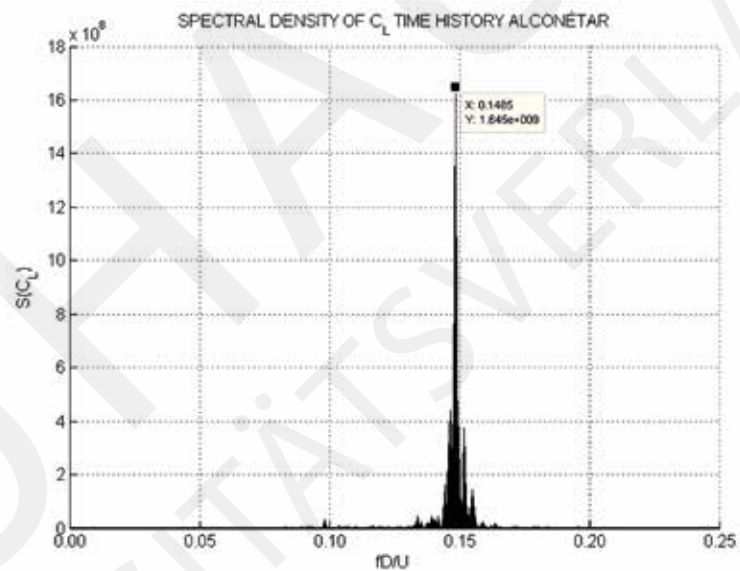


Out of the Strouhal number which results 0.1485 then the critical wind speed can be determined again.

$$St = \frac{fD}{U} => 0,1485 \frac{0,7 * 2,41}{U} <=> U = 11,36 \text{ m/s} \quad (4)$$

### Dynamic Simulations:
For dynamic simulation the same range of wind speed was chosen such as for the cross section (A). Again for each wind speed parameters were calculated for the cross section (B). Comparing the Figures 7 and 11, the vortex shedding formation is much higher in the cross section (A) than in the cross section (B) because of the chanalising effect of the deflectors.
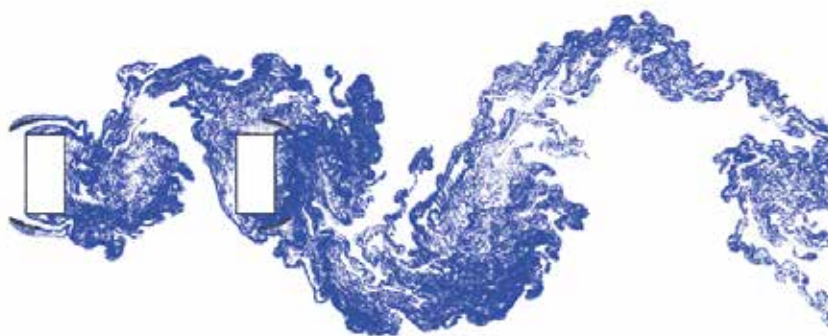
Figure 11 – Vortex shedding, cross section (B), U∞ = 9 m/s

In this case, the amplitude of the lift coefficient curve is more varying than in the case of cross section (A). It can be assumed that applying deflectors has a positive effect on the maximum displacement.
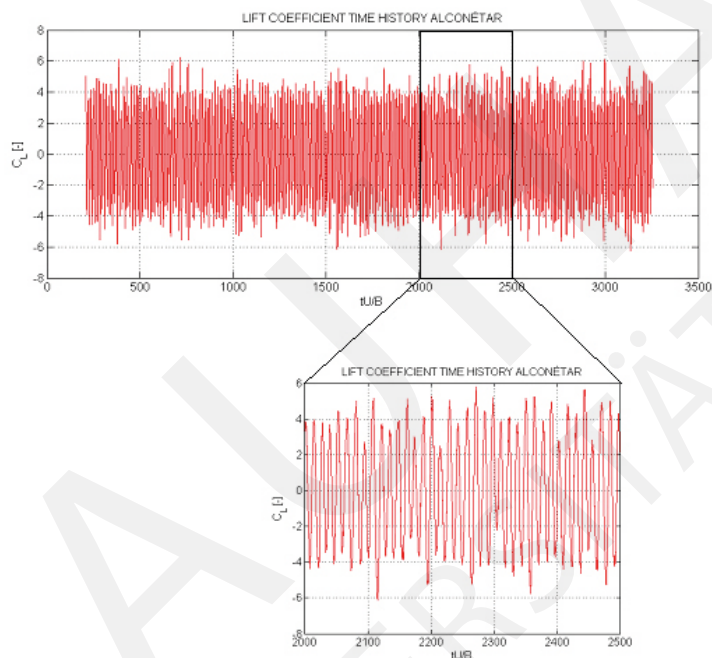


Figure 12 – Lift coefficient of cross section (B)

The results of vertical displacement of cross section (B) are shown at the figure 13.
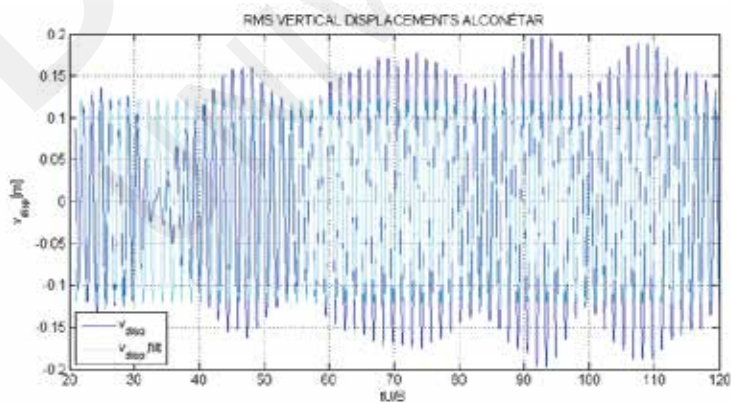


Figure 13 – Vertical displacement of cross

Figure 14 – Graph of
maximum displacement
versus wind speed
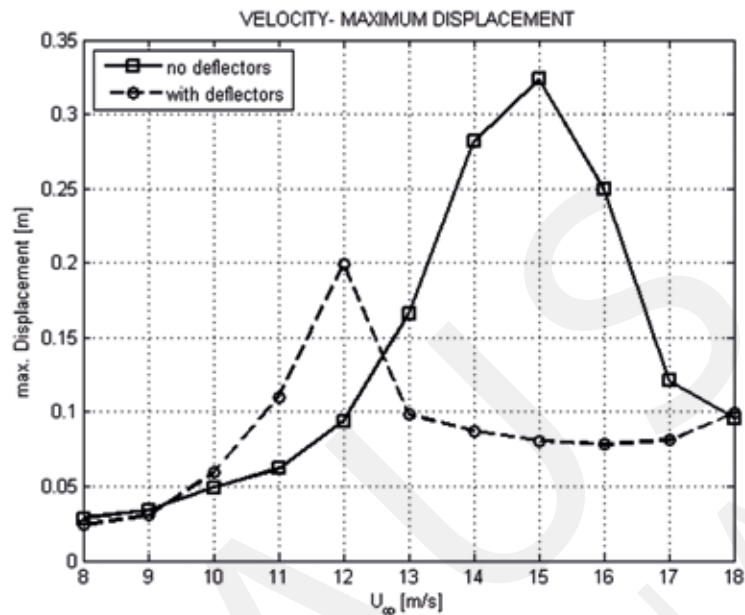


The average vertical displacement amplitude of the cross section
(B) is approximately 15 cm and it is smaller than the obtained for
the cross section (A).

The deflectors applied on the bridge change the aerodynamic
behaviour of the cross section and have a positive outcome on
various parameters. The Figure 14 shows that by using deflectors
the value of the maximum vertical displacement is reduced.

The maximum displacement of the cross section (A) is 33 cm
while this value obtained from the cross section with deflectors
is 20 centimetres. This is a good approximation of the measured
displacement of the cross section, which was about 40 cm. The
application of deflectors on the bridge has also reduced the wind
speed peak from 15 m/s to 12 m/s. This reduction of wind velocity
can be considered as a disadvantage since low wind speeds are
used to be more frequent.

## Conclusions

The arch of Alconétar Bridge showed a large displacement due to low but constant wind speed which excited the arch in their second eigenmode. After static analysis the critical speed was determined to 14 m/s and the range of wind velocity was chosen for dynamic analysis. As assumed there were high amplitudes of displacement for constant wind speed, the resonance phenomenon was observed for a wind speed of 15 m/s.

In order to improve the aerodynamic behaviour of the Alconétar Bridge deflectors were utilized to change the air flow´s trajectory. The study showed that the application of deflectors results in lower amplitudes of displacement and therefore it is a good method to face the problem.

Instead of reducing the amplitude by changing the shape of the cross section such as it was performed in this paper, there are also others possibilities like tuned mass dampers and active flaps, which avoid the creation of vortex.

## References

Morgenthal, G. (2012): "VXflow Primer" version 0.994, Weimar, Germany.

Simiu, E., Scanlan, R. (1996): "Wind Effects on Structures" John Wiley & Sons, Inc., New York, USA, Chaps. 6 and 14.

Jaques, J.A.L., Fort, J.R., Wörner, S.C. (2006): "Bridge over the river Tagus at Alcántara Reservoir Arcos de Alconétar", no 242, 4.° Trimester.

Morgenthal, G. (2002): "Aerodynamic Analysis of Structures Using High-resolution, Vortex Particle Methods", PhD Dissertation, Departament of Engineering, University of Cambridge, UK.

# Papers Contributed by the Participants

To read the reports in full go to: https://www.uni-weimar.de/summerschool/archiv

ABADIAS, David
Researcher engineer at
CIMNE

# Design of gravity-base sub-structures for offshore wind turbines in intermediate waters

## Abstract

In this Project, techniques for strengthening steel bridge in Jena (Thuringia, Germany) have been employed using carbon fiber reinforced polymers (CFRP). The CFRP plates were selected due to their outstanding mechanical characteristics, non-corrosive nature, and relative ease of application. The need for economical and fast rehabilitation solutions reflects the importance of using CFRP as a repair material. This Bridge was strengthened by installing CFRP plates to the bottom flange of steel girders in the positive moment regions. The strengthening system consists of preparation of the bonding surface and installing the CFRP plates to the beam surface with a high strength epoxy adhesive for the transfer of force to the high strength CFRP plates. Nonlinear finite element analysis software, ANSYS, and software optiSLang were used to verify and evaluate of the rehabilitation technique.

Figure 1 – Thornton Bank GBS (Peire et al, 2009)
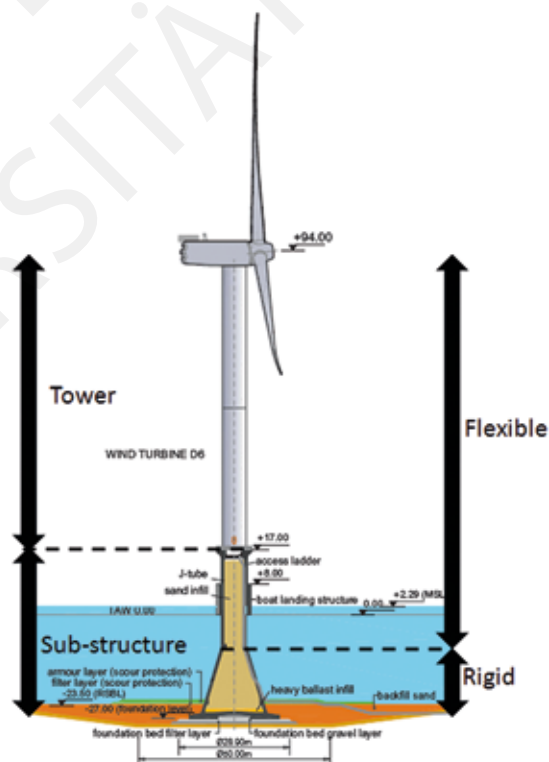
# Collapse Simulation of a fourlegged Masonry Minaret*

İ, KAZAZ,
Atatürk University,
Department of Civil
Engineering, Erzurum

AKANSEL,Vesile Hatun
Middle East Technical
University, Civil Eng.
Department, 06800, Ankara,
Turkey

GÜLKAN, Polat
Çankaya University, Civil
Eng. Department, 06800,
Ankara, Turkey

## Abstract

For the preservation of historical structures proper assessment, restoration and correct structural strengthening is needed. While the intervention methods depend mostly on the experience acquired by observing and interpreting past damage, complex structural analysis procedures progressively gain wide spread application to understand the behavior of historical masonry structures. In this study a special structure: the four-legged Minaret of Sheikh Mutahhar Mosque is analyzed to collapse under recorded earthquake ground motions, in order to demonstrate the effectiveness of such procedures in predicting the collapse behavior of masonry structures. The four-legged Minaret of Sheikh Mutahhar Mosque has been constructed in the early 16th century during the Akkoyunlu Period in Diyarbakır. The minaret is not connected to the body of the mosque, but is an adjacent and separate component. It is unique because the minaret body has been placed on four cylindrical stone columns. There is no positive connection between the columns and the minaret.

A model, which is very close to real structure, was generated with explicit dynamic code LS-DYNA using the architectural renderings of the minaret. The developed model takes into account the material nonlinearities and the interface friction and contact behavior between the masonry units. The modeling and analysis details for the minaret where the dynamic response is inherently nonlinear are presented and analysis results discussed in the manuscript. It was reported that the results of analysis, especially the disintegration of masonry units is strongly dependent on the employed friction coefficient and contact definitions in between the units.

Keywords: LS-DYNA, collapse, friction, contact, Sheik Mutahhar four-legged minaret, response history analysis.

BONIFÁCIO, Cristiana
University of Porto, Faculty
of Engineering,
Civil Department, Porto,
Portugal

RIBEIRO, Diogo
School of Engineering,
Polytechnic of Porto, Porto,
Portugal

CALÇADA, Rui
University of Porto, Faculty
of Engineering,
Civil Department, Porto,
Portugal

DELGADO, Raimundo
University of Porto, Faculty
of Engineering,
Civil Department, Porto,
Portugal

Figure 1 – Canelas Bridge:
general view*

# Dynamic behaviour of a short span railway bridge for high speed traffic

## Abstract

This article describes a 3D dynamic modelling and calibration of a railway bridge. The articulated train TGV-Double 3D rigid body model is described. This model allows performing moving loads and train-bridge interaction numerical analysis. The numerical results are compared with European Standards verifications and some particular aspects such as the consideration of an additional damping coefficient in moving loads numerical analysis, the track irregularities or the interaction effects of the two structural independent decks caused by the continuous ballast layer are analysed.

# Static plate load suitability when determining reinforcement soil stiffness – Model Validation and Simulation 2013

BRANDIS, Denis
University of Josip Juraj
Strossmayer, Osijek, Croatia

BUŠIĆ, Robert
University of Josip Juraj
Strossmayer, Osijek, Croatia

MINAŽEK, Krunoslav
University of Josip Juraj
Strossmayer, Osijek, Croatia

MULABDIĆ, Mensur
University of Josip Juraj
Strossmayer, Osijek, Croatia

## Abstract

With the road and railroad grid density increasing and the tendency for straight connection between point A and point B it is inevitable to cross soft subsoil areas. Furthermore, major settlements of road embankments made on such areas cause significant problems. In order to increase soil stiffness, a common solution imposes – geogrid reinforcement. Geogrid contribution to soil stiffness increase and reducing embankment settlements is indubitable because of sustainability concepts. However, providing optimal geogrid type, arrangement and efficiency control for certain soil type still remains vague due to the lack of a standard testing procedure for this purpose. Engineering practice requires a simple, reliable and quick testing procedure which is also applicable in the field to prove a construction quality when certain geogrid is used.

Figure 1 – Big pullout apparatus box



Figure 2 – Steel frame installation

DEHGHANIAN, Kaveh
Middle East Technical
University, Turkey

# The simplified methods for estimation of liquefaction potential based on shear wave

## Abstract

In- situ shear waves is being used widely in geotechnical engineering in recent years. Traditional methods are expensive and are not suitable for urbanized places. Surface wave dispersion methods have less limitation than body wave analysis which needs drilling. MASW technique is used to investigate site characterization in offshore, coastal and urban sites. In this paper, liquefaction assessment measure is described and a shear wave velocity based technique investigating liquefaction potential sites is studied.

Keywords: liquefaction potential assessment, shear wave, MASW.

Figure 1 – Schematic figure of typical MSAW (KGS, 2006)

# Dynamic analysis response in structural systems, accuracy and efficiency

DE MIGUEL TEJADA,
Alejandro
Department of Civil
Engineering. University of
Porto

## Abstract

The pros and cons (especially associated to both major accuracy and time of analysis) of time-dependent methods had been widely discussed over the years, being also recognized the importance of considering alternative and approximate methodologies to evaluate the structural response (displacements, shear efforts, flexure efforts…). Therefore, it is assessed the accuracy of the frequency domain method to the time domain method, through the analysis of SDOF responses. It has been detected that this accuracy is more remarkable if:

i) The truncate period, for the impulsive load and the response to a unit impulse function, is larger enough.

ii) A corrective response method is used. In this case, it is applied the well known corrective transient response based on initial conditions.

DRAGOS, Kosmas
Department of Civil
Engineering, Aristotle
University of Thessaloniki

# Dynamic Analysis of an Overpass Bridge from Field Measurements

## Abstract

The issue of dynamic behaviour of pedestrian bridges drew research attention following several incidents of unanticipated and unacceptable response under dynamic actions.
This behaviour could be partly attributed to the growing use of high-performance lightweight materials, which leads to slender structures particularly susceptible to oscillatory motion. Even in cases of footbridges designed in compliance with relatively recent code provisions in terms of ultimate limit state requirements, little or no allowance was made for in-service dynamic response.

The subsequent failure to meet serviceability criteria led to amendments in most codes of practice and the incorporation of relevant guidelines.
These issues were investigated through a case study of an R/C pedestrian bridge located in Thessaloniki. Numerical analysis of the bridge was performed parametrically, in the absence of detailed structural data, while further investigation involved instrumentation and ambient vibration testing. Modal identification was performed, using data from field measurements with the aid of specialised software, and the results showed good agreement between the numerical and experimental approach.

Figure 1 – The Millennium Bridge in London*

# Stability of Homogeneous Soil Slope

## Abstract

The paper deals with numerical patterns for assessment of the slope stability. Solutions are calculated with the finite element method using the ANSYS programme system. The results are compared with conventional approaches to determine the slope safety factor.

EKR, Jan
Brno University of Technology, Faculty of Civil Engineering, Department of Structural Mechanics, Veveří 95, 662 37 Brno, Czech Republic

GRATZA, Roman
Brno University of Technology, Faculty of Civil Engineering, Department of Structural Mechanics, Veveří 95, 662 37 Brno, Czech Republic

Figure 1 – Determining the slope geometry
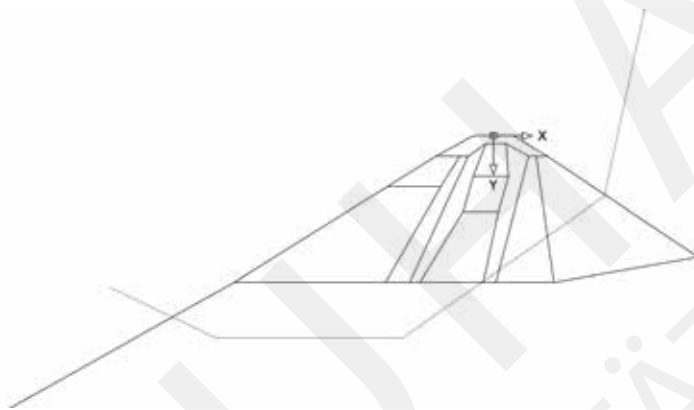
FELJA, Ivona
Faculty of Civil Engineering
Josip Juraj Strossmayer
University of Osijek, Croatia

# Earthquake resistance of bridges using KNE'X elements

## Abstract

University of California Berkeley announced the competition "Bridge Seismic Design Competition" for Civil Engineering undergraduate students to explore the effects of earthquakes on bridges. The research objective was to design the safest bridge for the San Francisco Bay Area, using the least amount of material possible that will suffer minimal damage when subjected to static and seismic loadings and constructed in the minimum time. The scaled model of the bridge is made up only of K'NEX elements without the use of glue or any additional elements.
On the Quanser Shake Table model was tested under earthquake excitation in the transverse direction of the bridge  The results showed that scaled bridge has enough resistance to withstand the static and dynamic load with minimum deflection.

Figure 1 – The scaled model of the bridge

# Study on Structural Performance of Loop Joints for Decked Bulb Tee Girder

JI,Sung-woong
Department of Civil
Engineering, College of
Engineering, Chung-Ang
University, Korea

## Abstract

The paper deals with numerical patterns for assessment of the slope stability. Solutions are calculated with the finite element method using the ANSYS programme system.
The results are compared with conventional approaches to determine the slope safety factor.
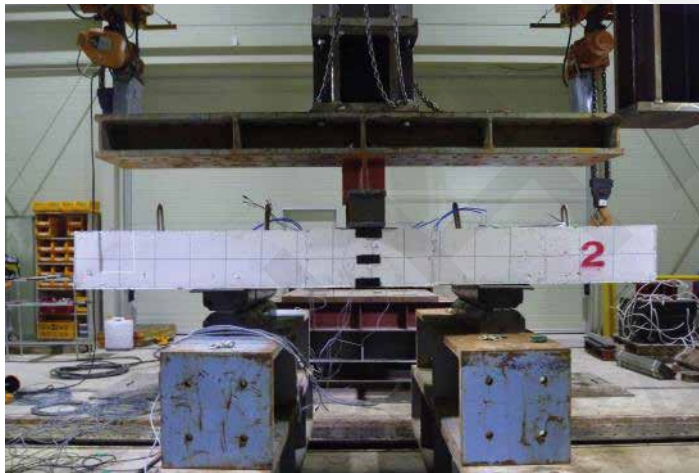
Figure 1 – Loading scheme of static test

KAMPENHUBER, David
Unit of Applied Mechanics,
University of Innsbruck,
Innsbruck, Austria

ADAM, Christoph
Unit of Applied Mechanics,
University of Innsbruck,
Innsbruck, Austria

# Collapse capacity of SDOF systems considering the P-delta effect and component degradation: A parametric study

## Abstract

This contribution to the summer school 2013 at Bauhaus University in Weimar deals with the quantification of the effect of component deterioration on the seismic collapse capacity of singledegree-of-freedom systems vulnerable to the destabilizing effect of gravity loads (P- delta effect).
The objective of this parameter study is to quantify how component degradation does influence the collapse capacity of P-delta sensitive SDOF systems. In other words, it is studied, which degradation parameter sets do affect the collapse capacity and which sets do not. In this study far-field ground motion records characterize the seismic input.

The outcomes are presented in terms of collapse capacity spectra, where for characteristic structural parameters the 16th percentile, the 84th percentile and the median of record-dependent collapse capacities are plotted against the initial structural period.

# Load time function calculation for assessment of structures subjected to aircraft impact load case

KLECHEROV, Ivaylo
Risk Engineering Ltd., Sofia, Bulgaria

NIKOLOV, Zhivko
Risk Engineering Ltd., Sofia, Bulgaria

## Abstract

After September 11, 2001 the awareness of the society for using a commercial airliner as a missile for damaging important public buildings, facilities and infrastructure was heightened.
That is why it is important to take into account the effects of such an impact on buildings with high societal risk as nuclear power plants or other important infrastructures. In the current paper we have examined two approaches for assessment of the loading intensity due to aircraft impact. The pioneering study of the aircraft impact problem is conducted by J.D. Riera (1968) and the developed method for a load time function calculation, known later as Riera's method, is still widely used today.

In this method, the impact force time history is first determined based on the aircraft mass distribution, crushing strength information and impulse conservation principles, assuming that the target is rigid. With the development of computer hardware, the computational analyses based on Finite Element Method (FEM) are becoming more widely used for assessment of engineering problems. In the last 10 years, significant progress has been made of explicit missile-target interaction analysis. In this method, a combined dynamic analysis model of both the missile and target is developed, and the dynamic response is determined as an initial velocity problem.
For the current study we have used FEM software LS-DYNA with explicit time integration. Sophisticated nonlinear material models and general contact algorithm are used. The load-time functions, calculated with both approaches are compared.

KONTOZOGLOU, Evangelos
Aristotle University of
Thessaloniki

MANOLIS, George
Aristotle
University of Thessaloniki

# Dynamic Analysis of an Onshore Wind Turbine Considering the Soil-Foundation-Structure Interaction (SFSI) Effects

## Abstract

The following paper concerns the dynamic analysis of an onshore wind turbine in which the Soil-Foundation-Structure Interaction (SFSI henceforth) effects are incorporated and their influence on the response of the wind-turbine is quantified and thoroughly explained. The wind turbine is modeled using two different Finite Element programs, namely ABAQUS and SAP2000, and a modal analysis is performed in both programs, in order to determine the fundamental frequencies and shape modes of vibration. Furthermore, a Response Spectrum Analysis is also performed for a variety of peak horizontal accelerations and types of the supporting soil medium. The circular foundation is modeled using static springs, dashpots, and lumped masses and the effects of the subsequent flexibility of the support are quantified and illustrated.

Figure 1 – The first 4 mode shapes of the wind turbine
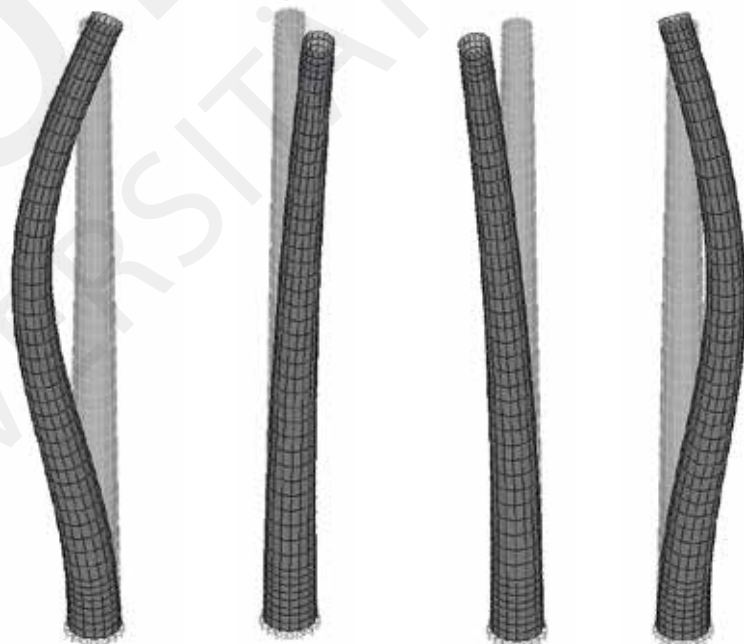
# Project for strengthening of Reinforced Concrete Bridge by carbon fiber composites

KULIKOFF, Rodrigo de Oliveira Bresser

School of Engineering of Sao Carlos University of Sao Paulo

CARRAZEDO, Ricardo
School of Engineering of Sao Carlos University of Sao Paulo

## Abstract

The fibers-reinforced polymers, also known as FRP systems for strengthening concrete structures, have emerged in recent years as attractive materials for use in civil engineering, especially for the rehabilitation of existing structures. Thus, it represents an immense potential not for the primarily markets, which were limited to aerospace, defense and transport industry, but also for use in civil infrastructure.

The FRP's light weight and the high mechanical characteristics, together with its resistance to corrosion and installation's facility, render these materials adequate to several uses in the field of construction industry, which allows innovative solutions, oftentimes impossible with conventional building materials.

The utilization of new strengthening techniques in structures emerges in accordance with the advent of new attractive materials to civil engineering. This demand is due to the rise in infrastructure constructions and also the ageing of existing structures, whether because of deterioration or having rendered obsolete.
This paper aims to perform the dimensioning of the strengthening of road bridge by carbon fiber composites, built in reinforced concrete and made to vehicle load called "class 30" from the Brazilian Standard ABNT NBR 7188/1984.

The bridge must have its bearing capacity increased in order to support the traffic of a special vehicle which should travel due to a substantial construction nearby.

The effects on the structure due to the addition of this new load will be analyzed, as well as the strengthening necessary for the bridge´s resistance to special vehicle loads. Finally, the sizing of the structural strengthening by carbon fiber composites is designed according to the American Standard ACI 440.2R-08.

MARCOS, Lara Kawai
School of Engineering of
São Carlos, University of São
Paulo

CARRAZEDO, Ricardo
School of Engineering of
São Carlos, University of São
Paulo

# Vibration sensitivity of hollow core slabs floor

## Abstract

Hollow core slabs are very efficient structural members, since their voids allow a significant reduction of self-weight. Moreover, prestressed concrete is commonly employed in this type of structure, allowing their use in large spans. Consequently, this is a very competitive solution. With these advantages, prestressed hollow core slabs are widely used in commercial and industrial buildings. However, there are reports on excessive vibrations in this type of floor. This research will analyze these elements' behavior against dynamic actions applied by people.

Firstly, the natural frequencies of a hollow core slab floor of 12 m of span were evaluated by numerical analysis. Then the frequencies were compared to excitation forces generated by people. This comparison showed that excessive vibration could occur in gymnasiums, dancing and concert halls and office buildings, and consequently a more complete analysis on this subject is necessary.

This study is in a preliminary phase and will comprise experimental determination of natural frequencies, mode shapes and damping ratios, as well as numerical simulation of vibration generated by people and their effects. Vibration levels will be then compared to comfort limits suggested by international standards.

Figure 1 – Pavement modelled in Abaqus®
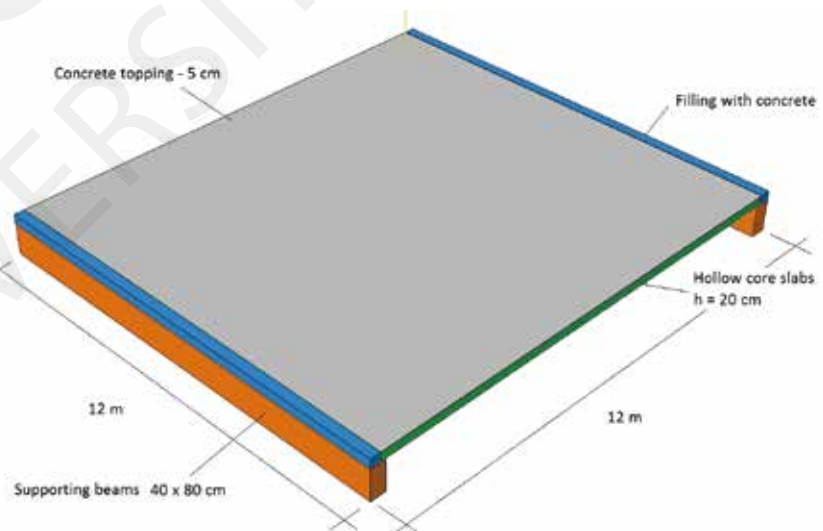
# Dynamic Behaviour of a Railway Viaduct with a Precast Deck under Traffic

## Abstract

In this paper, the dynamic effects resulting from the passage of the Alfa Pendular tilting train are evaluated on the Alverca viaduct, located in the Northern line of the Portuguese railway that establishes the connection between Lisbon and Porto. The dynamic analyses are performed using a train-bridge interaction model, considering the modal superposition method on the bridge model and the Newmark method on the train model. The analysis is focused on the three spans adjacent to the North abutment: one 16.5 m span and two 21.0 m spans. The numerical model of the bridge is a 3D finite-element model including the track developed in ANSYS software. The TGV-Double train is modelled as a rigid body and the Alfa Pendular train is also a 3D finite-element model which provides the deformability of the carbody, bogies and axles. Additionally, moving loads analysis is performed and the results from the two dynamic methodologies are compared.

The numerical results are assessed according to European Standards, as regards structural safety, track safety and passenger comfort.

MEIXEDO, Andreia
Department of Civil Engineering, Faculty of Engineering, University of Porto, Porto, Portugal

RIBEIRO, Diogo
Department of Civil Engineering, Polytechnic Institute of Porto, Porto, Portugal

CALÇADA, Rui
Department of Civil Engineering, Faculty of Engineering, University of Porto, Porto, Portugal

DELGADO, Raimundo
Department of Civil Engineering, Faculty of Engineering, University of

MOSCHEN, Lukas
Unit of Applied Mechanics,
University of Innsbruck,
Innsbruck, Austria

ADAM, Christoph
Unit of Applied Mechanics,
University of Innsbruck,
Innsbruck, Austria

# Introduction to parallel processing using the OpenSeesMP Interpreter

## Abstract

During the last decades, performance of workstations and desktop computers increased enormously. Nowadays, typical computers in companies or universities provide the user with several cores at each processor, with hyper-threading technology and a speed of more than 3Ghz. Software packages for structural analysis use already quite often several cores to assembly the stiffness matrix.
When the performance of structures subjected to seismic excitation is assessed, analysis is more sophisticated and time consuming. In such cases, very often multi-core-processing is not supported, or it is not applied by the end user due to lack of knowledge. In earthquake engineering nonlinear structural behaviour needs to be taken into account, in particular if it comes to the prediction of seismic collapse.

Furthermore, aleatory and epistemic uncertainties play an important role, and require in the most general case repeated nonlinear time-history analyses for a parametric study and subsequent statistical evaluation of the seismic structural behaviour. Scope of this paper is to provide users of OpenSees, which is the leading open source software package for earthquake analysis, with parallel techniques to accelerate the determination of their scientific results.

# Development of self-centering systems with rocking using CFDST columns made of ultra-high strength steel

NISHI Ryosuke
Department of Architecture and Architectural Engineering, Kyoto University

NAKASHIMA, Masayoshi
Disaster Prevention Research

## Abstract

Concrete filled steel tubes (CFTs) have been increasingly used for providing large stiffness and strength for the lateral-force resisting steel building structures. The first part of this paper presents an experimental investigation on a series of component tests of CFT and double skin CFT columns using ultra-high strength steel. The influence of seismic behavior of those columns specimens, CFTs and double-skinned CFTs, were evaluated regarding to many aspects, including initial stiffness, ultimate moment, strength deterioration, local buckling and fracture failure, in the study.
The test results show that the double skin CFT columns have comparable seismic performance of the CFT columns. In the second part of the study, tests of a self-centering frame specimen using the double skin CFT column inserted with post-tensioned high-strength steel bars to provide self-centering behavior was conducted. The cyclic behavior of the frame specimen was able to be accurately predicted by a developed analytical model using line-element with fiber sections.
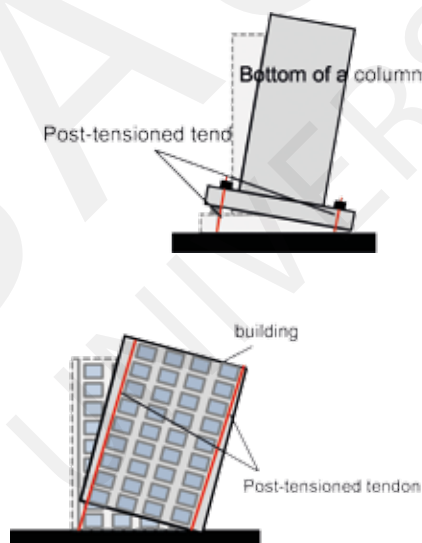
Figure 1 – the types of self-centering.
(a) self-centering components
(b) self-centering system

PAVEL, Florin
Department of Reinforced
Concrete Structures,
Technical University of Civil
Engineering Bucharest,
Bd. Lacul Tei no. 122-
124, Sector 2, 020396,
Bucharest, Romania

VACAREANU, Radu
Department of Reinforced
Concrete Structures,
Technical University of Civil
Engineering Bucharest,
Bd. Lacul Tei no. 122-

# Some comments on the variability of strong ground motions from Vrancea earthquakes

## Abstract

This research focuses on the analysis of the variability of strong ground motions recorded in intermediate-depth Vrancea earthquakes.

The variability is studied by using the Youngs et al. (1997) ground motion prediction equation (GMPE), which is among the candidate models for the prediction of spectral accelerations for Vrancea earthquakes, as recommended in Delavaud et al. (2012). Firstly, this GMPE is graded using several goodness-of-fit measures. Secondly, the single-station sigma approach is applied in order to reduce the variability of the predicted ground motions. Finally, the analysis of the variance (ANOVA) is performed. The results obtained revealed the extended influence of the seismic source on the amplitudes of the ground motions. The results of the single-station sigma approach also show a significant reduction of the standard deviations of the ground motions. The results from this paper which are part of a larger study shown in Pavel et al. (2014) reveal significant reductions of the ground motion standard deviation.

Figure 1 – Single-station standard deviations for the Youngs et al. (1997) GMPE*
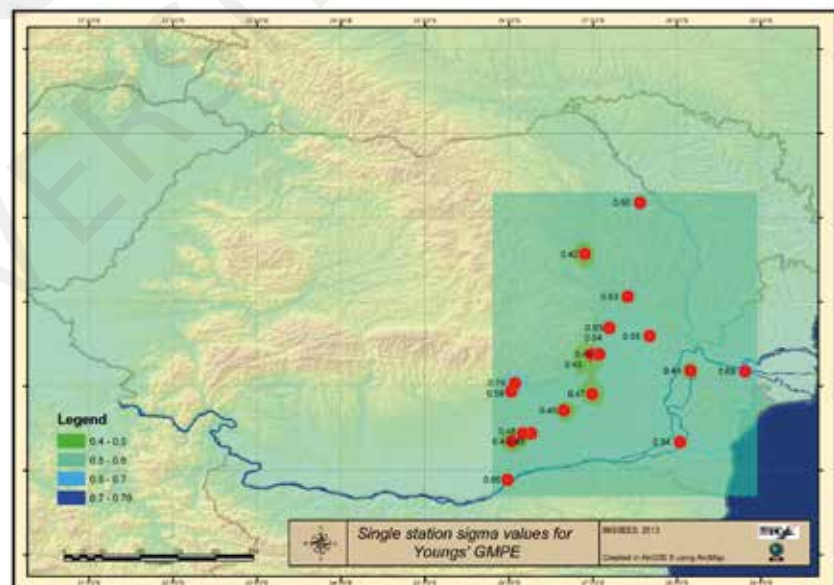


* Pavel, F., Vacareanu, R., Arion, C., Neagu, C. (2014). On the variability of strong ground motions recorded from Vrancea earthquakes. Earthquakes and Structures 6(1): 1-18.

# Optimization of an inter-story isolated structure using genetic algorithms

NISHI Ryosuke
Department of Architecture and Architectural Engineering, Kyoto University

NAKASHIMA, Masayoshi
Disaster Prevention Research

## Abstract

The paper aims to study the influence of an optimal inter-story isolation system on the seismic response of concrete structures. The inter-story isolation system consists in introducing lead rubber bearings at a certain level in the structure.

The analysis will be done for three pulse like records which can characterize the Vrancea source. The optimization problem will be addressed using genetic algorithms, which will aim to optimize the dimensions of the rubber bearings, an amount of additional mass above the rubber bearings and the story where the isolation occurs. The aim of the optimization process is to minimize the relative displacements of the structure.

A neural network is employed to build response surfaces for the structures and to analyze the influence of each parameter on the response of the structure.

ZARJOO, M.
Islamic Azad University-South Branch, Tehran, Iran

SASSANI, A.
Middle East Technical University, Ankara, Turkey

# Non-linear Finite Element analysis of the performance of Circular Bridge Piers reinforced with FRP composite laminates

## Abstract

Various factors such as design and execution mistakes, unsuitable execution, changing the occupancy of the buildings, and changes in the design and construction standards make it necessary to retrofit and enhance the structures during the service life. The application of innovative materials and methods has been proposed for retrofitting and enhancement of the buildings. Among these materials, FRP fibers have a high standing.

In this research the bending capacity and ductility of bridge piers with different FRP wrapping lengths have been investigated by the use of ABAQUS 6.9.1 software modeling. According to the findings of this research the needed wrapping length will be proposed with respect to the cost of this type of material.

# Numerical Analysis of Seismic Ground Response

HASSAN, Muhammad Shariq
School of Civil Engineering
National Technical University
of Athens, Greece

## Abstract

This paper contains nonlinear simulation result of layered soil from EERA program by considering Dobry-Vucetic and Mohr-Coulomb soil models. The effect of ground motion has adverse effect on layered soil compare to rock outcrop.

The two aforementioned design seismic excitations, considering two peak acceleration values (0.10g and 0.35g) for each excitation, were used to establish relations of soil response at ground surface and bedrock. Finally, analytical computation of maximum acceleration at soil surface is compared to the program ground acceleration results.

SINKOVIC, Klemen
University of Ljubljana,
Faculty of Civil and Geodetic
Engineering, Jamova 2, 1000
Ljubljana, Slovenia

# Assessment of seismic resistance of existing RC frame buildings

## Abstract

For assessing the seismic resistance of existing buildings, procedures at three levels of complexity are used.
At the lowest level the seismic resistance of the building is determined on the basis of a rapid screening of a building. At the middle level the seismic resistance is determined with a relatively simple analysis, while at a higher level a more advanced nonlinear method of analysis is applied, i.e. the N2 method.

At the first two levels, the existing approaches of Japanese method are used. There were made some modifications, which were primary related to determination of ductility and shear strength of RC columns. As an example, assessment of seismic resistance of an existing 4 storey RC frame building structure was made.

The response of the building and assessment of seismic resistance was then compared with the same building, designed according to Eurocode 8 standard, and with eight variants of the building, which were designed according to regulations, that were for the time of construction in force in former Republic of Yugoslavia.

# Beam – column sliding failure in R.C. frames with masonry infill panels

STRAMONDO, Paola Roberta
University of Catania,
Department of Civil and
Environmental Engineering,
Italy

## Abstract

A dangerous collapse mechanism can occur in reinforced concrete framed buildings during strong earthquakes.

This is the sliding shear failure between the top end of the column and the beam above, along the interface of the concrete casting. This kind of failure is essentially caused by the presence of masonry infill panels that develop a sort of strut under seismic actions. National and international regulations in seismic areas require an explicit test for this kind of collapse only for buildings with concrete walls.

Nevertheless, formulas used in regulations to evaluate the resistance against sliding at potential sliding shear planes are not directly applicable for the beam-column sliding resistance. A theoretical-experimental research has been developed at the University of Catania in order to evaluate different contributions to the beam-column sliding resistance and to provide and validate numerical relations for their calculation.

VELCHEVA, Vanya UACEG,
Bulgaria

BLAGOV, Dilyan UACEG,
Bulgaria

BONEV, Todor UACEG,
Bulgaria

# Seismic performance evaluation of reinforced concrete building in Bulgaria

## Abstract

There are plenty of old exciting buildings all over the world. They are considered to be momuments of culture – these are museums, galleries, schools, hotels and homes. We must admit these buildings represent architecture and culture over the centuries. Looking at them we can see architecture and civil engineering have developed during the years- bulldings have become more beautiful, broken up and safetier according to the theorries of static and dynamic behavior.

Unfortunately some of those buildings are situated in highly seismic regions whitch means our culture and homes might be in potential danger. Most people would say „Well, we're going to pray not to lose them" or „They are dangerous for out existance lets demolish them and build new ones. We can rebuild them, in order not lose our hystory and culture".

Nowadays both approaches are not efficient thanks to the development of modern engineering and technolgy. There are many ways of strenghtening a construction without significant architectural modifications. In this paper, a typical 2-storey reinforced concrete (RC) building frame is designed and analysed using SAP 2000. Based on the results of push over analysis we can conclude that the most efficient method for our building is strengthening by using steel diagonals

# Activities

# Activities

### Bauhaus Summer School

The Bauhaus Summer School is the summer programme of the Bauhaus-Universität Weimar and offers courses in Languages, Architecture, Art & Design, Culture & Media and Engineering & Environment.
It is open to prospective students, undergraduate and graduate students and alumni of the Bauhaus-Universität Weimar. Each year approximately 400 participants from over 60 countries around the world create a unique atmosphere.

The Bauhaus Summer School is a great opportunity to meet people all over the world, to connect to an international network and broaden cultural and academic horizons. Furthermore, the team of Bauhaus Summer School creates a diverse programme that participants can tailor to their interests.

Even if they would like to use the weekends to venture outside of Weimar or enjoy a reading, concert or film in the evenings.

The guided tours, the international gaming night, all Summer School parties and the film programme are free of charge for those who have a Bauhaus Summer School ID card. Moreover Bauhaus Summer School offers excursions at a reduced cost.

## Guided Tours



Every Wednesday between 14.00 and 17.00, participants can enjoy a cultural programme about the history of Thuringia, Weimar and the Bauhaus-Universität Weimar. The topics vary from week to week:

### Johann Wolfgang von Goethe: The Last Universal Genius
Travel cloak, volcanic rock, puppet theatre, Weimar?! On this tour, attendees learn what these things say about one of the most important dramatic artists of the German classical period and how they are connected. Goethe's complexity is as striking today as ever. He not only produced literary masterpieces such as Faust, but also was active in politics and art.

### In Henry van de Velde's Footprints
Henry van de Velde created one of his most significant spatial compositions and first 'total work of art' with the Nietzsche Archive. Here, Nietzsche's sister was hostess to one of the most modern salons in Europe, which also served to exploit Nietzsche for National Socialist ideology.

### Experience the World of Music from 200 Years Ago
Participants experience the music culture of the 18th and 19th centuries in an authentic environment as pianists bring historical grand pianos to life in rooms in the castle. Musicologists explain in which direction the sound aethetics of the piano moved and the role music played in cultural life around 1800.

### Discover the Green Heart of Weimar
Two hundred years ago, the Duchy of Weimar was little more than a tiny village with a burned-out castle and was almost bankrupt. A tour through the Park an der Ilm and Johann Wolfgang von

Goethe's garden house will show why this city succeeded within a span of 20 years in becoming a cultural centre with a European flair.

### Bauhaus Walk

Participants take a walk through Weimar, follow the traces of the early Bauhaus and experience the exciting past and present of the Bauhaus-Universität Weimar.

The beginnings of the Bauhaus-Universität Weimar can be traced back to the 19th century. Originally an art academy, it was enlarged after 1945 to include a number of engineering disciplines which gave the university a modern technical character. With the inclusion of the Faculty of Art and Design, founded in 1993, and the Faculty of Media, founded in 1996, the Bauhaus-Universität Weimar has once again coupled the fields of art and engineering into one institution and has been carrying the name of the famous school of design since 1996.

### Faculty Tour

The programme introduces prospective students to the Bauhaus-Universität Weimar, its laboratories and workshops. The programme aims to establish contact with these potential students and reduce their anxiety to study. Students can visit all faculties: Art & Design, Media, Architecture and Engineering. Afterwards they get an introduction in „How to study at Bauhaus-Universität Weimar".

## Summer School Parties

Three big parties traditionally take place during the Bauhaus Summer School. The first party, titled „Bonvena", welcomes all the participants to Weimar. Students discover that music and good food are the best ice-breakers. Everyone comes wearing the colours of their home country or those of the country whose
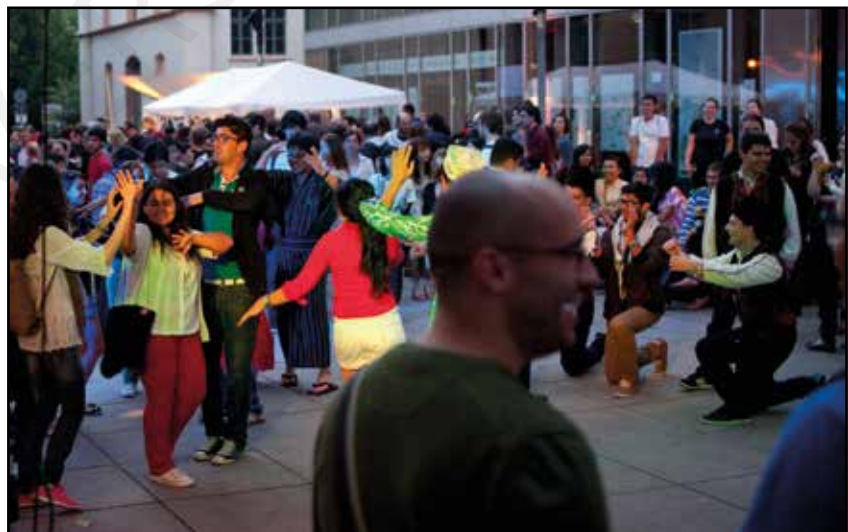
language they're going to learn at the Summer School.
Another great tradition is the „Bauhaus Gots Talent Show" held midway through the Bauhaus Summer School course. It's the last party for some participants, but for others, it marks the half-way point. A lot of fun for everyone involved.

Each year Bauhaus Summer School pick a different motto for the last big party. Here students can exchange telephone numbers and e-mail addresses, and celebrate the final hours of the Bauhaus Summer School together. And as always, dancing is strongly encouraged!

## International Gaming Night

Students make their learning process a game! What is the best way to get to know other people? Correct, the best way is to play games.
So, that is why attendees have the opportunity to participate in an international gaming night on every Monday during Bauhaus Summer School at 20:00, where they can meet other people from different courses. The purpose of this event is to overcome language barriers in a playful way.

## Excursions

### Berlin
Bauhaus Summer School offers a trip to one of the most fascinating cities in Europe. After a relaxing dinner on Friday evening, participants can go discover the nightlife of Berlin. On Saturday morning, they meet for a boat tour and cruise the Spree River while take in the sights and learn about the „New Berlin".

In the afternoon attendees can use their free time to visit museums, go shopping or just even enjoy the rhythm of Berlin. The weekend in the capitol city ends with a visit to the „Reichstagsgebäude".

### München

Participants can spend a fantastic weekend in the heart of Bavaria! On Saturday, they begin with a tour of the city and see the classic sights while hearing cool stories about Munich. Afterwards, students enjoy a hearty lunch and try a Hefeweizen at the world-famous Hofbräuhaus. On Sunday, they take a tour of the Olympic Park, where the attendees hear about the 1972 Olympics, walk through the famous Olympic Stadium, and learn about the impressive architecture and some of the most legendary musical acts to perform there!

## Rubber Rafting Tour

Participants enjoy an unforgettable experience with their fellow Bauhaus Summer school friends paddling down the Saale river from Camburg to Bad Kösen.
The rubber rafting tour takes attendees gently down the stream past castles, manors, vineyards, massive limestone cliffs and breathtaking landscapes. And the occasional rapids will certainly get their adrenaline pumping!

## Sports

Participants don't have to miss out on anything during Bauhaus Summer School, not even their weekly sport activities.
Every Tuesday, between 17:00 and 19:00, they can meet with other participants at the Falkenburg University Sports Centre and work up a sweat. There's something for everyone, from volleyball to badminton to football.

## Cinema

As every year the communal cinema mon amie in cooperation with the language centre and the Bauhaus Summer School will show several movies in their original language with German subtitles.

## Bauhaus Special

Students become a „Bauhaus Expert!" They learn about the Bauhaus and its core principles by going on the Bauhaus Lantern Walk in the first week. In addition, participants learn about the

Bauhaus masters in the Bauhaus Creative Workshop and take advantage of the opportunity to create their own personal work of art. On the weekend, they visit the designs of the Bauhaus in the city of Dessau. In the second week, the participants cook and enjoy an amazing Bauhaus-Dinner in a charming atmosphere. The Bauhaus Special ends with a tour of the Bauhaus Museum in Weimar.